DATA ANALYSIS AND NOISE PREDICTION
FOR THE QF-1B EXPERIMENTAL FAN STAGE

by D.B. Bliss, K.L. Chandiramani, and A.G. Piersol

BOLT BERANEK AND NEWMAN INC.

prepared for

NATIONAL AERONAUTICS AND SPACE ADMINISTRATION

NASA Lewis Research Center

Contract NAS3-19426

| 1 Report No CR-135066 | 2 Government Accession No | 3 Recipient's Catalog No |
|---|---|---|

| 4 Title and Subtitle DATA ANALYSIS AND NOISE PREDICTION FOR THE QF-1B EXPERIMENTAL FAN STAGE | 5 Report Date August 1976 |
| | 6 Performing Organization Code |

| 7 Author(s) D.B. Bliss, K.L. Chandiramani, and A.G. Piersol | 8 Performing Organization Report No 3338 |
| | 10 Work Unit No |

| 9 Performing Organization Name and Address Bolt Beranek and Newman Inc. 50 Moulton Street Cambridge, Mass. 02138 | 11 Contract or Grant No NAS3-19426 |
| | 13 Type of Report and Period Covered Contractor Report |

| 12 Sponsoring Agency Name and Address National Aeronautics and Space Administration Washington, D.C. 02138 | |
| | 14 Sponsoring Agency Code |

15 Supplementary Notes

16 Abstract    This report describes the results of a fan noise data analysis and prediction effort using experimental data obtained from tests on the QF-1B research fan at NASA Lewis. The data consisted of surface pressure measurements made with flush mounted sensors installed on selected rotor blades and stator vanes and corresponding noise measurements made by microphones located at the far field. The data analysis included  power spectral density analysis, time history studies, and calculation of coherence functions. The emphasis of these studies was on the characteristics of tones in the spectra. One important result of these investigations is that the amplitude behavior of spectral tones was found to have a large, often predominant, random component, suggesting that turbulent processes play an important role in the generation of tonal as well as broadband noise. Inputs from the data analysis were used in a prediction method developed by Heller and Widnall (1972) which assumes that acoustic dipoles, produced by unsteady blade and van forces, are the important source of fan noise. Some modifications were made to made the prediction method more compatible with the QF-1B fan configuration. The problem of rotor blade interaction with inflow distortions has been treated in more detail than in the original work. General agreement between predicted and measured tone levels was obtained for the lower harmonics of blade passage frequency but the predicted levels exceed the measured levels at higher harmonics The source of disagreement is believed to be related to the fact that some of the underlying assumptions of the prediction method are not satisfied by the actual fan configuration tested.

| 17 Key Words (Suggested by Author(s)) Fan Noise Trace speed criteria in stator noise | 18 Distribution Statement Unclassified – Unlimited |
|---|---|

| 19 Security Classif (of this report) Unclassified | 20 Security Classif (of this page) Unclassified | 21 No of Pages 117 | 22 Price* |
|---|---|---|---|

NASA-C-168 (Rev 10-75)

ORIGINAL PAGE IS
OF POOR QUALITY

# DATA ANALYSIS AND NOISE PREDICTION
# FOR THE QF-1B EXPERIMENTAL FAN STAGE

by D.B. Bliss, K.L. Chandiramani, and A.G. Piersol

BOLT BERANEK AND NEWMAN INC.

prepared for

NATIONAL AERONAUTICS AND SPACE ADMINISTRATION

NASA Lewis Research Center

# ABSTRACT

This report describes the results of a fan noise data analysis
and prediction effort using experimental data obtained from tests
on the QF-1B research fan at NASA Lewis.  The data consisted of
surface pressure measurements made with flush mounted sensors in-
stalled on selected rotor blades and stator vanes and correspond-
ing noise measurements made by microphones located in the far
field.  The data analysis included:  power spectral density
analysis, very narrowband spectral analysis, probability density
analysis, time history studies, and calculation of coherence
functions.  The emphasis of these studies was on the character-
istics of tones in the spectra.  One important result of these
investigations is that the amplitude behavior of spectral tones
was found to have a large, often predominant, random component,
suggesting that turbulent processes play an important role in the
generation of tonal  as well as broadband noise.  Inputs from the
data analysis were used in a prediction method developed by Heller
and Widnall (1972) which assumes that acoustic dipoles, produced
by unsteady blade and vane forces, are the important source of
fan noise.  Some modifications were made to make the prediction
method more compatible with the QF-1B fan configuration.  The
problem of rotor blade interaction with inflow distortions has
been treated in more detail than in the original work.  General
agreement between predicted and measured tone levels was obtained
for the lower harmonics of blade passage frequency but the pre-
dicted levels exceed the measured levels at higher harmonics.
The source of disagreement is believed to be related to the fact
that some of the underlying assumptions of the prediction method
are not satisfied by the actual fan configuration tested.

iii

# SUMMARY

The results of a data analysis and noise prediction effort conducted using experimental data obtained from tests on the QF-1B fan stage at NASA Lewis are described in this report. The rotor blades and stator vanes were instrumented with flush-mounted pressure sensors. Far field noise measurements were made with microphones located along a semi-circle on one side of the fan. A major goal of the study was to gain more understanding of the relationship between the unsteady surface pressures on blades and vanes and the far field noise, with particular emphasis on the characteristics of tones in the spectra.

The data analysis was performed at Bolt Beranek and Newman Inc. and at NASA Lewis. The analysis performed included:

Power spectral density analysis,

Very narrow band spectral analysis,

Narrowband possibility density analysis,

Calculation of coherence functions, and

Studies of time and phase delays between sensors.

The purpose of these analyses was to learn more about the statistical characteristics of the tones which occur at the harmonics of blade passage frequency and the harmonics of shaft rotation rate. Another reason for these analyses was to gain information about the nature of the aerodynamic interactions which produce unsteady pressure levels.

Some results from the data analysis were used in a fan noise prediction method that assumes that acoustic dipoles produced by net unsteady forces acting on the blades and vanes are the major source of fan noise. The method was modified in the case of rotor-wake/stator-vane interaction noise to make it more compatible with the physical nature of this interaction as it occurs on the QF-1B fan. The important features of the interaction are discussed in some detail. The prediction method was extended to treat specifically the use of a rotor operating in a distorted inflow. Predictions were made for both the rotor and stator noise sources and compared with far field noise levels. General agreement was obtained for the lower harmonics but the method overpredicted higher harmonic levels for both the rotor and stator. The possible reasons for this different trend with increasing frequency are discussed in some detail.

# TABLE OF CONTENTS

TABLE OF CONTENTS *(Cont.)*

# LIST OF FIGURES AND TABLES

LIST OF FIGURES AND TABLES *(Cont.)*

page

LIST OF FIGURES AND TABLES *(Cont.)*

# LIST OF SYMBOLS

Symbol

| | |
|---|---|
| B | Number of rotor blades. |
| d | Interelement spacing |
| $d_r$ | Interelement rotor spacing |
| $d_s$ | Interelement stator spacing |
| $f, \tilde{f}$ | Fourier Transform pair |
| f | Time history of fluctuating lift at either stator or rotor location |
| k | Acoustic wave number |
| $k_y$ | Wave number in the (unwrapped) y-direction |
| $L_s$ | Spanwise coherency length scale |
| $L_{ch}$ | Chordwise coherency length scale |
| $\ell_s$ | Effective spanwise length of stator over which the unsteady pressure acts |
| $\ell_{ch}$ | Chordwise length scale on stator over which the unsteady pressure acts |
| $\ell(t)$ | Lift due to impingement of a series of wakes |
| $\tilde{\ell}(\omega)$ | Fourier Transform of $\ell(t)$ |
| $p(x)$ | Probability density function |
| q | Harmonic number of rotor shaft speed |
| $q(y)\big|_{y=ut}$ | Circumferential distribution of fluctuating lift at the rotor location |
| $\tilde{q}$ | Fourier Transform of $q(y)\big|_{y=ut}$ |
| R | Signal-to-noise ratio |
| $R_o$ | Effective radial location of point forces on a stator/rotor blade |

x

| | |
|---|---|
| r | Radial coordinate |
| $r(y,t)$ | Fluctuating lift force per unit length in y-direction at rotor location |
| $\tilde{r}(k_y,\omega)$ | Double Fourier Transform of $r(y,t)$ |
| $S(y,t)$ | Fluctuating lift force per unit length in y-direction at stator location |
| $\tilde{S}(k_y,\omega)$ | Double Fourier Transform of $S(y,t)$ |
| u | Uniform rectilinear motion velocity in y-direction |
| V | Number of stator vanes |
| $V_z$ | Axial velocity component |
| $\bar{V}_z$ | The value of $V_z$ averaged in the z-direction between $Z_r$ and $Z_s$ |
| $V_\theta$ | Tangential velocity component |
| $V_{\theta f}$ | Tangential velocity in stator fixed coordinates |
| $\bar{V}_{\theta f}$ | The value of $V_{\theta f}$ averaged in z-direction between $Z_r$ and $Z_s$ |
| $V_{trace}$ | Trace velocity of the point of interaction along radial edge of a stator vane |
| $W_1$ | Resultant downstream mean velocity in rotor fixed coordinates |
| $W_2$ | Resultant downstream velocity in the rotor wake in rotor fixed coordinates |
| x,y | Cartesian coordinates in the plane normal to fan axis |
| y | Circumferential direction in the two-dimensional (unwrapped) analog of a row of blades or vanes |
| z | Axial coordinate |

# LIST OF SYMBOLS (*Continued*)

$\hat{z}$ — Unit vector in axial direction

$z_r$ — Axial location of rotor trailing edge

$z_s$ — Axial location of stator leading edge

## Greek

$\alpha$ — Slope of the wake in x-y plane

$\tilde{\alpha}$ — Interaction angle between rotor wake and stator vane leading edge

$\beta$ — Average setting angle of stator vanes, degrees

$\delta$ — Dirac-Delta function

$\theta$ — Circumferential coordinate

$\hat{\theta}$ — Unit vector in the circumferential direction

$\theta_r$ — Circumferential location of rotor trailing edge

$\theta_{tip}$ — Circumferential location of the rotor wake at the tip of the stator inlet plane

$\theta_{hub}$ — Circumferential location of the rotor wake at the hub of the stator inlet plane

$\lambda$ — Acoustic wave length

$\rho$ — Medium density

$\sigma_n$ — Standard deviation of the noise

$\sigma_s$ — Standard deviation of the signal

$\phi$ — Slope of wake in the $\theta$-z plane

$\phi_\ell(\omega)$ — Frequency spectral density of fluctuating lift

$\phi_p(\omega)$ — Farfield pressure spectral density

$\phi_{dp}(\omega)$ — Spectral density of the differential pressure field

$\phi_{\pi rad}(\omega)$ — Frequency spectral density of radiated acoustic power

$\Omega$ — Rotor shaft speed

$\omega_r$ — Blade passage frequency

$< >$ — Average value

# INTRODUCTION

The fan stage of a high-bypass-ratio turbofan engine is a major aircraft noise source. In order to attain long range goals for noise reduction, a better understanding of the basic aeroacoustic sources of fan noise must be achieved. The purpose of this report is to describe the results of an experimental and analytical study to improve the understanding of fan noise mechanisms.

Prior to the beginning of the present study, aeroacoustic data was taken on the QF-1B fan stage using the full scale fan test rig at NASA Lewis. The aeroacoustic data consisted primarily of unsteady surface pressure measurements taken at a number of locations on the rotor blades and stator vanes using flush-mounted sensors.* Microphone measurements of the far field noise were made simultaneously. The experimental arrangement is described in the next chapter. The present study deals with the analysis and interpretation of some of this data and its use in a particular fan noise prediction method. This report is not intended to provide a detailed compilation of the data obtained, of which there is a considerable quantity, but rather to summarize the important results for typical cases and to discuss the most interesting and important characteristics of the data that emerged during its analysis.

The occurrence of unsteady loading on the rotor blades and stator vanes is a major source of fan noise. The most important cause of this unsteady loading is the interaction of the rotor and stator with non-uniformities and turbulence in the incident flow. The rotor blade wakes are the primary source of inflow distortion to the stator vanes; these wakes possess a periodic mean shape on which a turbulent structure is superimposed. The nature of disturbances to the rotor inflow is less structured and more complex. Typical mean and turbulent disturbances to the rotor inflow include: gross flow distortions and the wakes from objects upstream; the possible presence of inlet vortices (rising from the ground or an external object); and elongated eddies sucked into the fan from turbulence in the atmosphere. The unsteady surface pressures measured on the blades and vanes arise primarily from these effects. The analysis and interpretation of the surface pressure data and the corresponding far field noise measurements is described in the third chapter.

---

*The instrumentation of the blades and vanes was performed by Bolt Beranek and Newman Inc., Cambridge, Mass., under Contract NAS3-17852.

Following the data analysis, the surface pressure data (converted to blade and vane forces) was used as an input to a fan noise prediction method originally developed by Heller and Widnall (1972). Because this method represents a rather basic fan noise model, both its degree of success and its shortcomings in predicting the fan noise are of interest. The use of surface pressure data as an input simplifies the problem since a detailed characterization of the inflow velocity distortions and the blade aerodynamic response is largely avoided. The assumptions underlying the fan noise model, its use in the present program, and an interpretation of its results are found in the fourth chapter.

# DESCRIPTION OF THE EXPERIMENT

The experiment was conducted on the NASA Lewis QF-1B Fan Stage in a full-scale outdoor fan noise test facility. Descriptions of the fan and the facility, and the results of some previous test programs are found in Leonard, *et al.*, (1970); Goldstein, *et al.*, (1970); and Povinelli, *et al.*, (1972). The fan is illustrated in Fig. 1 and its pertinent design parameters are summarized in Table 1.

The fan is mounted on a pedestal so that its axis is about 19 ft above the ground. The fan is externally driven by a long shaft connected to a drive motor. The drive shaft requires an extensive support structure. The fan is partially surrounded by an arc of far field microphones for noise measurements. A photograph of the general arrangement is shown in Fig. 2. The fan can be operated in two ways: a front drive installation where the drive shaft comes in through the inlet (as shown in Figs. 1 and 2), and a rear drive installation where the shaft enters the fan from behind. The most important difference between the front drive and rear drive cases is that the shaft support structure does not interfere with the fan inlet flow when rear drive is used. The two drive installations are shown in the plan views of Fig. 3 along with the pertinent dimensions for the two cases. The angular designations for the far field microphones are also indicated in Fig. 3 for each case.

A schematic drawing summarizing the instrumentation installed in the fan is shown in Fig. 4. The rotor blades and stator vanes were instrumented with BBN Model 381 flush-mounted surface pressure sensors. Some sensors were single-sided, whereas others were double-sided and these could be used either individually or differentially (to measure lift pressure). The designations used throughout the report to identify the individual instrumented rotor blades and stator vanes are also indicated in Fig. 4. The data analysis and interpretation discussed in the following section deals with the surface pressure measurements on the blades and vanes, and the noise measurements in the far field.

The BBN Model 381 is a rugged single- or double-sided piezoelectric dynamic pressure sensor with an internal preamplifier. The sensor thickness is 3.18 mm (0.125 in), measured between sensor faces, and the total diameter is 6.35 mm (0.250 in) at the measurement surface. The actual sensing area has a diameter of 5.59 mm (0.220 in). The nominal sensitivity is 0.055 mV/(N/m$^2$) (380 mV/psi) with a frequency response of 10 Hz to 20 kHz at ±1 dB and a dynamic range of 94 dB. Figures 5a and 5b show photographs of the sensors installed in the rotor blades and stator vanes.
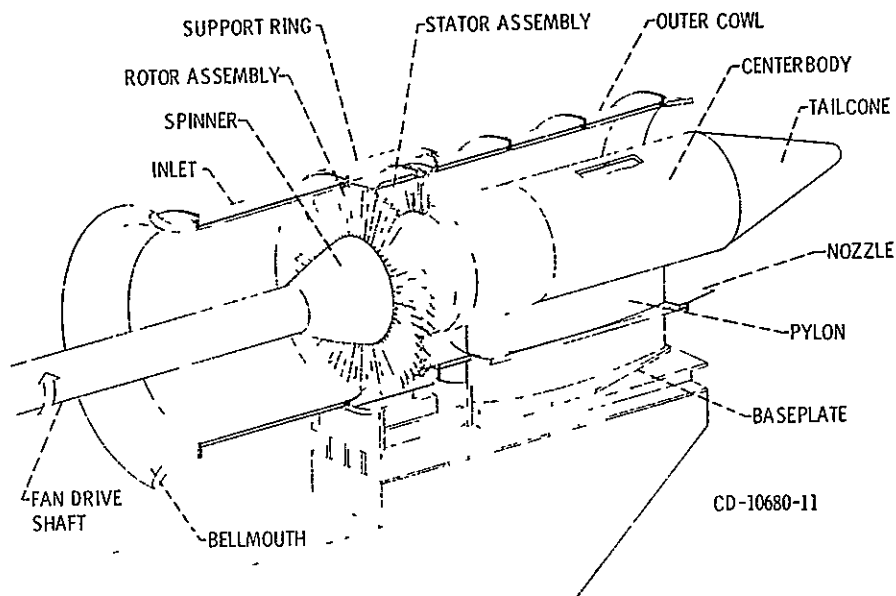
FIG. 1. SKETCH OF QF-1 FAN NACELLE ASSEMBLY, FRONT DRIVE ARRANGEMENT (From Povinelli, *et al.*, 1972).
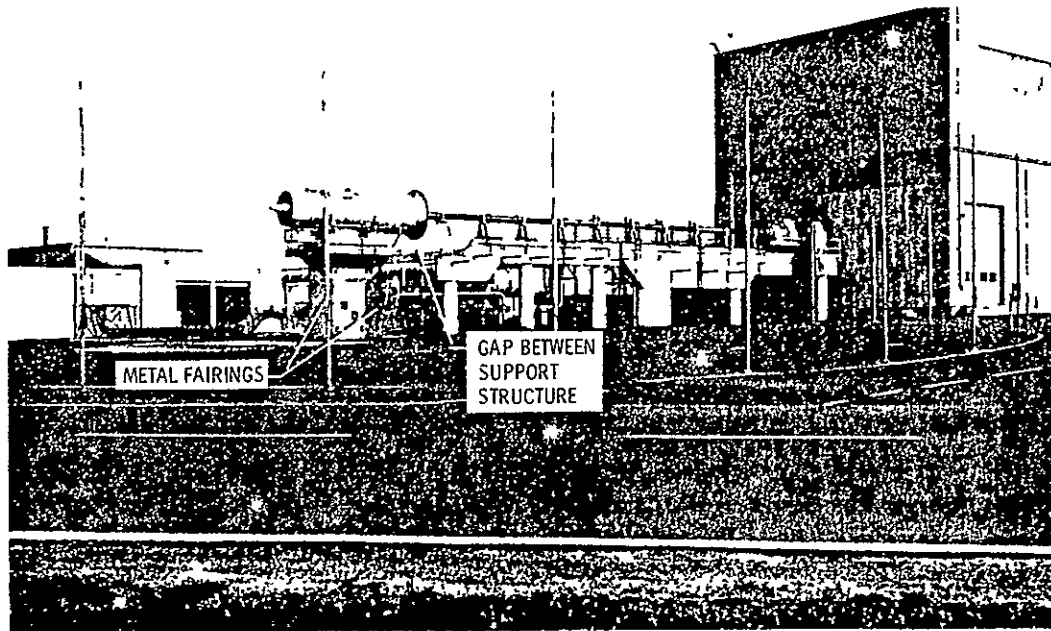


FIG. 2. PHOTOGRAPH OF THE TEST SITE.

## TABLE 1. FAN DESIGN PARAMETERS

Rotor tip diameter, m (in.)......................... 1.824 (71.81)

Stator tip diameter, m (in.)....................... 1.726 (67.94)

Rotor tip speed (cruise design value, corrected),
    m/sec (ft/sec)................................. 337.4 (1107)

Design stagnation pressure ratio............................. 1.5

Design weight flow (corrected), kg/sec (lbm/sec)....... 396 (873)

Rotor hub-tip radius ratio (inflow face).................... 0.50

Stator hub-tip radius ratio................................. 0.59

Rotor-stator spacing (rotor trailing edge to stator
    leading edge at the hub), cm (in.).................. 50.8 (20)

Number of rotor blades........................................ 53

Number of stator blades...................................... 112

Rotor chord length, cm (in.)......................... 13.97 (5.5)

Stator chord length, cm (in.)........................ 6.83 (2.69)

Note: Aerodynamic parameters have been corrected to NACA standard
      sea-level atmospheric conditions of 288.2K (518.7°R) and
      $1.013 \times 10^5$ newtons per square meter (2116.2 $lbf/ft^2$).
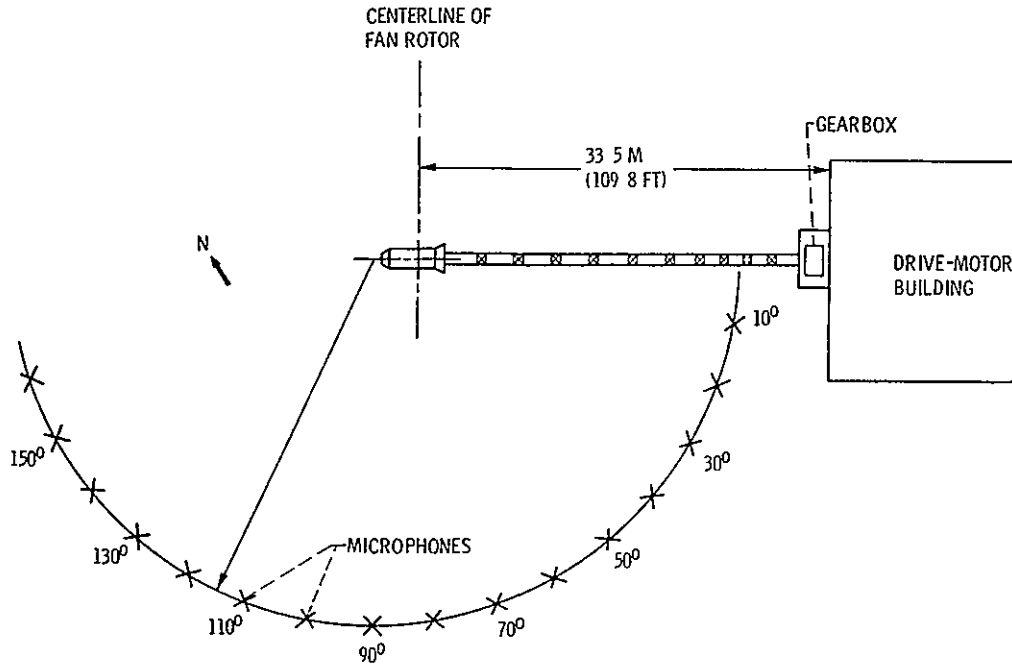
(a)   Front Drive Installation.
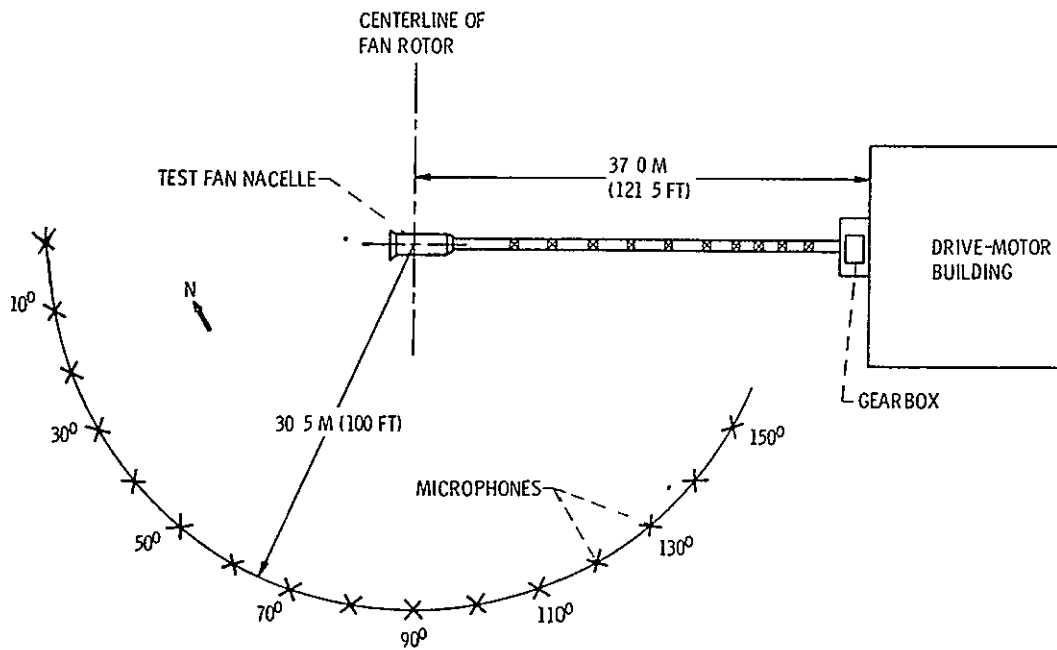


(b)   Rear Drive Installation.

FIG. 3.   PLAN VIEWS OF TEST SITE SHOWING FRONT AND REAR DRIVE
          INSTALLATIONS AND THE CORRESPONDING MICROPHONE LOCATIONS.

6
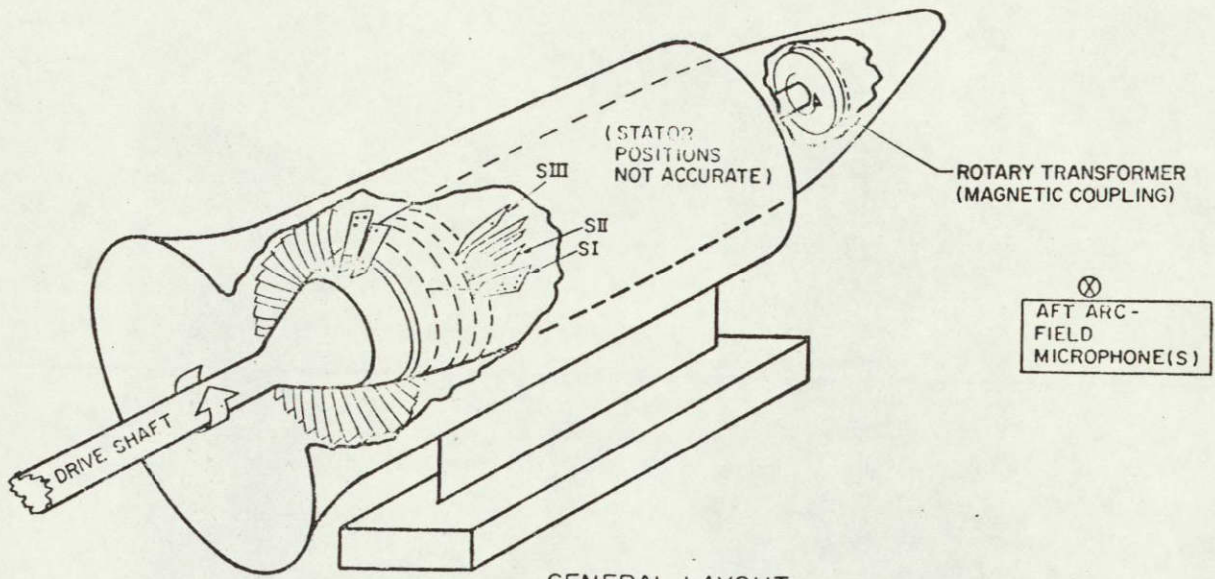
GENERAL LAYOUT

O — SINGLE-SIDED SENSOR
● — DOUBLE-SIDED SENSOR (OR 2 SINGLES)

ROTOR DETAIL

STATOR DETAIL
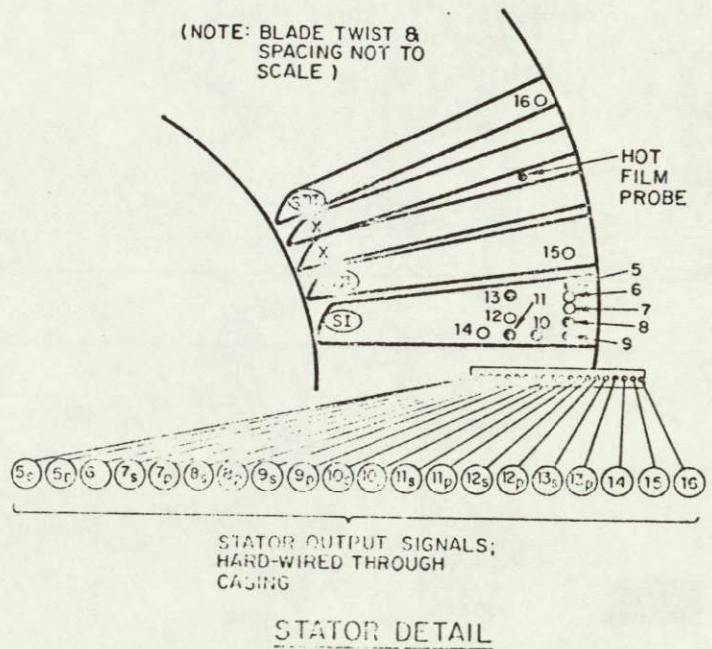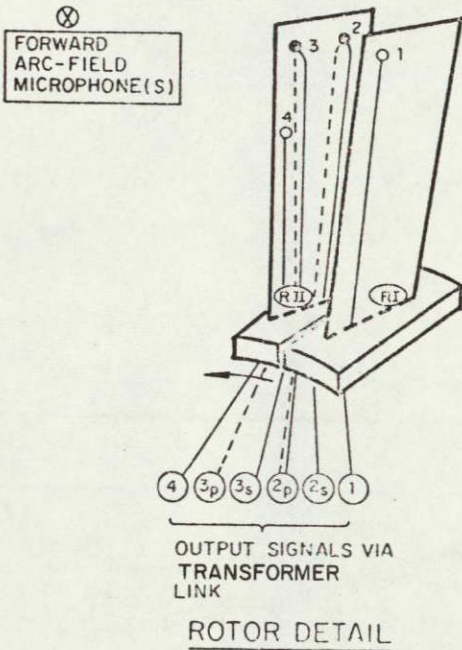
FIG. 4.   SCHEMATIC SUMMARIZING FAN INSTRUMENTATION.
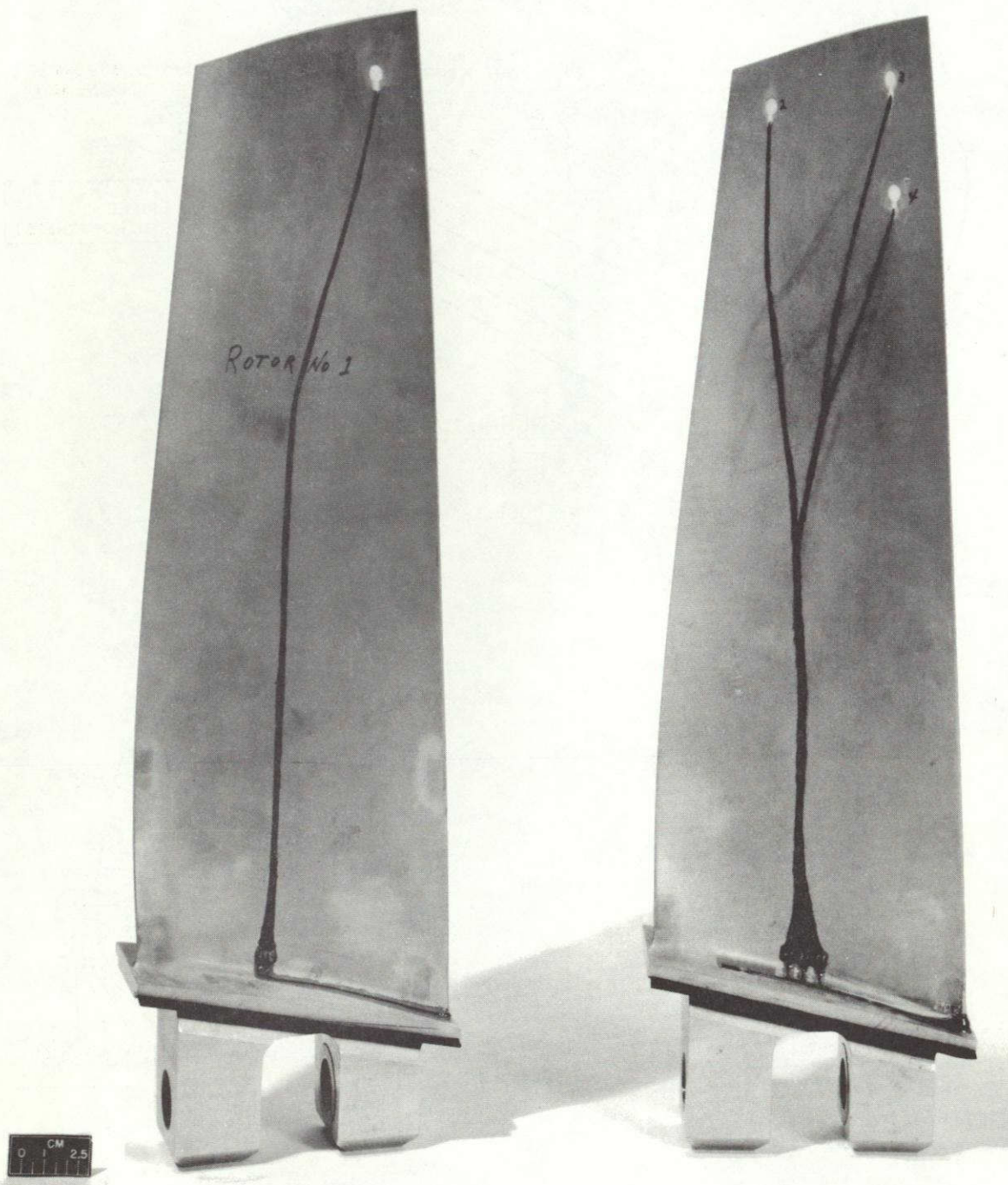
FIG. 5a.  SENSORS INSTALLED IN ROTOR BLADES.
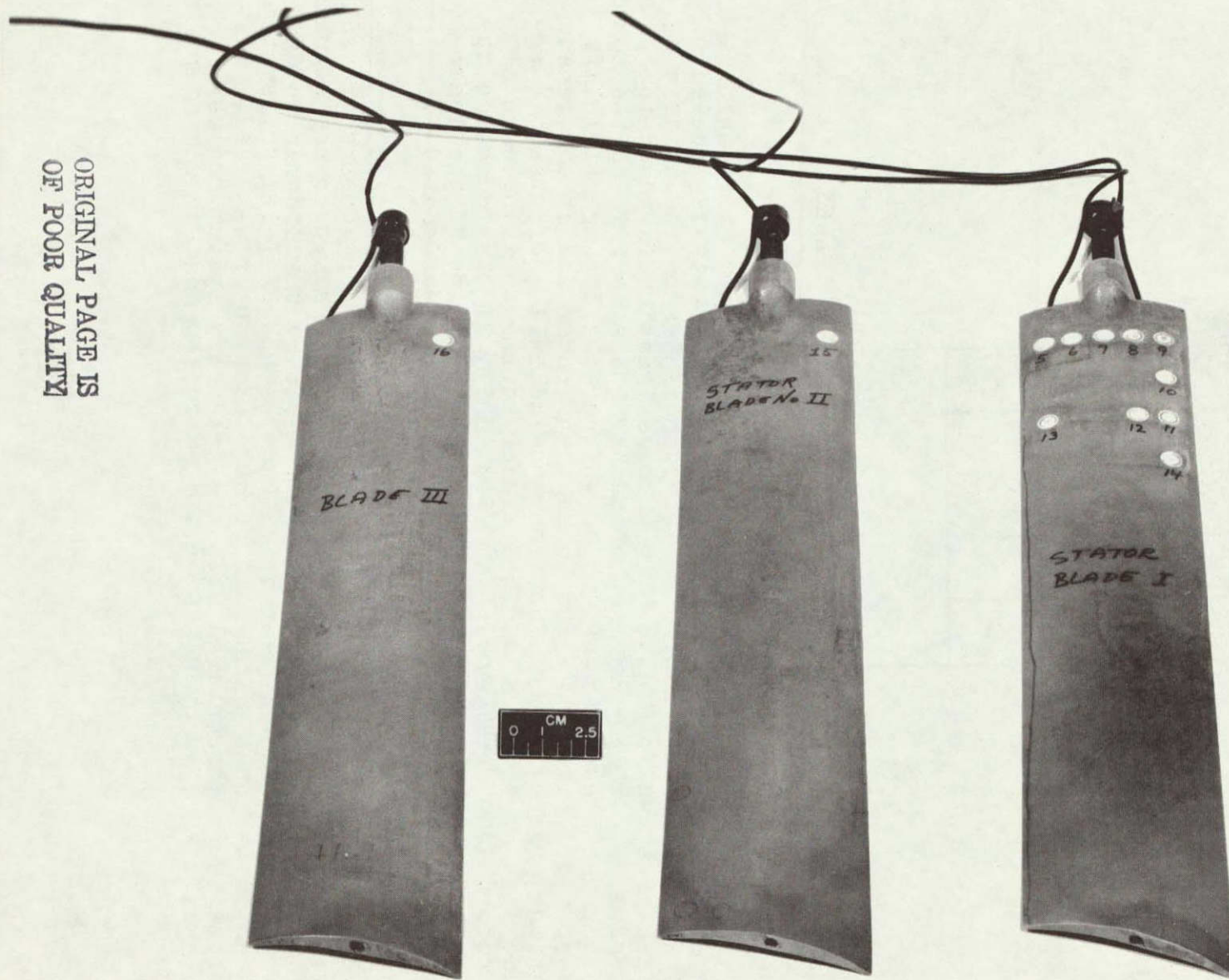
FIG. 5b.   SENSORS INSTALLED IN STATOR BLADES.
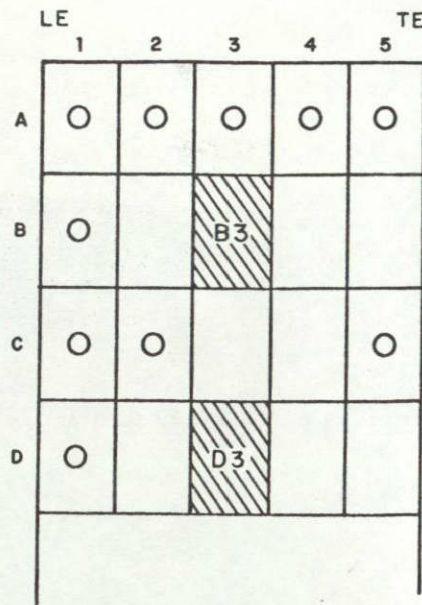
FIG. 6.   DEFINITION OF BLADE SURFACE SPACES.

The location of a specific sensor is defined by identifica-
tion of the rotor blade or stator vane on which it is located,
followed by the designation of its coordinates on the blade sur-
face space shown in Fig. 6.   To this designation is added the
letters s, p, or $\ell$ depending on whether the sensor is on the suction
surface, the pressure surface, or whether the differential lift
is computed.   Figures 7a and 7b show the rotor and stator sensor
locations, respectively.   For instance RII/A5$\ell$ indicates the un-
steady lift of the double-sided sensor at the trailing edge of
the rotor blade designated RII.   Similarly, SI/DIs indicates the
unsteady pressure measurement on the suction side of the inner-
most sensor on the leading edge of the stator designated SI.

The stator output signal lines were hard-wired through the
fan casing.   Acquiring the signals from the rotor sensors proved
to be more difficult.   In the front drive installation the signals
were transmitted through a Himmelstein rotary transformer in the
fan tail cone.   In the rear drive case, a BBN FM Telemetry system
mounted in the nose spinner in front of the rotor was used.   Dif-
ficulties were encountered with the telemetry system and very
little data were recovered from the rotor sensors for the rear
drive case.

10

LE        TE        LE        TE

RⅡ        RI

⊕ DOUBLE SIDED SENSOR
○ SINGLE SIDED SENSOR

(a) Rotor Blade Instrumentation

DIRECTION OF ROTOR ROTATION

TE    LE

SⅢ             SⅡ    SI

● DOUBLE SIDED SENSOR, OR TWO SINGLE SIDED SENSORS
○ SINGLE SIDED SENSOR
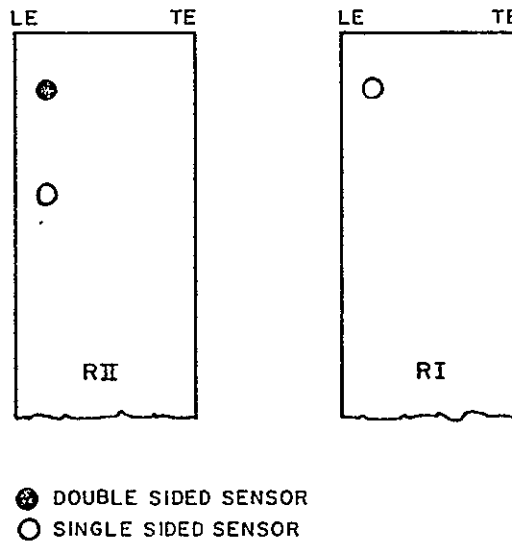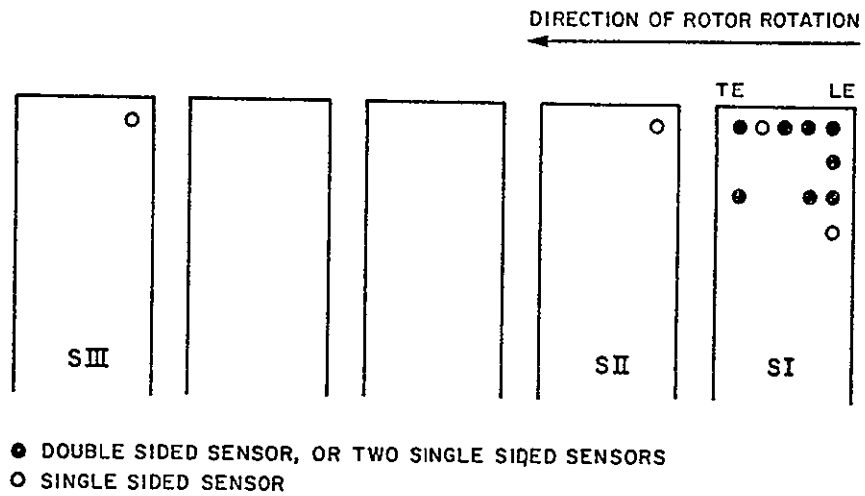
(b) Stator Blade Instrumentation

FIG. 7.  BLADE AND VANE INSTRUMENTATION.

The experiment was conducted and the data acquired by NASA personnel using the facilities and equipment available at NASA Lewis. Measurements were taken for two test cases:

    Case 1: Front drive, no wind.

    Case 2: Rear drive, no wind.

For each case, measurements were made at four speeds: 60%, 70%, 80% and 90% of design speed. (Therefore the rotor tip speed was always subsonic.) The data analysis and interpretation in this report concerns both Cases 1 and 2, primarily for the 80% speed case.

## DATA ANALYSIS AND INTERPRETATION

### Introductory Comments

The data analysis and interpretation effort was undertaken with three particular objectives. The first was to determine the unsteady pressure levels on the rotor blades and stator vanes. and in the far field. These levels were used to investigate the relationship between blade and vane surface pressures and far field noise using a fan noise prediction method. The prediction method is discussed in the next chapter.

The second objective was to study the statistical character-istics of tones in the surface pressure and fan noise spectra. Such a study not only increases the understanding of noise generating mechanisms, but it may ultimately aid in the develop-ment of more advanced fan noise prediction methods which include the statistical characteristics of these mechanisms. The study is also of interest since certain fan noise sources which are encountered in static tests, such as noise produced by inflow distortions, may not be as important under flight conditions. There may be identifiable differences in the characteristics of tones produced by different sources.

The third objective was to learn more about the rotor wake structure and its interaction geometry with the stator vanes. This information can form an important input to more refined fan noise models. Unfortunately, problems with spurious phase shifts in the data somewhat limited progress in this area. The data analyses directed towards this objective are discussed in the final section of this chapter. Some aspects of the rotor-wake/stator-blade interaction problem and its importance to the noise generation process are discussed in the next chapter.

The major analyses performed, which are discussed in the subsequent sections of the chapter, are as follows:

- Power (auto) spectral density analysis,
- Very narrowband spectral analysis,
- Narrowband probability density analysis,
- Time history studies,
- Calculation of coherence functions,
- Studies of time and phase delays between sensors.

In addition, broadband auto- and cross-correlations and cross-spectra were computed, but, for reasons to be discussed, this data proved to be less useful and therefore does not receive much attention. A background reference for these types of data analysis is the textbook by Bendat and Piersol (1971).

It is worthwhile to discuss briefly the types of pressure signals encountered at different sensor locations. The far field noise spectra are characterized by a series of discrete tones rising above a broadband distribution. Intense tones occur at blade passage frequency and its harmonics; tones having lower levels occur at shaft frequency and its harmonics. The tones at blade passage frequency and its harmonics are generated primarily by the following effects:

- Gutin sound associated with the rotating rotor potential field (not a major source for a subsonic rotor with many blades),.
- The interaction of the stator vanes with the rotor blade wakes.
- The interaction of the rotor blades with inlet flow distortions.

It should be noted that on the QF-1B installation, the rotor-wake/stator-blade interaction is subject to duct mode cut-off at the fundamental blade passage frequency. Thus, the far field noise at the fundamental blade passage frequency is due primarily to the interaction of the rotor blades with inlet flow distortions.

Sound at rotor shaft rotation frequency and harmonics occurs due to small asymmetries in the rotor construction and the resulting variations in aerodynamic behavior. These asymmetries may arise, for instance, as the result of blade-to-blade manufacturing differences in camber thickness, and setting angle. These variations modulate the sound sources mentioned above.

The unsteady pressures measured on the rotor and stator are the result of local aerodynamic processes which act as sound sources, rather than being the actual acoustic pressures themselves. In other words, these pressures are associated with the unsteady *aerodynamic* response of the blades and vanes, which are not, by any means, converted entirely to acoustic pressures in the far field. The pressures measured in the fixed stator blades, due primarily to interaction with the rotor wakes, occur at the same frequency as the sound they ultimately produce. Unsteady pressure peaks on the stator blade sensors occur at blade passage frequency and its harmonics and (at lower intensity) at shaft frequency and its harmonics. However, pressures measured on the rotating rotor blades do not generally produce sound at the same

14

frequency as the measurement frequency. As an example, suppose the rotor is subjected to a steady inlet flow distortion. A pressure sensor in the rotor surveys this distortion once per shaft revolution. The harmonics of shaft frequency reflect the detailed circumferential structure of the distortion. If all the rotor blades were exactly identical, then tones would be produced only at blade passage frequency and its harmonics, even though the source of this noise occurs at harmonics of shaft speed when sensed traveling with the rotor. Notice, furthermore, that there is no direct relation between the pressure signals measured on the rotor at shaft speed and its harmonics and those measured on the stator or in the far field at these same frequencies.

A number of practical difficulties arose during the data analysis and these should now be mentioned. Some of these problems will receive further discussion later in the chapter.

Four of the blade pressure transducers did not function during the experiment. All four were on one side of a suction-pressure combination and, hence, eliminated four potential lift measurements. A fifth lift measurement was lost because one channel malfunctioned on the recording of a suction-pressure combination, although the suction and pressure signals in question were individually retrieved on other recorders. A summary of the data which were retrieved and analyzed is presented in Table 2. Note that beyond the dead channels indicated in Table 2, a number of additional transducer channels produced signals with obvious anomalies. Nevertheless, all channels producing measurable signals were analyzed.

Another difficulty encountered was mechanical vibration of the stator vanes which produced extraneous tonal peaks in the stator pressure sensor data. These tonal peaks occurred at frequencies which were essentially independent of speed (see Fig. 8 in the next section). A detailed investigation of the characteristics of the peaks has provided strong evidence that (at least) most of them are due to blade vibration. This evidence may be summarized as follows:

    (a) The phase shift between different points on the stator at the frequencies of these peaks appears to be either zero or 180°.

    (b) The energy at these frequencies does not appear to propagate, since it is not evident in the far field data.

TABLE 2.  SUMMARY OF DATA CHANNELS FOR QF-1B BLADE PRESSURE
DATA (Case 1-80% rpm).

| Blade | Location | Suction | Pressure | Lift |
|---|---|---|---|---|
| Rotor I | A1 | yes[†] | no* | no |
| Rotor II | A1 | yes | yes[†] | yes |
| | C1 | yes | no* | no |
| Stator I | A1 | yes | dead | no |
| | A2 | dead | yes | no |
| | A3 | dead | yes | no |
| | A4 | yes | no* | no |
| | A5 | yes | yes | yes |
| | B1 | yes[†] | yes | yes |
| | C1 | yes | yes | yes |
| | C2 | yes | yes | no |
| | C5 | yes | yes | yes |
| | D1 | yes | no* | no |
| Stator II | A1 | yes | no* | no |
| Stator III | A1 | yes | no* | no |

*No transducer installed.

[†]The data analysis suggested anomalies in the data from these
transducer channels.

16

(c) The amplitude characteristics of the indicated pressures at these frequencies is strongly Gaussian, as one would expect for a normal mode response to random excitation.

(d) The normal mode frequencies of the stator blade, as subsequently calculated by LeRC in both bending and torsion, agree reasonably well with the frequencies for most of the observed spectral peaks in the data.

The value of the stator vanes pressure data was somewhat compromised by the apparent sensitivity of the stator vane pressure transducers to vibration. In particular, the vibration-induced signals make it difficult or impossible to determine the wave form of the wakes striking the stator blades. They further eliminate the possibility of obtaining useful information through broadband correlation analysis of the stator blade data. On the other hand, once the suspect spectral peaks were identified as spurious, specialized analysis techniques were formulated which might yield much of the desired information.

Beyond the vibration problem, there was another difficulty which limited the usefulness of certain types of data provided by correlation analysis procedures. Specifically, at least some of the data channels apparently suffered from spurious phase shifts in the data acquisition system. This problem is discussed in the final section of this chapter.

Calculation of Surface Pressure and Far Field Noise Spectra

Autospectra were computed for the Case 1 data at 80% speed and for the Case 2 data at all four speeds. This portion of the data reduction was done primarily by NASA personnel using the facilities at NASA Lewis.

Figure 8 shows typical autospectra taken from the stator data. The spectra clearly show the blade passage frequency and harmonics and the spurious peaks due to vane vibration. The broadband levels tend to be higher on the suction side of the blade.

Figure 9 shows typical autospectra for sensors on the rotor. The substantial low frequency roll-off beginning around 500 Hz is due to the low frequency behavior of the rotary transformer (magnetic coupling) which was used to retrieve the signal from the rotating blades. The low frequency values were corrected
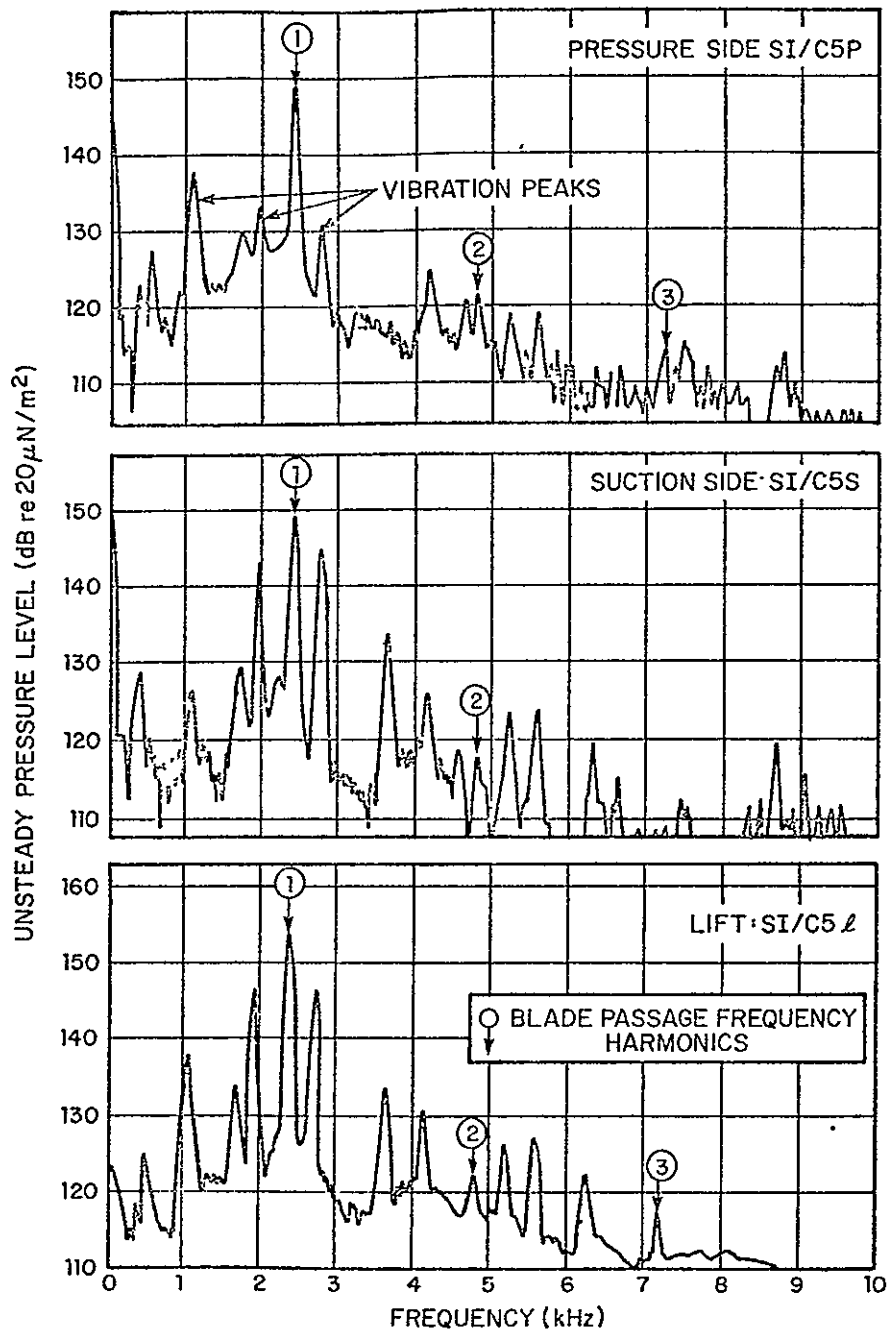
FIG. 8. TYPICAL AUTOSPECTRA OF STATOR BLADE SENSOR SIGNALS.

18
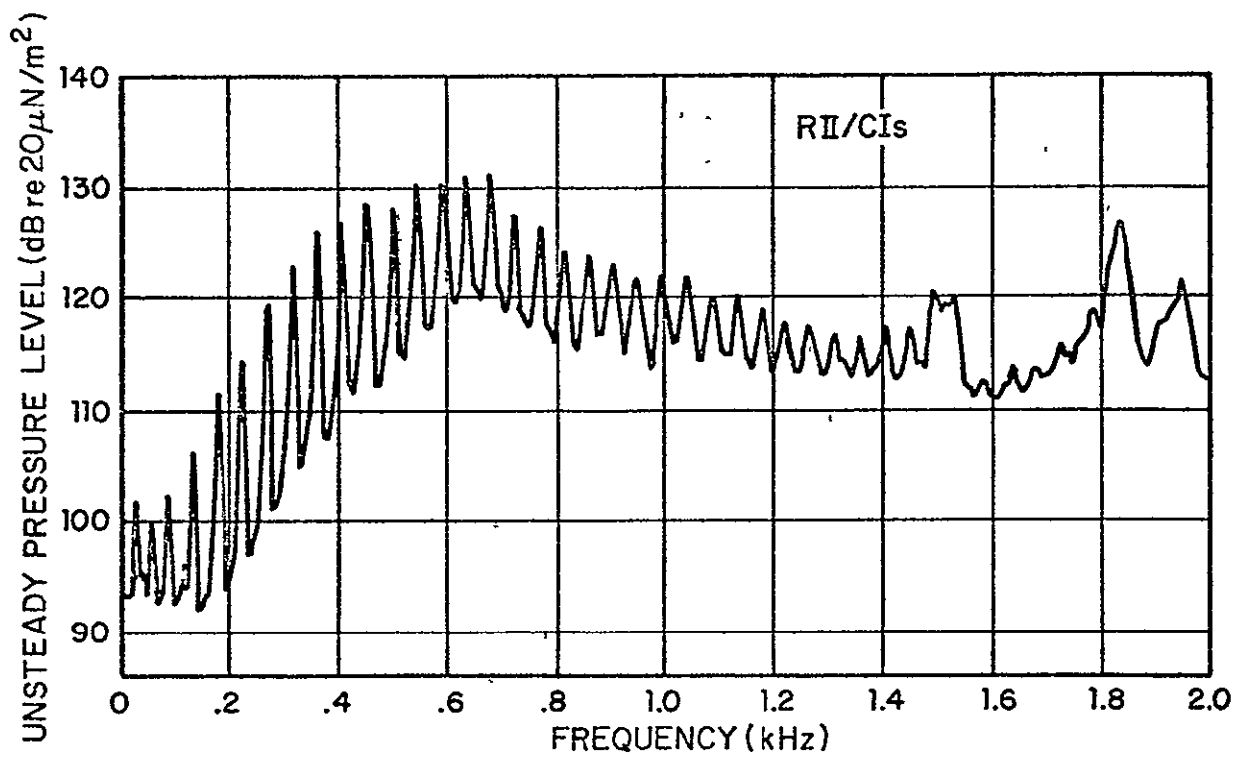
a) Autospectrum to 2kHz
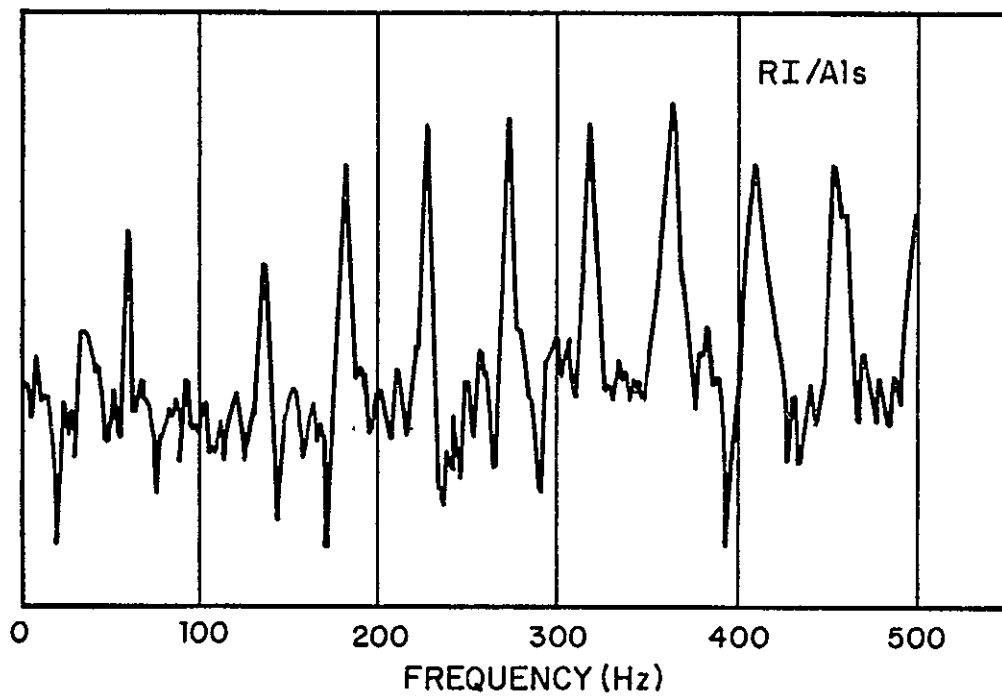


b) Autospectrum to 500 Hz

FIG. 9. TYPICAL AUTOSPECTRA FOR ROTOR SENSORS

19
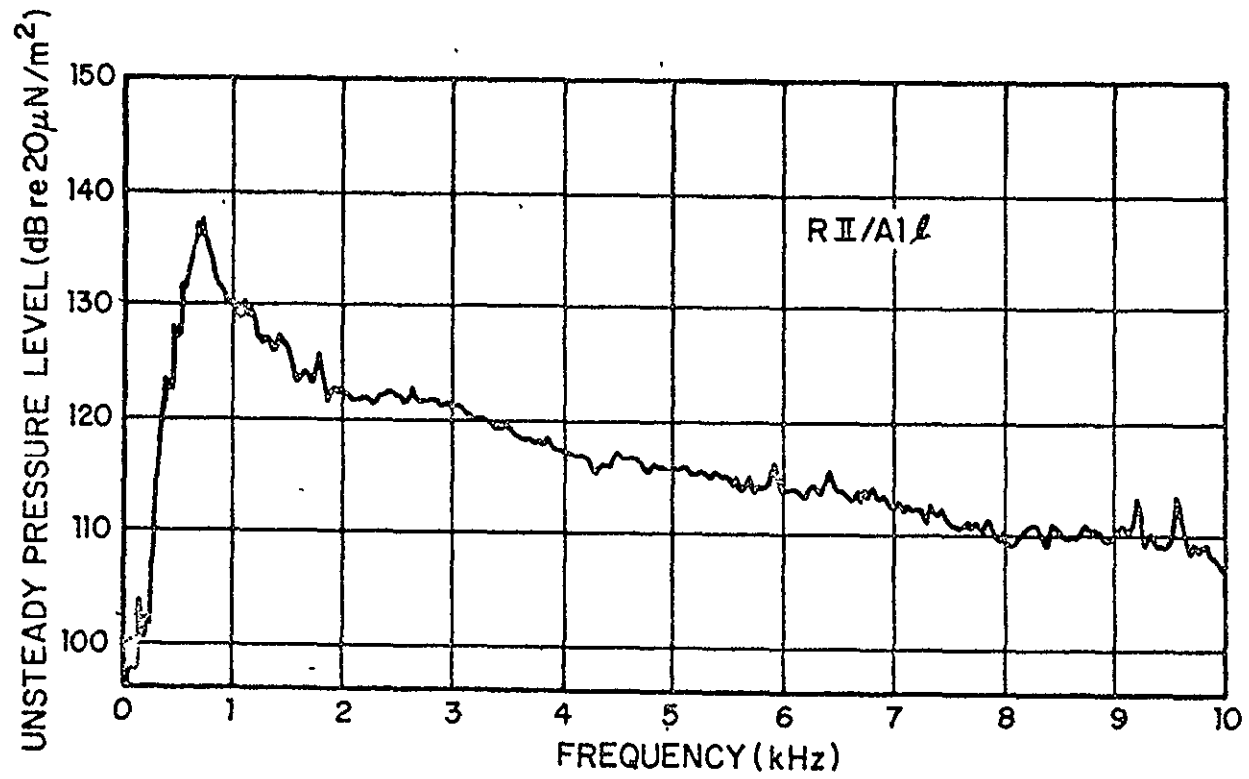
c)  Autospectrum to 10 kHz

FIG. 9.  TYPICAL AUTOSPECTRA FOR ROTOR SENSORS

using the calibration factor for the data retrieval system presented in Fig. 9b. As expected, discrete peaks from very many shaft harmonics can be seen. The rotor data appear to be free from any problem associated with blade vibration.

Figure 10 shows typical autospectra from the far field data. Although blade passage frequency and its harmonics are clearly evident, the vibration-related spikes seen in the stator data are not present.

Table 3 summarizes the frequency of the blade passage tones measured in the Case 1 and Case 2 data. Table 4 presents the rms values for both the overall and the blade passage components at all locations on the stator, and the overall rms level on the rotor (blade passage frequency does not have the same importance on the rotor due to the different frame of reference).

Table A.1 summarizes the stator and far field tone levels for blade passage frequency and its harmonics for Case 1 at 80% speed and Case 2 at all four speeds. Because of its considerable length, Table A.1 has been placed in the Appendix. Referring to the stator blade pressure data in Table A.1, the Case 1 data at 80% rpm are reasonably consistent with the Case 2 data, except for a few cases which may be due to a calibration problem. On balance, the Case 1 stator blade pressures appear to be somewhat higher than the corresponding Case 2 data. On the other hand, the Case 2 far field noise levels appear to be higher than for the Case 1 data at all locations. This surprising result may eventually be resolved by future experiments at NASA Lewis.
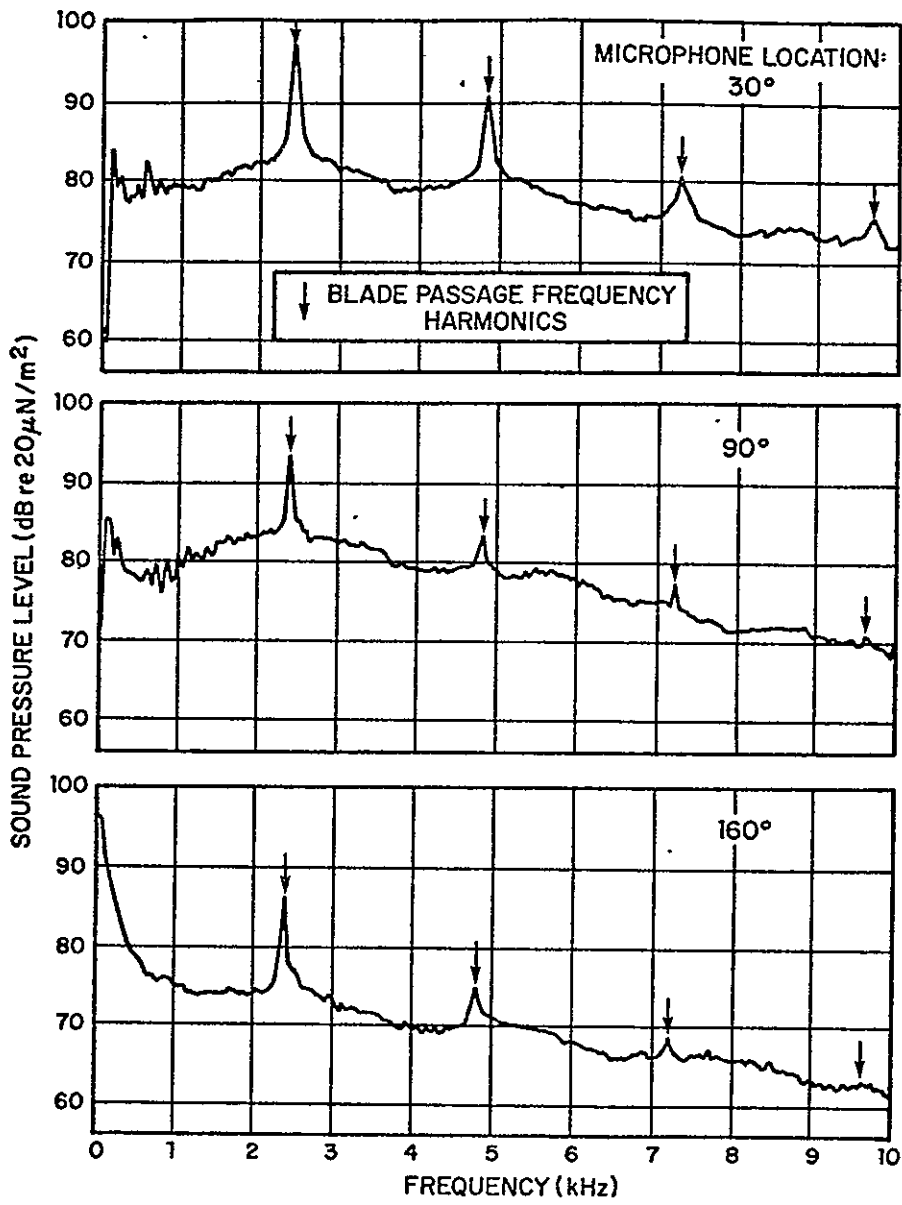
(a)  Spectra to 10 kHz Showing Blade Passage Harmonics

FIG. 10.  TYPICAL FAR FIELD NOISE SPECTRA
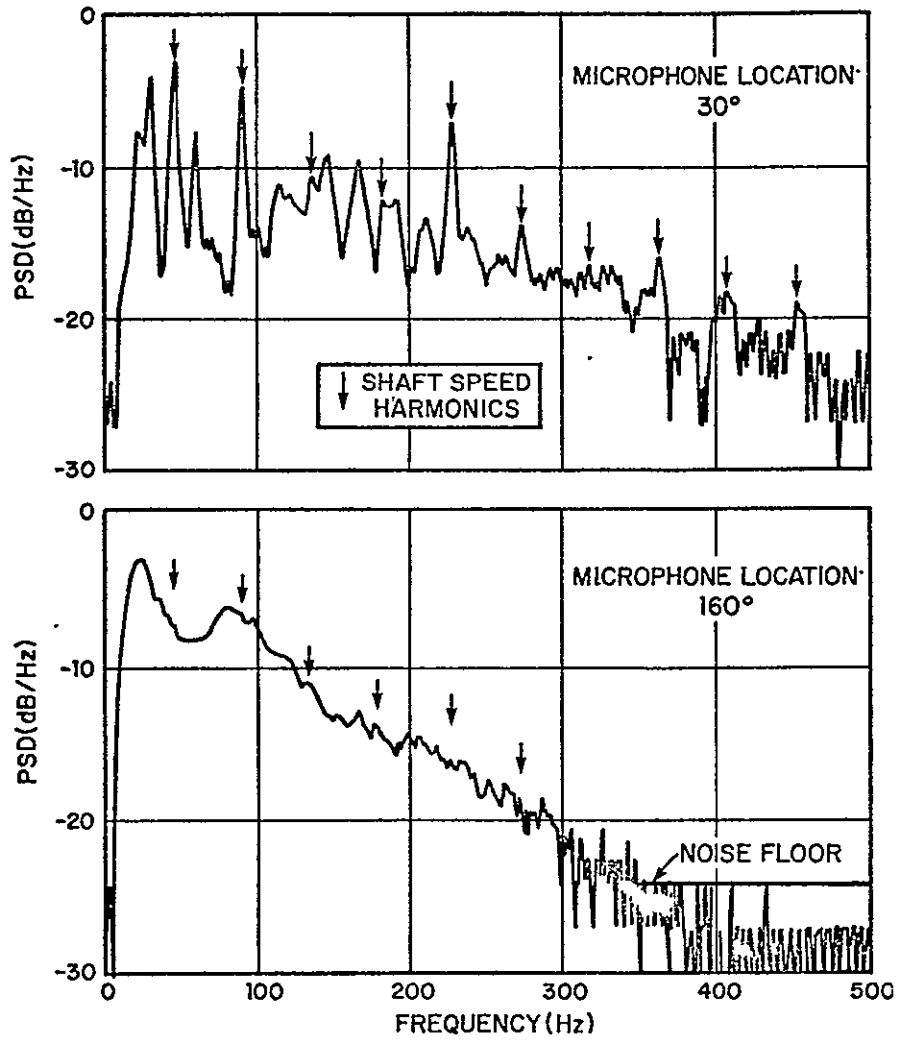
(b) Spectra to 500 Hz Showing Shaft Speed
Harmonics

FIG. 10. Cont'd

TABLE 3. SUMMARY OF FREQUENCIES FOR BLADE PASSAGE TONES.

| Case No. | rpm (%) | Frequency of Tone in Hz | | | |
|---|---|---|---|---|---|
| | | 1st tone | 2nd tone | 3rd tone | 4th tone |
| 2 | 60 | 1860 | 3720 | 5580 | 7440 |
| 2 | 70 | 2170 | 4340 | 6510 | 8680 |
| 2 | 80 | 2480 | 4960 | 7440 | 9920 |
| 1 | 80 | 2410 | 4820 | 7230 | 9640 |
| 2 | 90 | 2790 | 5580 | 8370 | 11160 |

TABLE 4. SUMMARY OF BLADE PRESSURE RMS VALUES FOR CASE 1, 80% SPEED.

| Blade | Location | rms Value of Blade Pressure in dB | | | | | |
|---|---|---|---|---|---|---|---|
| | | Pressure Side | | Suction Side | | Lift | |
| | | Overall | 2.4 kHz | Overall | 2.4 kHz | Overall | 2.4 kHz |
| Rotor I | A1 | – | – | 134* | – | – | – |
| Rotor II | A1 | 141 | – | 156 | – | 155 | – |
| | C1 | – | – | 168 | – | – | – |
| Stator I | A1 | – | – | 162 | 143 | – | – |
| | A2 | 160 | 152 | – | – | – | – |
| | A3 | 157 | 153 | – | – | – | – |
| | A4 | – | – | 161 | 152 | – | – |
| | A5 | 156 | 152 | 158 | 149 | 160 | 155 |
| | B1 | 158 | 154 | 173* | 161* | 175* | 165* |
| | C1 | 159 | 153 | 162 | 156 | 164 | 157 |
| | C2 | 158 | 152 | – | – | – | – |
| | C5 | 157 | 151 | 160 | 153 | 163 | 156 |
| | D1 | – | – | 162 | 146 | – | – |
| Stator II | A1 | – | – | 158 | 145 | – | – |
| Stator III | A1 | – | – | 157 | 147 | – | – |

*Suction side transducer believed to have a calibration problem.

24

## Evaluation of the Characteristics of Blade
## Passage Frequency and Rotor Speed Tones

This section presents the results of an investigation of blade passage frequency and rotor speed tones for the rotor and stator surface pressures, and for the far field noise signature. Understanding the characteristics and structure of these tones gives insight into the nature of basic fan noise mechanisms. In addition, information is provided which may be useful in the future development of theoretical fan noise models which include the statistical characteristics of the noise generating process.

For Case 1 of the QF-1B fan noise experiment, the fan was driven from the front, meaning there was considerable structure forward of the inlet. This structure is believed to have been responsible for a degree of inlet distortion, hereafter referred to as the "steady" inlet distortion. Very likely there is a certain amount of flow turbulence associated with this distortion. Beyond these effects, there is also the possibility of an environmentally induced distortion due to such factors as atmospheric turbulence and wind gusts. Hanson (1974) has suggested that atmospheric eddies that are sucked into a fan during static tests produce significant inflow distortion. The large scale eddies are elongated and intensified (by vortex stretching) as the flow is pulled into the fan. Because the stretched eddies may be very many fan diameters in length, these disturbances may produce quasi-periodic tones at blade passage frequency and its harmonics.

In either case, the distortions should appear in the rotor sensor data as sharply defined components at the rotational frequency of the rotor and its harmonics. However, there should be a subtle but important difference between the two types of distortion in that the steady distortion would be expected to appear as a true periodic component, while the environmentally induced distortion would probably be time varying in character. The environmentally induced distortion should appear more like narrowband noise than a true periodic component.

If the above thesis is accepted, it follows that a distinction might be made between the contributions of steady and environmentally induced flow distortions to the fan noise by a careful study of the probability structure of the fluctuating pressures on the rotor blades which occur at the rotor speed and its harmonics.

Also, of considerable interest is the probability structure of tones at blade passage frequency and its harmonics which appear on the stator vanes and in the far field noise levels. As mentioned earlier, the rotor-wake/stator-vane interaction tone is subject to duct mode cut-off at the fundamental blade passage frequency. Therefore, the far field noise at this frequency must be due entirely to the interaction of the rotor with inflow distortions. The far field tones at the harmonics of blade passage frequency will be due to both inflow distortions and rotor-wake/stator-vane interaction. Analysis of blade passage tones on the stator vane surfaces will provide information about the rotor wake structure. Also of interest is the probability structure of the rotor speed tones which appear on the stator in the far field noise levels.

The data discussed in the following sections were taken from Case 1 at 80% speed. Some of the same analyses were performed as Case 2 data and the same general conclusions were reached. Unfortunately, the rotor blade data could not be compared for the two cases since there was no reliable rotor blade data for Case 2.

## Investigation of Techniques

There are a number of possible procedures which might be used to separate the periodic and random portions of a narrow-band waveform. Those considered for this study include (a) narrowband spectrum analysis, (b) narrowband signal enhancement, (c) narrowband correlation analysis, and (d) narrowband probability density analysis. The last of these possibilities was chosen, but some discussion of the others is in order.

*Narrowband Spectrum Analysis.* The autospectrum of a sine wave is theoretically a delta function, while the autospectrum of narrowband noise will have both a finite density and bandwidth. It then follows theoretically that one should be able to distinguish between the two situations by performing a spectral analysis with a sufficiently narrow resolution bandwidth. Such a procedure was attempted on the QF-1B fan noise data with negative results. The problem is that the rotor speed is not perfectly constant; it varies during any given run by about 0.4%. Hence, even a steady distortion will cause tones which appear to have finite density and bandwidth.

The above fact is illustrated in Fig. 11 which shows the spectrum of a rotor speed signal along with the spectrum of a blade passage tone as seen on stator blade I at location C3. In both cases, the spectrum analysis was performed using a resolution
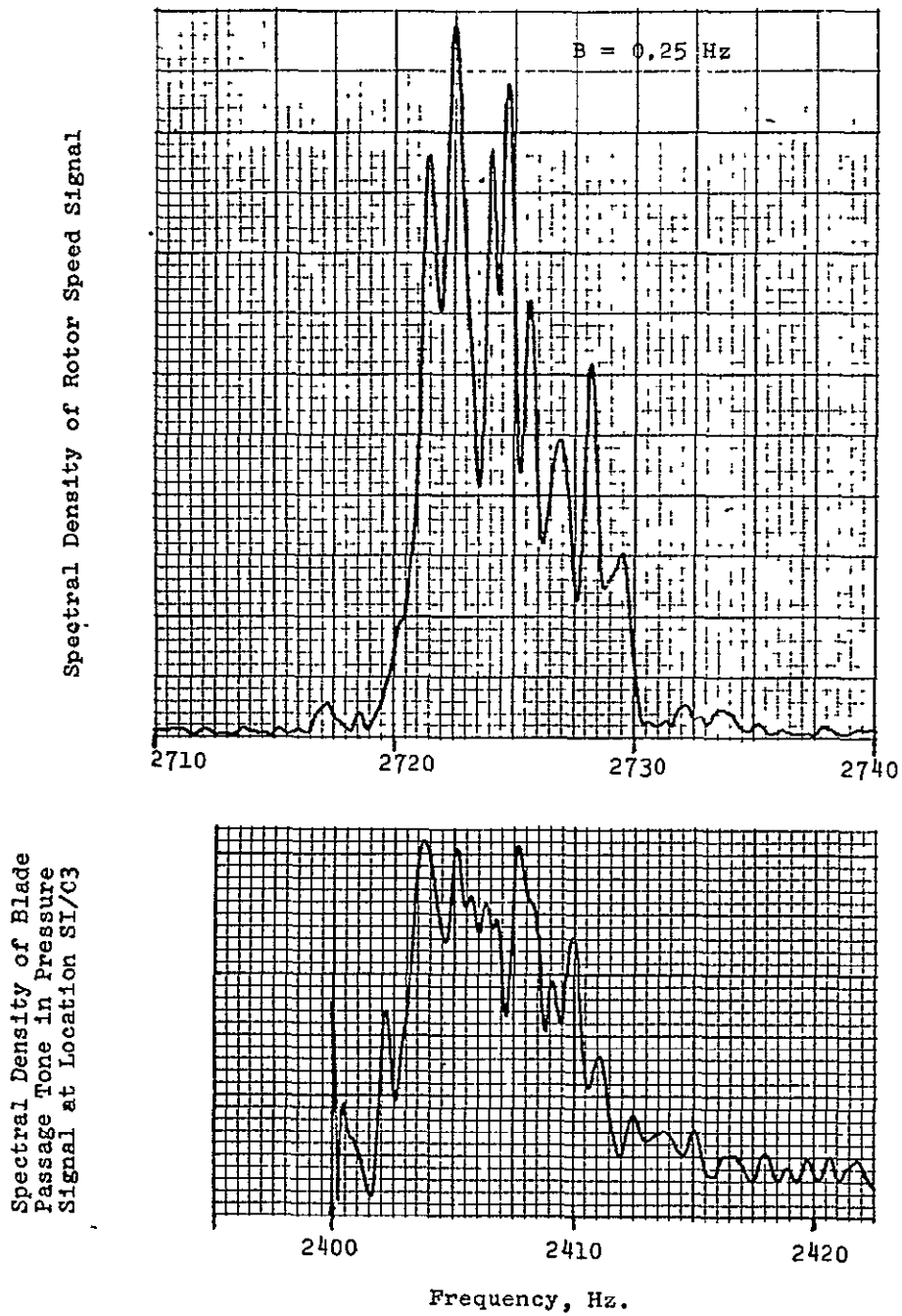
FIG. 11. COMPARISON OF BLADE PASSAGE TONE AND ROTOR
SPEED SIGNAL BANDWIDTHS.

bandwidth of B = 0.25 Hz.* Although the frequencies of the speed
signal and blade passage tones are slightly different, it is
clear from Fig. 11 that the bandwidths of the two signals are
similar on a percentage basis; i.e., both signals have a band-
width of about 0.4% of center frequency. It should be mentioned
that this bandwidth might be due to time base errors in the
recording and/or playback of the data, particularly since a dub-
bing operation was involved in the analysis. No calibration
signals were inserted on the original tapes during the experiment,
so the net time base errors in the recording, dubbing, and play-
back operation could not be checked. However, the time base
errors for tape recorders of the type involved in the analysis
are characteristically on the order of 0.25%. In any case, it
makes little difference what the source of the indicated speed
variations might be, since speed variations of any type restrict
the effectiveness of narrowband spectrum analysis as a technique
for distinguishing between narrowband noise and sine waves.

*Narrowband Signal Enhancement*. A common technique for ex-
tracting deterministic components, such as sine waves, from a
stochastic background is to collect repeated samples of the data
on a common time base, and average the data at specific times
over the resulting ensemble of records. Such a procedure was
given a preliminary investigation by capturing repeated samples
of selected data signals and displaying them on a scope. How-
ever, the final average of the repeated samples would have re-
quired some special computer programming which was not undertaken
because it was felt that other data analysis techniques would
provide the same information more easily.

*Narrowband Correlation Analysis*. If a narrowband signal
includes both a sine wave and a stochastic component, then the
envelope of the autocorrelation function should decay from a
value equal to the total mean square value of the signal at zero
time delay to a value equal to the mean square value of the sine
wave alone at long time delays. The problem with this procedure
for the current study is that the rotor speed was not perfectly
constant. Hence, even steady distortion will appear as frequency
modulated tones. The autocorrelation function for a frequency
modulated sine wave tends to decay, particularly when the modu-
lation frequency is low as it appears to be in the QF-1B fan
data. In spite of this problem, the narrowband correlation
technique was employed in some cases.

*Narrowband Probability Analysis*. This is the type of analy-
sis procedure used most extensively in this study. The theory
is based on the fact that a sine wave will cause a dished shaped

---

*The blade passage frequency is 53 times the shaft speed, whereas
 the speed signal occurs at a frequency corresponding to 60 times
 the shaft speed.

28

probability density function, while narrowband noise will be approximately Gaussian in character. The combination of the two will have a probability density function given by (Rice, 1954, page 105)

$$p(x) = \frac{1}{\pi \sigma_n \sqrt{2\pi}} \int_0^{\pi} \exp[-(x - \sqrt{2}\ \sigma_s \cos\theta)/2\sigma_n^2]d\theta \qquad (1)$$

where $\sigma_s$ in the rms value of the sine wave portion of $x(t)$ and $\sigma_n$ is the rms value of the noise portion. Typical plots of $p(x)$ for various ratios of $R = \sigma_s^2/\sigma_n^2$ are shown in Fig. 12. The relative contributions of a sine wave and noise portion of a signal can be identified by comparing the signal's probability density function to plots of the type shown in Fig. 12, assuming the noise portion of the signal is Gaussian.

The advantage of the above procedure is that variations in the frequency of the sine wave and/or noise do not alter the resulting probability density function. The disadvantage is that the probability density function is not very sensitive to changes in the signal-to-noise ratio in the regions $R < 1$ and $R > 10$.

## Data Analysis Procedures

All correlation and probability density functions were computed using a SAICOR SAI-43A analyzer. Spectral densities were calculated using the SAICOR correlator in conjunction with an SAI-470 Fourier Transform Analyzer. Specific spectral components of interest were isolated for detailed analysis by heterodyning the data signal past a crystal filter set with a 30 dB form factor of less than 1.5; i.e., the bandwidth of the filter at the 30 dB down points is less than 50% greater than the bandwidth at the 3 dB down points. The filter set included filters with nominal bandwidths of 5, 10, and 50 Hz. Other bandwidths could be achieved by using different data playback speeds. Finally, low pass filtering to suppress aliasing in the spectral analysis was achieved using a Khronhite filter with a 24 dB/octave cutoff.

One significant problem was encountered during the probability density analysis which effects the calibration accuracy of the resulting plots. Specifically, the calibration of the probability density analyzer is based upon the application of the
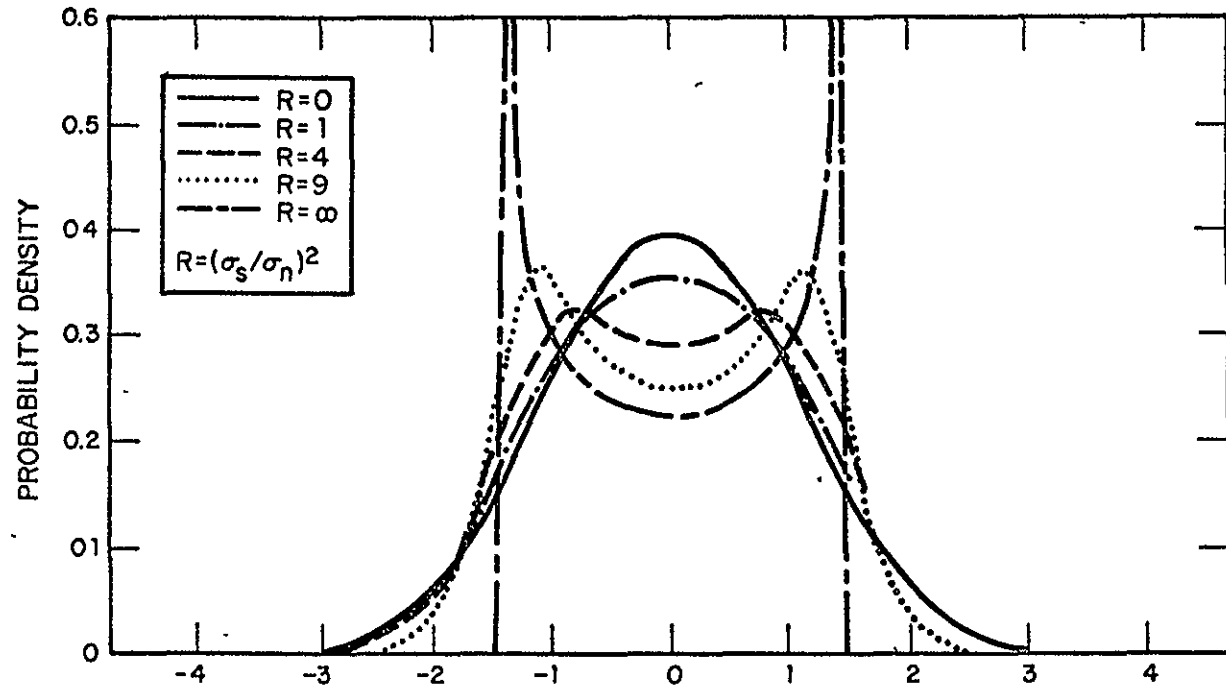
FIG. 12.   PROBABILITY DENSITY FUNCTIONS OF SINE WAVE IN GAUSSIAN NOISE.

data with a fixed rms value at the input to the analyzer. If the rms value of the data is different from the specified amount, both the amplitude (abscissa) and density (ordinate) scales will be in error. Every effort was made to maintain a constant input level during the analyses. However, many of the isolated tones selected for analysis varied in amplitude widely (over 10 dB in some cases) during the analysis period, making it difficult to accurately set the input level to the analyzer. Hence, the accuracy of the scaling on the probability density plots is rather poor in some cases.

For the purpose of this study, the above noted problem can be circumvented by evaluating the shape of the probability density function in terms of a ratio of the maximum probability density to the probability density at zero amplitude, hereafter referred to as the PDR. For signal (sine wave) to noise ratios of R>1.5, the PDR will be greater than unity, and will define the relative contributions of the sine wave and noise independent of the scale factors. Representative values of the PDR for different R values are presented in Table 5.

TABLE 5.  PDR VALUES FOR VARIOUS SIGNAL TO NOISE RATIOS

| $R=\sigma_s^2/\sigma_n^2$ | 1 | 2 | 3 | 4 | 6 | 8 | 12 | 16 | 24 | 32 | $\infty$ |
|---|---|---|---|---|---|---|---|---|---|---|---|
| PDR | 1 | 1.06 | 1.15 | 1.25 | 1.4 | 1.5 | 1.65 | 1.8 | 1.9 | 2.0 | $\infty$ |

Rotor Blade Pressure Data

Probability density functions for selected rotor speed tones in the rotor blade pressure data are presented in Fig. 13 and are summarized in Table 6. Note that the last three columns in this table are of 'primary interest. The column labelled "Measured PDR" is the ratio of the maximum density to the density at zero amplitude determined from the measured probability density plots. The column labelled "Corresponding R" is the approximate signal (sine wave) to noise ratio corresponding to the measured PDR, as determined from Table 1. In two cases where autocorrelation data are presented, the value in this column is the signal to noise ratio determined from the correlation plots. The final column labelled "R from PSD" presents an estimate for the signal to noise ratio as determined from low frequency spectral density data supplied by NASA. This value was computed by first correcting

31

TABLE 6.   SUMMARY OF ROTOR BLADE PRESSURE DATA.

| Blade No. | Loca-tion | Pressure, Súction, or Lift | Tone Freq.* | | Func-tion | Mea-sured PDR | Corres-ponding R | R from PSD |
|---|---|---|---|---|---|---|---|---|
| | | | Har-monic | Hz | | | | |
| RII | A1 | lift | | | | | | |
| | | | 1 | 45.3 | PDF | 1.4 | 6 | ** |
| | | | 1 | 45.3 | ACF | – | 4 | ** |
| | | | 2 | 90.6 | PDF | 1.2 | 3.5 | ** |
| | | | 2 | 90.6 | ACF | – | 2 | ** |
| | | | 10 | 453 | PDF | 1 | <1.5 | 125 |
| RII | A1 | pressure | | | | | | |
| | | | 1 | 45.3 | PDF | 1 | <1.5 | ** |
| | | | 5 | 226 | PDF | 1 | <1.5 | 24 |
| RII | A1 | suction | | | | | | |
| | | | 1 | 45.3 | PDF | 1.5 | 8 | 24 |
| | | | 5 | 226 | PDF | 1 | <1.5 | 78 |
| RII | C1 | suction | | | | | | |
| | | | 1 | 45.3 | PDF | 1.4 | 6 | 7 |
| | | | 2 | 90.6 | PDF | 1.13 | 3 | 3 |
| | | | 3 | 136 | PDF | 1 | <1.5 | 11 |
| | | | 5 | 226 | PDF | 1 | <1.5 | 14 |
| RI | A1 | suction | | | | | | |
| | | | 1 | 45.3 | PDF | 1 | <1.5 | 10 |
| | | | 5 | 226 | PDF | 1 | <1.5 | 30 |

*Isolated for analysis by 5 Hz wide bandpass filter.

**Spectral peak off scale or otherwise not apparent in data.
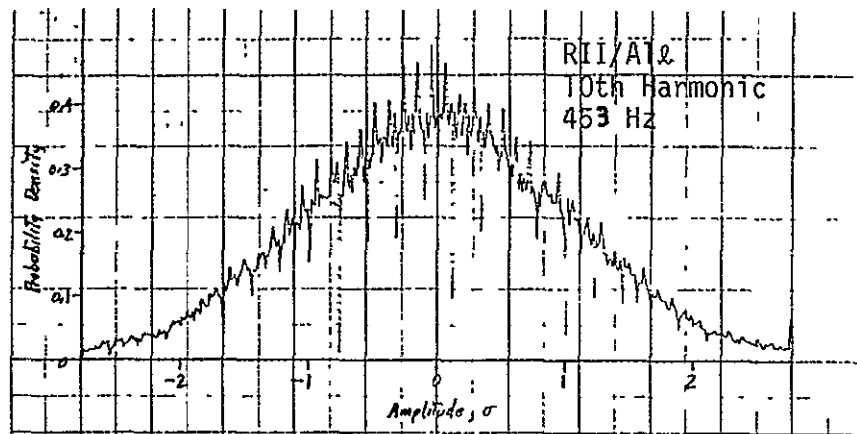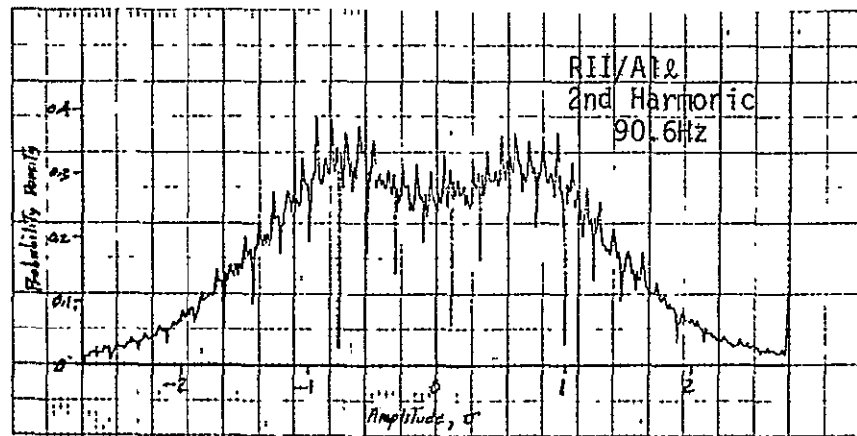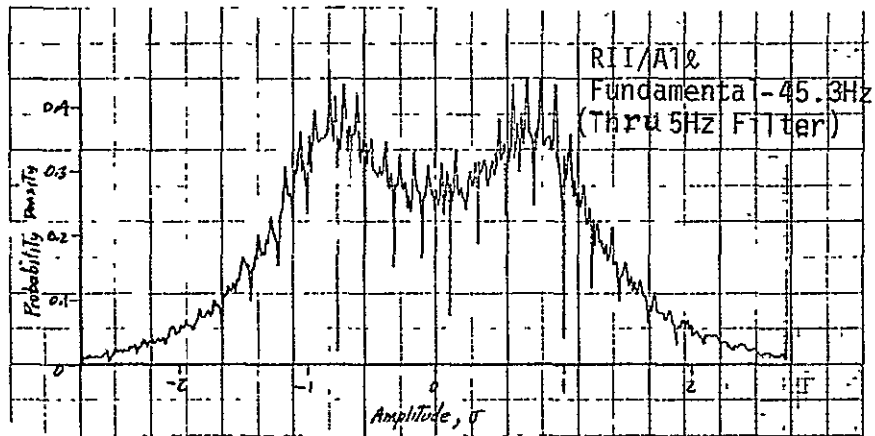
(a)  First, Second, and Tenth Harmonics for a Rotor
     Lift Measurement

FIG. 13.   PROBABILITY DENSITY FUNCTIONS OF SELECTED ROTOR
           SPEED TONES MEASURED ON THE ROTOR.
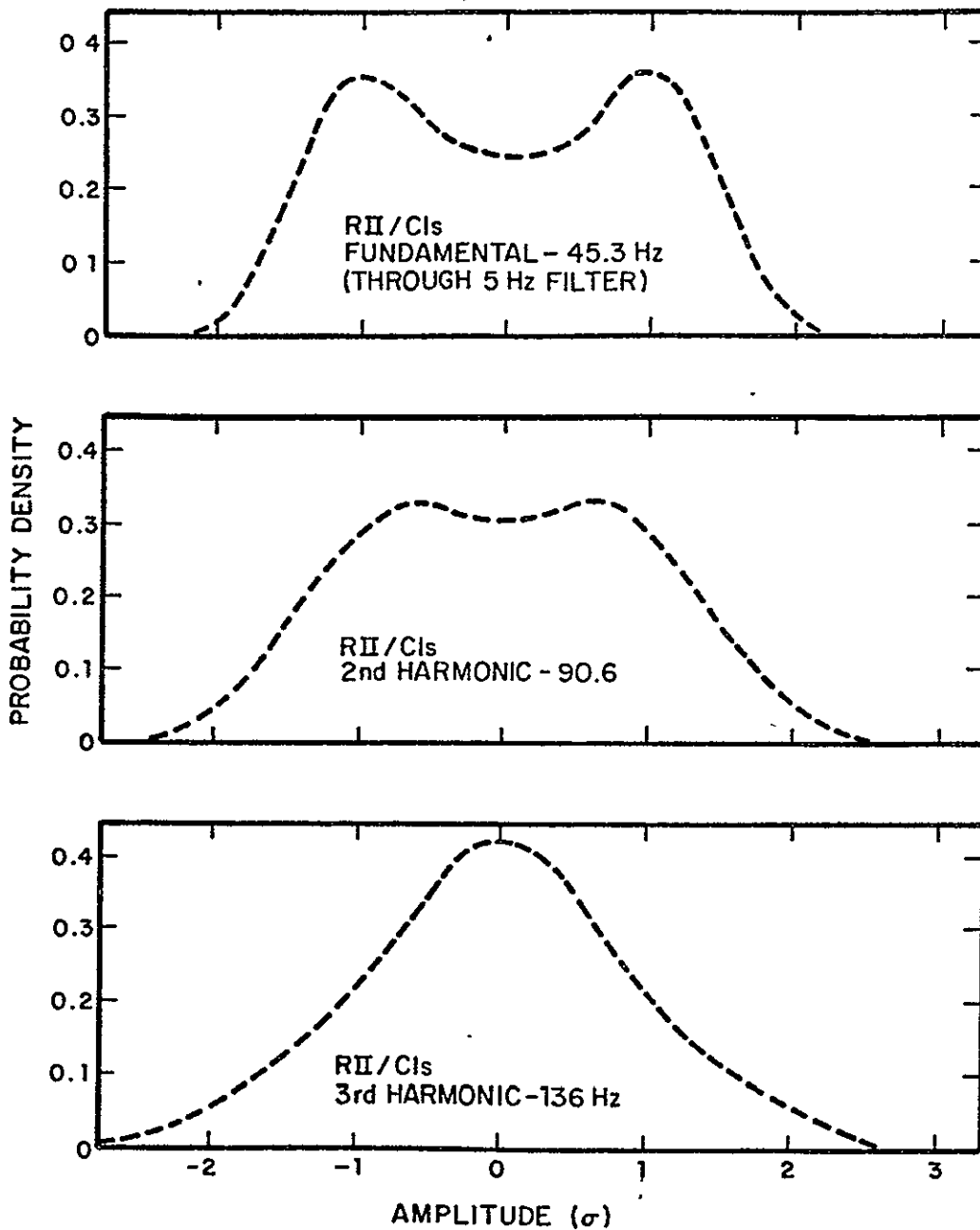
(b)   First, Second, and Third Harmonics for a Rotor Suction
      Side Measurement

FIG. 13.   Cont'd

an indicated spectral peak for the background random noise which would be passed by the 5 Hz filter used to isolate the peak, and then dividing by the same background noise level. In all cases, the background noise was estimated using the broadband spectral density levels on either side of the peak in question, as given by the zero to 2 kHz spectral data provided by NASA. Appropriate corrections were made to account for the 6 Hz noise bandwidth resolution inherent in the NASA data analysis system.

The "R from PSD" value discussed above represents, in effect, the signal to noise ratio of a given peak where the signal may be a sine wave, narrowband noise, or a combination of the two; i.e., any narrowband random noise at the blade passage frequency will add to the "R from PSD" value. On the other hand, the "R from PDF" value reflects only the influence of a sinusoidal component of the blade passage frequency; narrow band noise at the blade passage frequency adds to the noise, not the signal in the "R from PDF" value. Hence, a comparison of the two results can provide a measure of the relative contributions of sine and narrowband random components in any given peak.

Since the number of rotor sensors is very limited, the analysis of the signal from each sensor is discussed. Referring first to the lift data at location RII/A1 in Table 6, two important observations should be made. First, the probability density function (PDF) for the fundamental shaft frequency at 45.3 Hz dishes sharply, corresponding to a sine wave with a mean square value of about 6 times the mean square value of the random energy in a 5 Hz bandwidth about the tone. An autocorrelation function (ACF) plot of this same tone, however, suggests a somewhat lower signal-to-noise ratio of about 4. A similar discrepancy is seen in the signal-to-noise ratio indicated by the PDF and ACF plots for the second harmonic at 90.6 Hz. This discrepancy is probably indicative of the sensitivity of the autocorrelation function of a sine wave to slight variations in the sinusoidal frequency. As mentioned earlier, the correlation function of a frequency modulated sine wave will decay with increasing delay time, just as if noise were present. On the other hand, the probability density function is generally unaltered by frequency modulation. These results clearly demonstrate the superiority of PDF analysis over ACF analysis for the application at hand.

The second important result in the RII/Al lift data is the
lack of measurable sinusoidal character in the tones at har-
monics above the third, in spite of the fact that these higher
harmonics stand out strongly in the NASA spectral density.  This
lack of sinusoidal character is illustrated for the 10th harmonic
in Fig. 13.  These results suggest that although the fundamental
tone is quite periodic, the higher order tones are more stochas-
tic in character, becoming almost totally random at the higher
harmonics.

The individual pressure and suction side measurements at loca-
tion RII/Al is now considered.  The pressure side measurement re-
veals almost no sinusoidal character, even at the fundamental.  Re-
ferring back to Table 4, the pressure side measurement at this loca-
tion produced unusually low levels, raising suspicion about this mea-
surement.  The data in Table 6 tend to increase that suspicion.  This,
of course, raises doubts about the RII/Al lift measurement as well.

Referring now to the results for the suction side measure-
ment at location RII/Cl, the PDF data behave very much like the
data at location RII/Al.  Specifically, the indicated signal
to noise ratio is very strong at the fundamental (R=6) and
moderately strong at the second harmonic (R=3).  In both cases,
the signal to noise ratio is about the same as would be expected
for a pure sine wave in broadboard noise from the spectral data.
However, there is very little evidence of sinusoidal character
in the third harmonic and higher, in spite of relatively intense
spectral peaks at the higher harmonics.  These results again
suggest that the rotor frequency tones become increasingly sto-
chastic at the higher harmonics.

The suction data at location RI/Al shows no significant sinu-
soidal content.  As for the pressure data at RII/Al, this particular
measurement is suspect.  In spite of uncertainty about some of the
rotor data, there is a clear indication that only the first couple
of rotor speed harmonics have a dominant sinusoidal character as
would be expected for a steady inflow distortion.  These results sug-
gest that the inflow distortions to the rotor are strongly influ-
enced by disturbances having a stochastic character.


Stator Blade Pressure Data

Probability density functions of the first three rotor speed
tones in the stator blade pressure data are presented in Fig. 14.


36
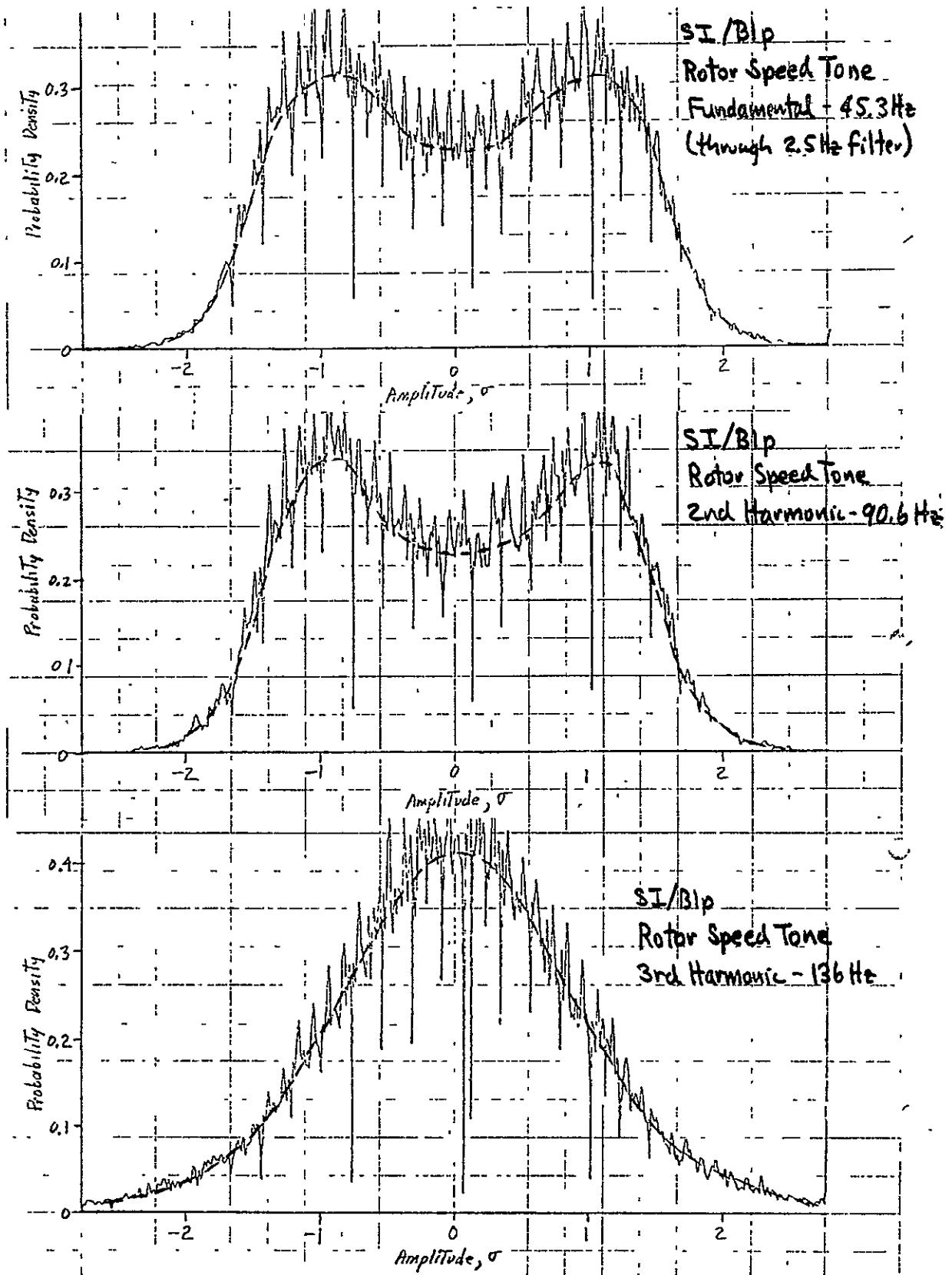
FIG. 14.   PROBABILITY DENSITY FUNCTIONS FOR THE FIRST THREE
           ROTOR SPEED HARMONICS MEASURED BY A STATOR PRESSURE
           SIDE SENSOR.

Probability density functions of the first two rotor blade passage tones are shown in Fig. 15. These data are summarized in Table 7. The interpretations of the last three columns of Table 7 are exactly the same as previously discussed for Table 6. The spectral data supplied by NASA were used to arrive at the "R from PDS" values in the last column for the data at blade passage frequencies. The low frequency spectral data needed to determine the "R from PSD" values at the rotor speed frequencies were computed at only one stator location where a good lift signal was measured.

Referring first to the rotor speed tones, the data presented in Table 7 are for only those locations where the rotor speed tones are most pronounced. At many of the A locations, for example, the PDF at the rotor speed fundamental revealed little or no sinusoidal content. On the other hand, the sinusoidal content is quite strong at the B and C locations, particularly in the pressure side measurements. For these measurements, the general trend is exactly the same as observed in the rotor blade data in the previous section; specifically, the sinusoidal content is very strong in the fundamental (almost 30 times the noise power in one case), moderately strong in the second harmonic (up to 10 times the noise power), and weak or negligible in the third harmonic and higher. (This is not to imply a relationship between rotor data and stator data at these frequencies; as mentioned earlier, these data are essentially physically unrelated.)

For the lift data at location SI/C5, a signal-to-noise ratio was estimated for the first two rotor speed tones from the auto-correlation function as well as the probability density function. At the fundamental, the values of R from the ACF and PDF are in close agreement. At the second harmonic, however, the ACF result is significantly less than the PDF result, exactly as observed in similar comparisons involving the rotor data. The reason for the discrepancy is probably the same as for the rotor data, specifically, rotor speed variations reduce the R value determined by the ACF but not by the PDF.

Now referring to the PDF data at the blade passage frequency and its harmonics, although the pressures at these frequencies appear as strong tones in the spectral data, they display very little sinusoidal content in the PDF results. The first and second blade passage tones at all stator locations were examined.
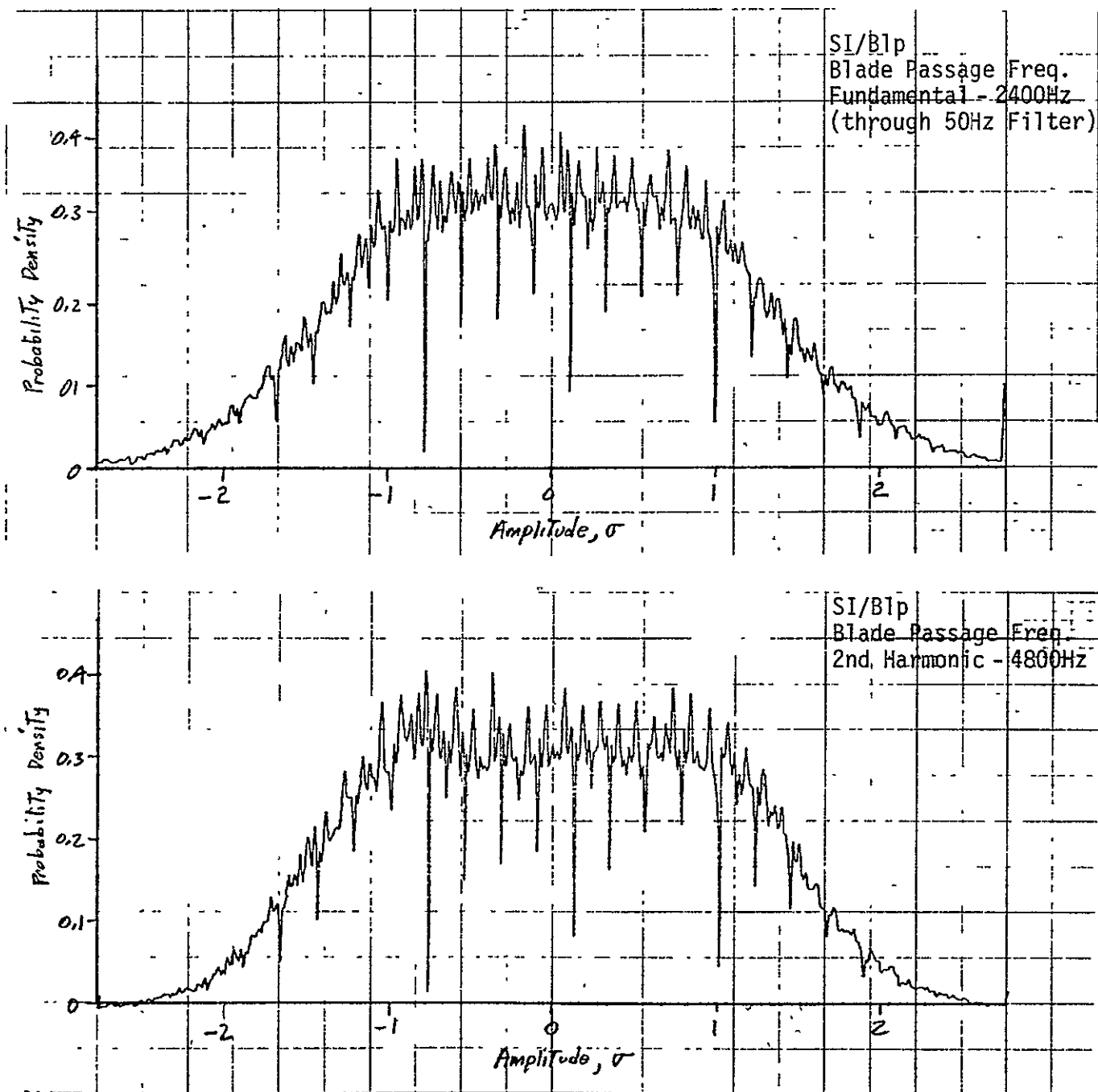
FIG. 15. PROBABILITY DENSITY FUNCTIONS FOR THE FIRST TWO HARMONICS
OF BLADE PASSAGE FREQUENCY MEASURED BY A STATOR PRESSURE
SIDE SENSOR.

TABLE 7. SUMMARY OF STATOR BLADE PRESSURE DATA.

| Blade No. | Loca-tion | Pressure, Suction, or Lift | Tone Freq.* | | Func-tion | Mea-sured PDR | Corres-ponding R | R from PSD |
|---|---|---|---|---|---|---|---|---|
| | | | Har-monic | Hz | | | | |
| SI | C5 | lift | 1 | 45.3 | PDF | 1.5 | 8 | 8.5 |
| | | | 1 | 45.3 | ACF | – | 7.5 | 8.5 |
| | | | 2 | 90.6 | PDF | 1.3 | 5 | 5 |
| | | | 2 | 90.6 | ACF | – | 2.6 | 5 |
| | | pressure | 1 | 45.3 | PDF | 1.2 | 3.5 | 3.5 |
| | | suction | 1 | 45.3 | PDF | 1 | 0 | 4 |
| SI | B1 | pressure | 1 | 45.3 | PDF | 1.75 | 15 | ** |
| | | | 2 | 90.6 | PDF | 1.55 | 9 | ** |
| | | | 3 | 136 | PDF | 1 | 0 | ** |
| | | suction | 1 | 45.3 | PDF | 1.15 | 3 | ** |
| SI | C1 | pressure | 1 | 45.3 | PDF | 1.95 | 28 | ** |
| | | | 2 | 90.6 | PDF | 1.60 | 11 | ** |
| | | | 3 | 136 | PDF | 1 | <1.5 | ** |
| | | suction | 1 | 45.3 | PDF | 1.15 | 3 | ** |
| SI | B1 | pressure | 1 | 2400 | PDF | 1.03 | 1.5 | 150 |
| | | | 2 | 4800 | PDF | 1.07 | 2 | 2 |
| SI | C1 | pressure | 1 | 2400 | PDF | 1 | <1.5 | 30 |

*Rotor speed tones isolated by 2.5 Hz wide bandpass filter.
Blade passage tones isolated by 50 Hz wide bandpass filter.

**Low frequency spectra needed to determine "R from PSD" not computed.

and no tone indicated a signal-to-noise ratio of more than R=2.*
Further discussions of the blade passage tones as seen in the
stator pressure signals are included under the discussion of
time history data later in this chapter.

## Far Field Noise Data

Spectral density plots and probability density functions were
generated for the first two or three rotor speed tones in the
far field noise data and are summarized in Table 8. The inter-
pretations of the results in the last three columns of Table 8
are exactly the same as previously discussed for Table 6. The
probability density functions for the third and higher harmonics
of the rotor speed tones were basically Gaussian at all but two
locations, 50° and 60°.

The results in Table 8 reveal a generally consistent pat-
tern; specifically, the fundamental tends to be strongly sinu-
soidal at angles of 110° or less, but the sinusoidal content
falls off rapidly in the higher harmonics. The data for loca-
tions at angles greater than 110° reveal very little or no
sinusoidal content even at the fundamental rotor speed frequency.
There are a few unusual characteristics in the results. For
example, the fundamental at 30° shows negligible sinusoidal
character, while the second harmonic at this same location re-
veals a strong sinusoidal property. At 60°, the third harmonic
appears somewhat more sinusoidal than the second. At 100°, none
of the harmonics reveal a significant sine wave contribution,
although sine waves are present in the fundamental at both the
90° and 110° locations. There is no obvious explanation for
these apparent anomalies, except that they may be related to
the radiation pattern of the fan noise.

Now concerning the tones due to the rotor blade passage
frequency, the probability density functions of the funda-
mental and second harmonic of the blade passage frequency were

---

*At the blade passage frequencies, the stator blade pressures
 for Case 4 appear to display slightly greater "dishing" in some
 cases than the Case 1 data. For example, the measured PDR
 (rate of maximum to minimum probability density) for the blade
 passage tone at SI/Clp was 1.2 for the Case 4 data as compared
 to 1.0 for the Case 1 data. On balance, however, the differences
 were not found to be very great.

TABLE 8. SUMMARY OF POLAR MICROPHONE NOISE DATA FOR ROTOR SPEED TONES.

| Location (degrees) | Tone Freq.* Harmonic | Hz | Function | Measured PDR | Corresponding R | R from PDS |
|---|---|---|---|---|---|---|
| 10 | all | all | PSD | – | – | – |
|  | 1 | 45.3 | PDF | 1.35 | 6 | 20 |
|  | 2 | 90.6 | PDF | 1.15 | 3 | 15 |
| 20 | all | all | PSD | – | – | – |
|  | 1 | 45.3 | PDF | 1.06 | 2 | 2 |
|  | 2 | 90.6 | PDF | 1 | <1.5 | 2 |
| 30 | all | all | PSD | – | – | – |
|  | 1 | 45.3 | PDF | 1 | <1.5 | 7 |
|  | 2 | 90.6 | PDF | 1.42 | 6 | 20 |
| 40 | all | all | PSD | – | – | – |
|  | 1 | 45.3 | PDF | 1.75 | 14 | 15 |
|  | 2 | 90.6 | PDF | 1.35 | 5 | 11 |
| 50 | all | all | PSD | – | – | – |
|  | 1 | 45.3 | PDF | 1.35 | 5 | 7 |
|  | 2 | 90.6 | PDF | 1.20 | 3.5 | 19 |
|  | 3 | 226 | PDF | 1.15 | 3 | 1 |
| 60 | all | all | PSD | – | – | – |
|  | 1 | 45.3 | PDF | 1.75 | 14 | 14 |
|  | 2 | 90.6 | PDF | 1.09 | 2 | 12 |
|  | 3 | 226 | PDF | 1.27 | 4 | 1 |
| 70 | all | all | PSD | – | – | – |
|  | 1 | 45.3 | PDF | 1.30 | 4.5 | 7 |
|  | 2 | 90.6 | PDF | 1.11 | 2.5 | 5 |
| 80 | all | all | PSD | – | – | – |
|  | 1 | 45.3 | PDF | 1.67 | 12 | 30 |
|  | 2 | 90.6 | PDF | 1 | <1.5 | 4 |
| 90 | all | all | PSD | – | – | – |
|  | 1 | 45.3 | PDF | 1.11 | 2.5 | 10 |
|  | 2 | 90.6 | PDF | 1 | <1.5 | 10 |
| 100 | all | all | PSD | – | – | – |
|  | 1 | 45.3 | PDF | 1 | <1.5 | <0.5 |
|  | 2 | 90.6 | PDF | 1 | <1.5 | 2 |

*Isolated for analysis using a 2.5 Hz wide bandpass filter.

42

TABLE 8. *(Continued)*.

| Location (degrees) | Tone Freq.* | | Function | Measured PDR | Corresponding R | R from PDS |
| | Harmonic | Hz. | | | | |
|---|---|---|---|---|---|---|
| 110 | all | all | PSD | – | – | – |
| | 1 | 45.3 | PDF | 1.20 | 3.5 | 13 |
| | 2 | 90.6 | PDF | 1.52 | 8 | 18 |
| 120 | all | all | PSD | – | – | – |
| | 1 | 45.3 | PDF | 1 | <1.5 | <0.5 |
| | 2 | 90.6 | PDF | 1 | <1.5 | 1 |
| 130 | all | all | PSD | – | – | – |
| | 1 | 45.3 | PDF | 1 | <1.5 | <0.5 |
| | 2 | 90.6 | PDF | 1 | 0 | 0.8 |
| 140 | all | all | PSD | – | – | – |
| | 1 | 45.3 | PDF | 1 | <1.5 | 1 |
| | 2 | 90.6 | PDF | 1 | 0 | 0.5 |
| 150 | all | all | PSD | – | – | – |
| | 1 | 45.3 | PDF | 1 | 0 | <0.5 |
| | 2 | 90.6 | PDF | 1 | 0 | <0.5 |
| 160 | all | all | PSD | – | – | – |
| | 1 | 45.3 | PSD | 1 | 0 | <0.5 |
| | 2 | 90.6 | PDF | 1 | 0 | <0.5 |

*Isolated for analysis using a 2.5 Hz wide bandpass filter.

surveyed for all far field microphone positions.  At no location was a significant sinusoidal character observed in the data (R < 1.5 in all cases).  This was true in spite of the fact that the blade passage tones are pronounced in the spectra of the far field data out to the third or fourth harmonic.

## Time History Studies

The results of the two previous sections suggest that the rotor blade passage tones, as seen in both the stator blade pressure signals and the far field noise data, generally appear more like narrowband noise than sine waves in terms of their probability structure.  To be more specific, the probability density functions of the blade passage tones indicate that less than 67% of the tone power in all cases, and less than 50% in most cases, can be attributed to a constant amplitude sine wave.  The implication here is that the rotor generated wakes striking the stator blades are heavily stochastic in character.  Since this is an important conclusion, additional studies of the blade passage tones were pursued by investigation of the tone time histories.

The pressure time history studies were performed using a Biomation Model 802 Transient Recorder which was triggered using the once per revolution signal on the data tape recording.  This permitted an ensemble of pressure time histories to be generated on a common time base.  The studies were limited to the pressure side signal recorded on Stator Blade I at location B1 (SI/B1p).  This signal was chosen for two reasons.  First, the spectrum of the signal at this location revealed a strong blade passage tone which is substantially more intense than other extraneous tones believed to be due to blade vibration.  Second, this signal revealed the strongest indication of a periodic character at 2400 Hz of all the stator blade pressure signals.

First consider the unfiltered time history of the pressure signal at location SI/B1p.  Three sample records measured on a common time base of 20 msecs duration (about one rotor revolution) are shown in Fig. 16.  All of these time histories reveal a certain systematic character including a dominant oscillation at about 2400 Hz.  However, there is clearly a strong stochastic character in the time histories indicated by significant differences from one rotor revolution to another.
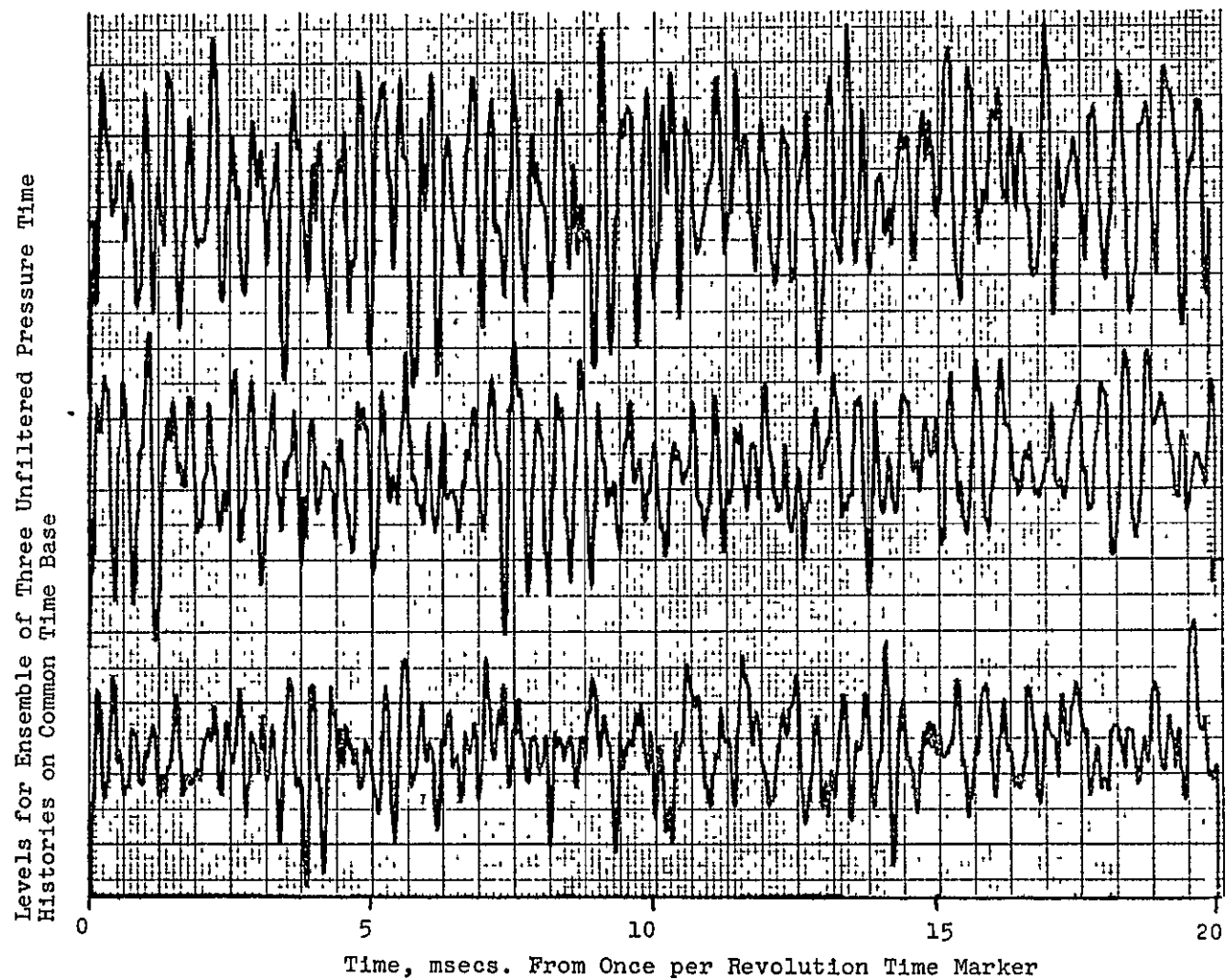
FIG. 16.   ENSEMBLE OF UNFILTERED PRESSURE TIME HISTORIES AT LOCATION
SI/B1p (20 msec. Time Base).
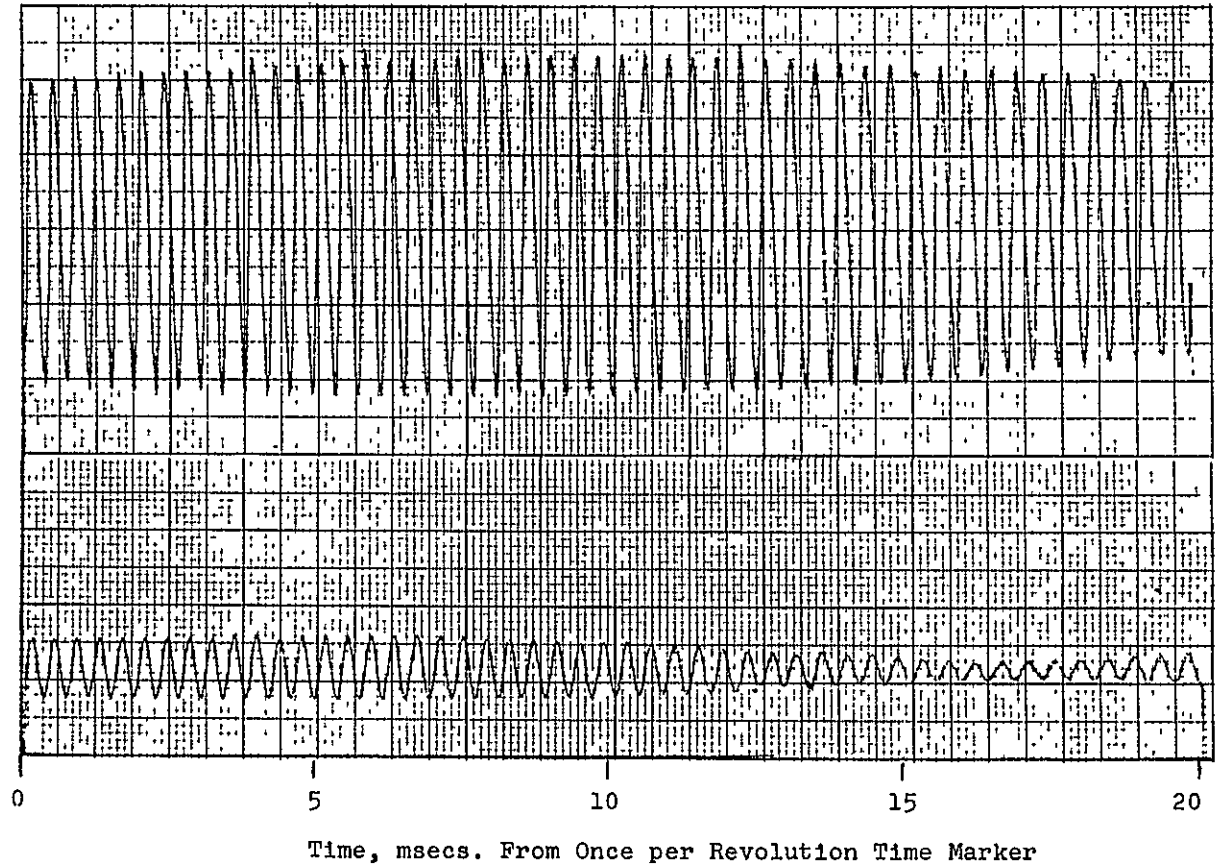
FIG. 17.  ENSEMBLE OF FILTERED PRESSURE TIME HISTORIES AT LOCATION
SI/B1p (20 msec. Time Base).

FIG. 18. ENSEMBLE OF FILTERED PRESSURE TIME HISTORIES AT LOCATION SI/Blp (50 msec. Time Base)
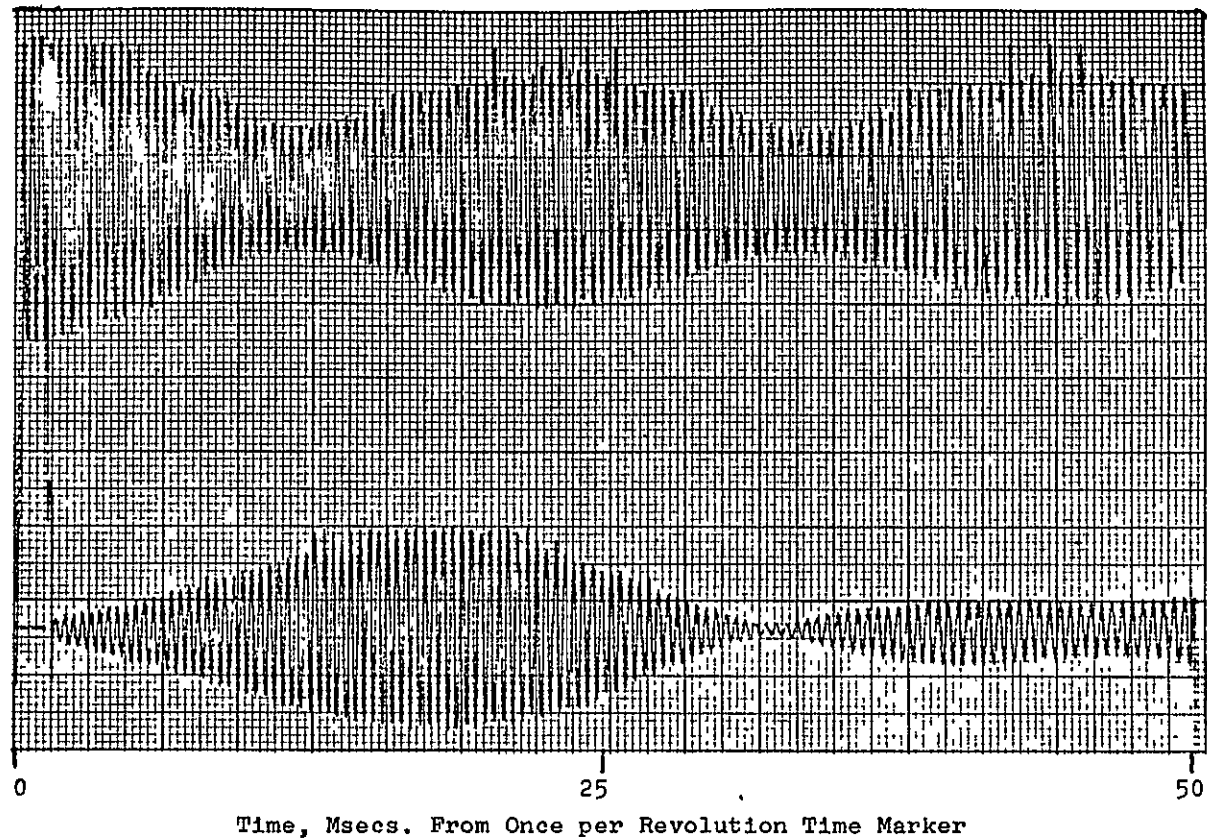
FIG. 19.   ENSEMBLE OF FILTERED PRESSURE TIME HISTORIES AT LOCATION
SI/B1p (5 sec. Time Base)
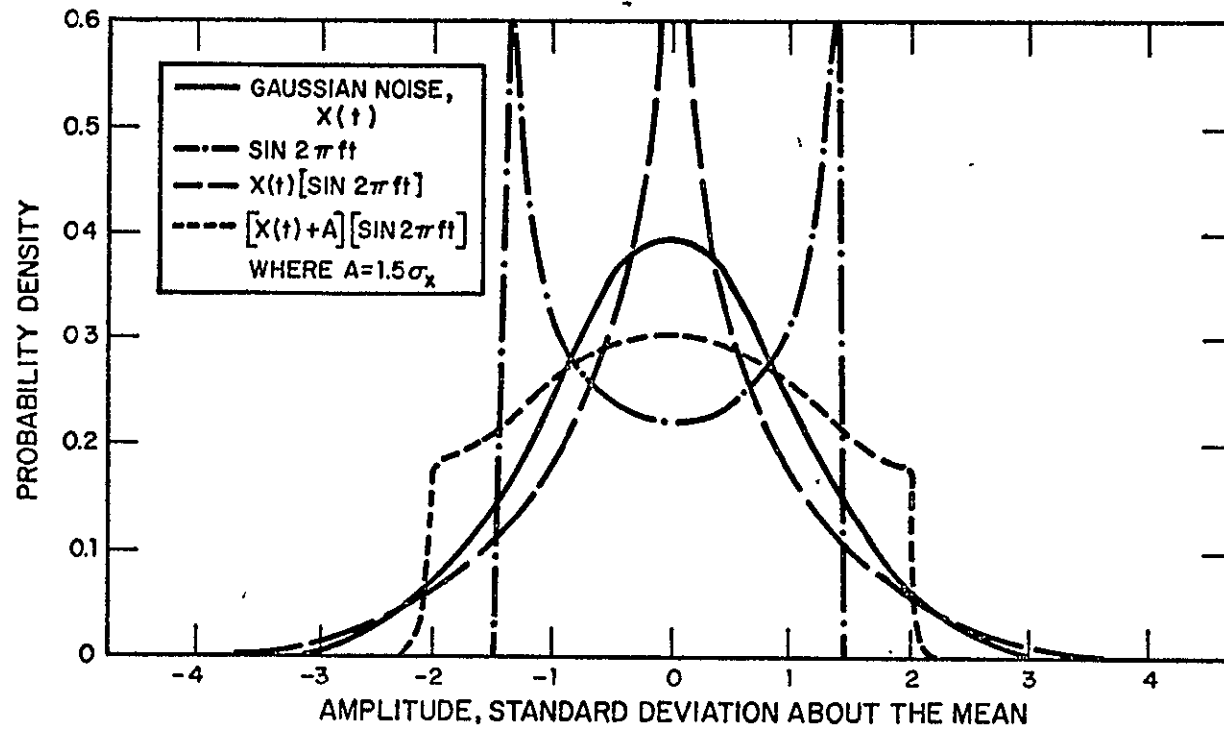
FIG. 20. PROBABILITY DENSITY FUNCTIONS OF IDEAL WAVE FORMS.

Now consider that portion of the pressure time history at location SI/Blp which falls in a 50 Hz band centered at 2400 Hz (the rotor stator blade passage frequency). Two sample records on the same 20 msec time base are presented in Fig. 17. Note that the filtered time histories appear almost as sine waves over the duration of a single rotor revolution. However, the level from one revolution to another is quite different; i.e., the level of the sine wave is varying quite dramatically over long time intervals. This is more clearly seen by expanding the time base, first to 50 msec (about 2-1/2 revolutions) in Fig. 18, and then to a full 5 sec in Fig. 19. In Fig. 19, note that the time histories appear much like narrowband noise with an average number of envelope maxima of perhaps 6 or 7 per sec. This is in agreement with the theoretical value of 6.4 maxima per sec given by Rice's formula (Rice, 1954, p. 222) for noise with a 10 Hz bandwidth (the bandwidth of the blade passage tones is about 10 Hz, as shown in Fig. 11).

At first glance, the above discussions tend to support the conclusion that the blade passage tone in the stator blade pressure signals is more nearly like narrowband noise rather than a sine wave, as indicated previously by the probability density plots. This conclusion, however, might be misleading in physical terms. Specifically, it may be important in the interpretation of the data in terms of physical mechanisms to distinguish between narrowband noise and an amplitude modulated sine wave. It is true that a full amplitude modulation of a sine wave will not produce a probability density function similar to those measured. The probability density function of a full randomly modulated sine wave will generally include a large peak in the density at zero amplitude, as shown in Fig. 20. However, if a static term is included in the modulation, then probability density functions similar to those measured might result, as also shown in Fig. 20.

## Summary of Findings on Tone Characteristics

The results of the preceding sections on the evaluation of the characteristics of blade passage frequency and rotor speed tones can be summarized as follows:

1. The rotor blade pressures, stator blade pressures, and far field noise data all reveal a spectral component at the rotor rotational frequency which has the probability characteristics of a strongly sinusoidal signal. The second harmonic of the rotor frequency also displays a sinusoidal character, but not as strongly as the

fundamental. The third harmonic displays at most a light sinusoidal character. The higher harmonics appear as Gaussian noise, inspite of the fact that they often stand out strongly in the spectral data.

2. The stator blade pressures include strong spectral components at the rotor blade passage frequency and its harmonics. However, the isolated blade passage tones display surprising little sinusoidal character. The probability structure of the blade passage tones in the far field noise data is even less sinusoidal. The fundamental and all harmonic tones in the far field data appear to be almost Gaussian; because of duct mode cut-off, the fundamental tone is due entirely to the rotor response to inflow distortions. However, both the rotor and the stator contribute to the harmonics of blade passage frequency.

3. Studies of ensembles of stator blade pressure time histories in a frequency interval about the blade passage frequency indicate the time histories of the tones behave much more like narrowband noise than a sine wave, at least in terms of their amplitudes; i.e., the envelop of the time histories varies randomly with time in a manner consistent with narrowband noise. However, there is an important distinction between the time histories and true narrowband noise. Specifically, the time histories have systematic zero crossings, as opposed to narrowband noise which has some random variability in the zero crossing rate. The random character of the blade passage tones in the stator data indicates that the wakes striking the stator blades, although systematic in time, have a strongly stochastic amplitude character. To be more specific, the wakes are in fact pulses of highly turbulent flow.

## Experimental Studies of the Interaction Between the Rotor Wakes and the Stator Vanes

This section presents the results of studies to understand more about the rotor wake structure and its interaction with the stator vanes, primarily by means of simultaneously processing signals from pairs of stator vane sensors. Unfortunately, this effort was hampered by several problems with the experimental data and, as a result, progress was limited.

The intent was to study the spanwise, chordwise, and circumferential structure of the rotor wake as seen by the stator vane sensors. Both the turbulent and mean properties of the wake were of interest. The turbulence characteristics of general interest are the values of the broadband cross-correlation function and the coherence function between different vane locations. Mean wake properties of interest include the waveform of the wake-induced pressure signal, and the wake trace speed along the vane as described below.

Because of the characteristics of the swirling flow behind the rotor, the generators of the surface which defines a wake centerline do not remain radial. The wakes are swept over so that the hub region leads the tip region. Thus, a given wake first meets a given vane at the hub and the interaction region travels towards the tip as the wake passes. The wake trace speed along the vane is important to the acoustic radiation which results from the wake/vane interaction. The trace speed concept and the wake/vane interaction are discussed in more detail in the next chapter. An area of interest in the data analysis was to measure experimentally the wake trace speed along the vane by determining the time delay between different sensor locations.

Difficulties were encountered in some of the above-mentioned areas. For instance, meaningful broadband cross-correlations could not be determined from the data because of the presence of the previously-mentioned vibration related peaks in the stator vane pressure spectra. Their presence distorts the shape and the time delay at the peak of the cross-correlation function. As a result, no useful information could be extracted from this data. However, even if the vibration peaks were not present, spurious phase delays in the data would have still altered the time delays, as discussed later.

Because of the stochastic character of the vibration peaks, it is possible that they would not have prevented the determination of the mean wake-induced pressure waveform by ensemble averaging signals. The averaging was not attempted because Table A.1 shows that the harmonics of blade passage frequency are typically 10 to 15 dB below the fundamental. This suggests that the mean waveform of the wakes is predominately sinusoidal in character at the blade passage frequency.

52

The remaining tools to study the wakes and their interaction with the vanes are coherence functions* and time delays determined from narrow-band cross-correlations. These are now discussed.

Coherence data on the stator at the blade passage frequency is summarized in Table 9. As indicated in the table, the coherence data was calculated at three separate facilities: Mechanics Research Inc. (MRI) in Los Angeles, Bolt Beranek and Newman Inc. (BBN), and NASA Lewis. The BBN and MRI data apply to Case 1 (front drive) at 80% speed, whereas the NASA data applies to Case 2 (rear drive) at 80% speed. The procedure used at NASA Lewis illustrates a typical way in which coherence functions are obtained. Two time history records of interest were passed through matched 50 Hz wide narrow-band filters tuned to the blade passage frequency for this case (about 2480 Hz), and the filter outputs were cross-correlated. The square of the narrow-band cross-correlation function, after proper normalization, gives the desired coherence function.

Reviewing the data in Table 9 shows it to be reasonably · consistent except for most values on the suction side involving an A location, i.e., the values nearest the tip of the vane. To be specific, extremely low coherence values occur in measurements involving location A1 with only one exception (SI/A4s versus SI/A5s). Furthermore, referring back to the spectral data, the signal at location SI/A1s was very unusual in that the blade passage tone barely appeared in a spectrum that was otherwise rich in blade vibration contributions. Referring to Table A-1, the magnitude of the blade passage tone at location SI/A1s was substantially lower than measured at other SI/A locations

There are two possible explanations for this behavior. The data from location SI/A1s may well be anomalous. Alterna-, tively, the flow field may be very complex in the suction side leading edge region very near the tip, causing the unsteady pressure response in this region to be drastically altered.

If measurements involving suction pressures at the A locations are ignored, the remaining data cluster nicely around a decaying spatial coherence along the stator blade chord, as shown by the empirical fit in Fig. 21. The coherence data for stator blade pressures is sufficient to conclude that the spatial coherence of the blade passage tone falls off gradually (perhaps in an exponential way) to about 0.3 between the leading and trailing edges of the stator blades. Unfortunately, the data are not sufficient to draw a complete picture of the spatial coherence in the spanwise direction. However, the one reliable measurement between SI/B1p and SI/C1p suggests the spanwise coherence may be similar to the chordwise coherence.

--------

*See Bendat and Piersol (1971) for definition and discussion of coherence functions.

TABLE 9.   SUMMARY OF COHERENCE AND TIME DELAY DATA AT BLADE PASSAGE FREQUENCY.

| Locations | Chordwise, Spanwise, Bladewise | Pressure, Suction or Lift | Test Case No. | Coherence Value | | | Time Delay (msec) |
|---|---|---|---|---|---|---|---|
| | | | | BBN | MRI | LeRC | |
| SI/A2 to SI/A3 | chordwise | pressure | 1 | 0.83 | – | 0.82 | 0.017 |
| "        " | | | 2 | – | – | 0.69 | 0.022 |
| SI/A3 to SI/A5 | | | 2 | – | – | 0.72 | 0.055 |
| SI/A2 to SI/A5 | | | 1 | 0.44 | – | – | – |
| "        " | | | 2 | – | – | 0.63 | 0.078 |
| SI/C1 to SI/C2 | | | 1 | 0.78 | – | 0.44 | 0 |
| "        " | | | 2 | – | – | 0.52 | 0 |
| SI/C2 to SI/C5 | | | 2 | – | – | 0.25 | –0.033 |
| SI/C1 to SI/C5 | | | 1 | 0.25 | 0.20 | 0.27 | –0.022 |
| "        " | | pressure | 2 | – | – | 0.29 | –0.073 |
| SI/A1 to SI/A2 | | suction | 2 | – | – | – | –0.143 |
| SI/A2 to SI/A4 | | | 2 | – | – | – | 0.143 |
| SI/A4 to SI/A5 | | | 1 | 0.18 | – | – | – |
| "        " | | | 2 | – | – | 0.46 | –0.020 |
| SI/A1 to SI/A5 | | | 1 | 0.03 | – | – | – |
| SI/C1 to SI/C5 | | suction | 1 | 0.40 | – | – | – |
| SI/C1 to SI/C5 | chordwise | lift | 1 | 0.35 | – | – | – |
| SI/B1 to SI/C1 | spanwise | pressure | 1 | 0.85 | 0.76 | 0.89 | 0.012 |
| SI/A2 to SI/C2 | | | 2 | – | – | 0.07 | 0.200 |
| SI/A5 to SI/C5 | | | 1 | – | 0.24 | – | – |
| "        " | | pressure | 2 | – | – | 0.48 | 0.044 |
| SI/A1 to SI/B1 | | suction | 1 | 0.13 | 0.07 | – | –0.009 |
| "        " | | | 2 | – | – | 0.04 | –0.018 |
| SI/B1 to SI/C1 | | | 2 | – | – | – | 0.006 |
| SI/A1 to SI/C1 | | | 2 | 0.03 | – | – | 0.020 |
| SI/A1 to SI/D1 | | | 1 | 0.06 | 0.33 | – | – |
| SI/B1 to SI/D1 | spanwise | suction | 2 | – | – | 0.09 | 0.115 |
| SI/A1 to SII/A1 | bladewise | suction | 1 | 0.10 | 0.63 | – | – |
| "        " | | | 2 | – | – | 0.11 | 0.110 |
| SI/A1 to SIII/A1 | | | 1 | 0.02 | 0.01 | – | –0.097 |
| "        " | | | 2 | – | – | 0.10 | –0.077 |
| SII/A1 to SIII/A1 | bladewise | suction | 2 | – | – | 0.03 | 0.030 |

*The absence of an entry, denoted by a dash, indicates that the analysis could not be performed because sensor outputs were not on the same tape.
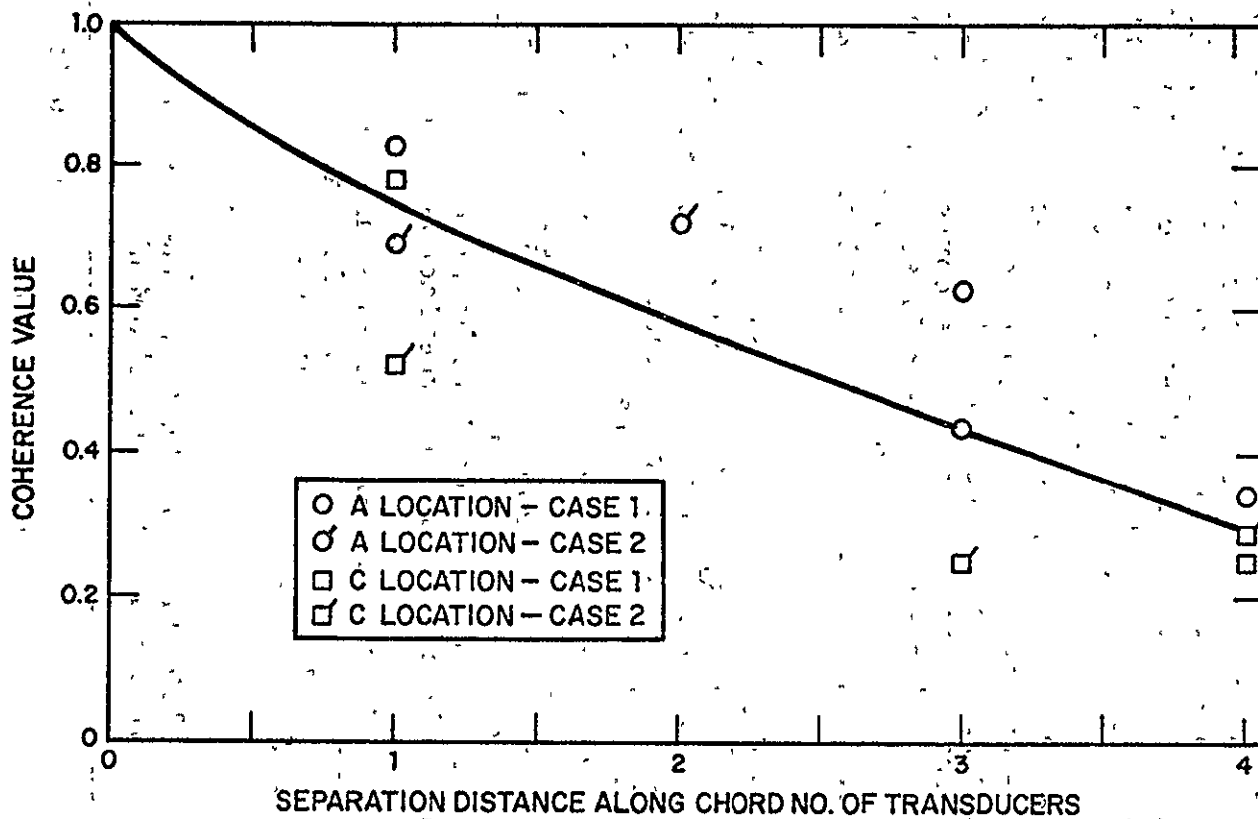
FIG. 21. SPATIAL COHERENCE OF STATOR BLADE PRESSURES AT BLADE PASSAGE FREQUENCY ALONG THE BLADE CHORD.

Because of the interest in wake trace speed along the stator, time delays for the propagation of the blade passage tones between various transducer pairs were computed. These are shown in Table 9 for the Case 2 experimental data. These time delays were determined from the cross-correlation peaks computed for the pairs of signals after narrow-band filtering to isolate the blade passage tone at 2480 Hz. Narrow-band filtering avoids problems with the vibration-related peaks in the stator data. The correlation data were carefully calibrated using a common signal to correct for static time delays due to the slightly different phase characteristics of the isolation filters. Because of the very slow decay of the cross-correlation function between two narrow-band filtered signals, it is possible that some of the results in Table 9 might be off by one or more correlation function periods equal to 0.404 msecs for Case 2 data. Hence, some of the time delays in Table 9 might require an adjustment by ±0.404 n msecs; n = 1,2,3,..., particularly for widely separated transducers.

Even allowing for the possible corrections discussed above, the time delay data in Table 9 are inconsistent. For example, at spanwise location A, the time delays across the chord suggest the propagation on the pressure side is forward across the blade, while at span location C, the propagation is aft. Time delays for spanwise time delays also show unusual behavior including sign reversals. These inconsistencies suggest that phase shifts occurred in at least some channels of the data acquisition equipment during the experiments. Because of this possibility, it has not been possible to make any definitive statements about the wake trace speed on the basis of the experimental data.

To investigate this issue further, coherence and time delay data were computed between the pressure and suction side measurements at various stator blade locations during the Case 2 experiment. The results are shown in Table 10.

TABLE 10.    COHERENCE AND TIME DELAY AT BLADE PASSAGE FREQUENCY
            FOR PRESSURE TO SUCTION SIDE MEASUREMENTS

| Locations | Coherence | Time Delay (msecs) |
|---|---|---|
| SI/A2p *vs.* SI/A2s | 0.27 | 0.102 |
| SI/A5p *vs.* SI/A5s | 0.79 | 0.172 |
| SI/C1p *vs.* SI/C1s | 0.44 | 0.084 |
| SI/C2p *vs.* SI/C2s | 0.52 | 0.172 |
| SI/C5p *vs.* SI/C5s | 0.21 | -0.150 |

Even when a factor of ±.202 msecs is added to these results to account for a 180° phase shift between suction and pressure surfaces, it is seen that significant time delays are indicated between the pressure and suction side measurements at all locations, often exceeding the time delays between different locations in Table 9. One would expect the time delays between the pressure and suction side at the same location on the blade to be very small, particularly near the leading edge (for instance SI/Clp vs SI/Cls). Hence, these results also suggest that phase errors may have been introduced during the experiment by the data acquisition equipment, probably in the amplifiers involved in the sensors or data retrieval system rather than the tape recorders, which should be reasonably accurate at the frequency in question.

# FAN NOISE PREDICTION METHOD

## Introductory Comments

This chapter describes the use of the QF-1B blade and vane surface pressure data in a fan noise prediction method. The calculated sound power is compared with values based on the far field microphone measurements. The prediction method was developed by Heller and Widnall (1972) and utilizes a rather basic analytical model for the fan noise sources and the fan geometry. A few modifications have been made in order to better represent the role of the rotor-wake/stator-vane interaction in the noise producing process. The surface pressure data is used as an input to estimate the unsteady blade and vane forces that are required in the prediction method. Because of the basic nature of the analytical model, both its degree of success and its shortcomings are of considerable interest. The use of measured surface pressures provides a degree of simplification, since a detailed characterization of wakes and inflow distortions and the calculation of the associated aerodynamic response are not required.

In the following sections, the underlying physical assumptions of the Heller and Widnall (1972) prediction method are first reviewed, followed by a discussion of the rotor-wake/stator-vane interaction process. The detailed use of the prediction method is then described and the implications of the results are discussed.

## Review of the Prediction Procedure Assumptions

This section reviews the underlying assumptions of the fan noise prediction method proposed by Heller and Widnall (1972). A full mathematical review of the method is not provided, and a knowledge of the basic reference is therefore assumed.

The noise prediction method assumes that acoustic dipoles produced by unsteady forces on the blades and vanes are responsible for fan noise. These unsteady forces are caused by rotor/stator and stator/rotor interactions. Typical sources of the interaction are the wakes and potential fields of the blades and vanes. As previously discussed, the sources of unsteady loading of interest for the QF-1B are rotor wakes interacting with stator vanes, and rotor blades interacting with inflow distortions. Potential field effects are not important because of the relatively large spacing between the rotor and stator in the QF-1B. In the context of the Heller and Widnall method, a rotor operating in a

58

distorted inflow bears a relation to a rotor interacting with an upstream stator, and can be treated accordingly if the proper factors are taken into account.

The acoustic dipoles excited by the unsteady loading on a blade or vane are assumed to act along a single radial line, i.e., a chordwise distribution of acoustic sources is not considered. The dipole strength and orientation is assumed constant along the span (along the radial line). Furthermore, the dipoles are assumed to behave coherently along the span, i.e., they radiate exactly in phase. As will become evident, this last assumption may constitute a serious limitation of the method.

In addition to the above, certain important assumptions are made to simplify the mathematical analysis. The hub/tip ratio of the fan is assumed to be near unity so that the blades and vanes lie in a narrow passage. When the passage height is sufficiently small compared to the fan radius, the effects of curvature can be largely ignored. This fact, along with the assumption of coherent acoustic sources of constant spanwise strength, reduces the problem to that of a two-dimensional sound field in a narrow duct. Figure 22 illustrates the analogy between a rotor or stator in a narrow semi-infinite duct and the essentially two-dimensional arrangement of blades or vanes between two semi-infinite plates. The prediction method is based on the solution of this two-dimensional analog problem with the further assumption that the separation distance between the plates is less than half an acoustic wavelength. To calculate the radiated sound power, the transition from the two-dimensional to the three-dimensional environment must be considered, and the method takes these effects into account. However, the method also allows the calculation of radiated power when the rotor is unducted, assuming a line of point dipoles. These two calculations should provide bounds on the effect of the duct, subject, of course, to the other assumptions and limitations of the model.

Finally, it should be noted that the effects of the flow field on the sound field are not considered, i.e., moving media effects are ignored.

## Wake/Vane Interaction Geometry

The character of the rotor-wake/stator-vane interaction geometry in a fan such as the QF-1B is now discussed. This interaction is of interest because it can significantly affect the noise produced by this source. Furthermore, it is of interest because of the assumption of spanwise coherence in the Heller and Widnall prediction method.

Y-DIRECTION
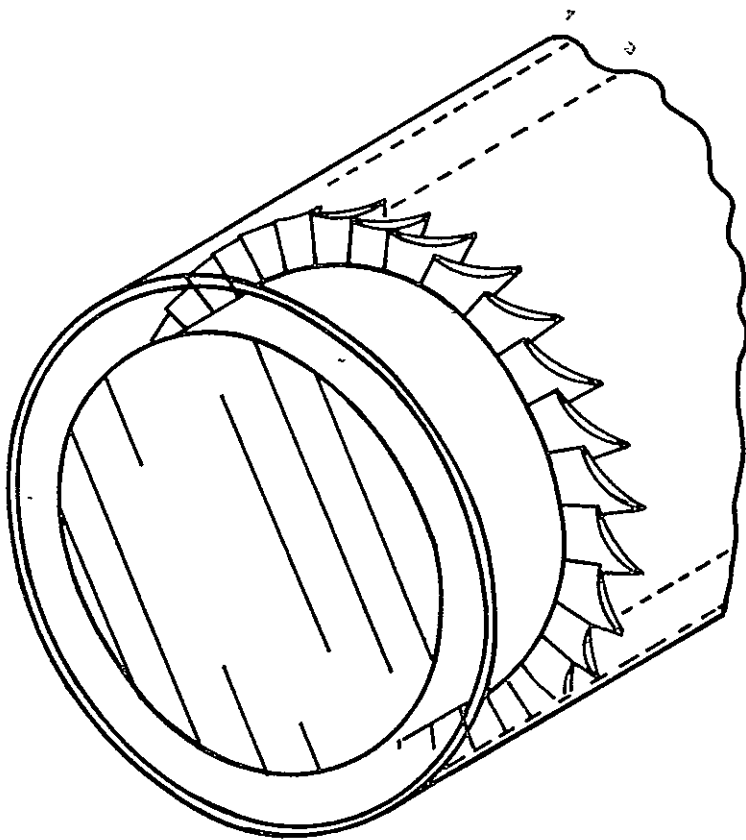
COMPRESSOR
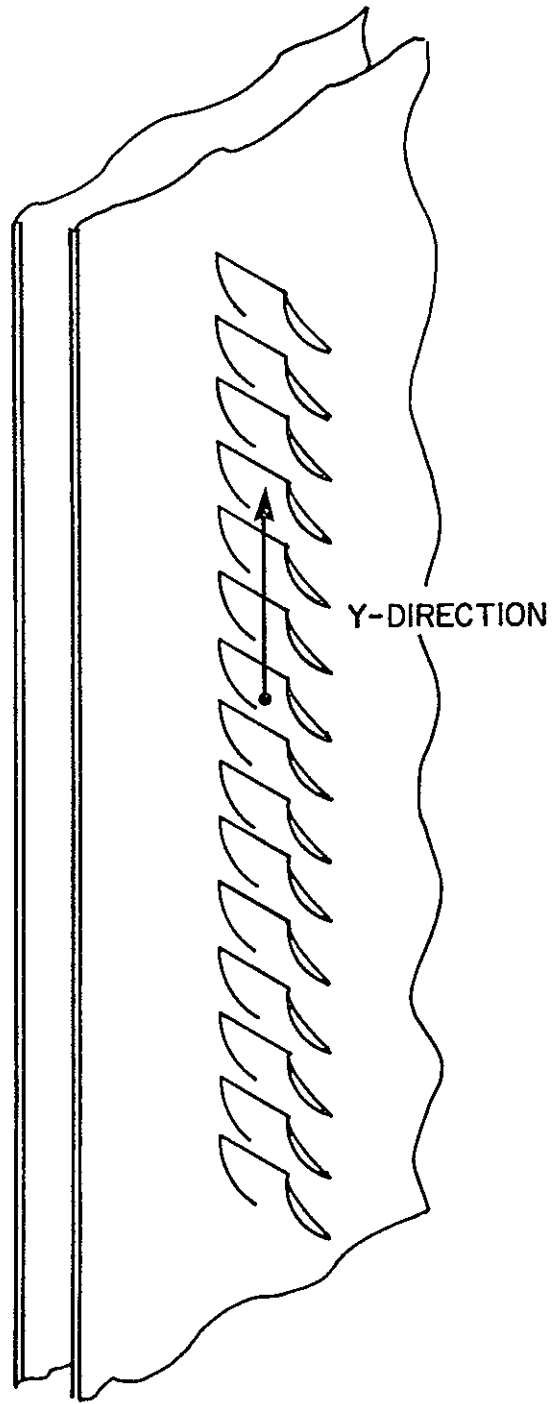
TWO-DIMENSIONAL MODEL
(THRUST + DRAG FORCES)

FIG. 22.   ROTOR IN NARROW SEMI-INFINITE DUCT AND TWO-DIMENSIONAL
ANALOG.

60

Figure 23 illustrates the interaction of a row of stator vanes with rotor wakes when viewed on a surface of constant radius from the fan axis. The mean and turbulent components of the wake produce perturbation velocities at the stator vane which produce unsteady lift. However, the aerodynamic interaction is not really two-dimensional as this illustration seems to suggest.

Figure 24 shows a sketch of a three-dimensional wake/vane interaction in a fan. The structure of the viscous, usually turbulent, rotor wakes which trail each lifting fan blade is complex. However, on the average, these wakes can be considered as being convected with the mean flow in which they are imbedded. The nature of the downstream mean flow is such that the convection process will distort the wakes from their original shape. Suppose, for instance, the rotor is designed to give a mean flow which has a uniform axial velocity distribution and a free vortex tangential velocity distribution. Assuming the wakes are radial at the rotor trailing edge, it is clear that the tangential velocity component will act to skew the wakes over, with the hub region leading the tip region. This situation is illustrated in Fig. 24. In this case, the interaction of a given wake with a given stator vane does not occur simultaneously all along the stator vane span. Instead, the instantaneous spanwise interaction region will extend over only a portion of the vane and will sweep along the vane leading edge, beginning at the hub and ending at the tip. Indeed, the skewing of the wake due to convection by the downstream mean flow can be sufficient to involve several stator vane with a given wake at the same time.

The downstream flow can be thought of as possessing a mean wake component which is steady when viewed moving with the rotor. The shape and strength of this component can be expected to vary from hub-to-tip. The surfaces around which these mean wakes are centered will be skewed by the convection of the mean flow, as discussed above. To complete this picture of the downstream flow field, one must consider any unsteady components. The unsteady component accounts for the turbulent structure of the wakes and for any other sources of inhomogenieties in the flow, e.g., inlet flow distortions, large-scale flow instabilities, and blading errors. In general, the statistical properties of this unsteady component can be expected to vary axially, circumferentially, and radially.

Both the mean and unsteady components of the wake induce unsteady loads on the stator vanes. The mean component will produce a load distribution which travels from hub-to-tip, changing shape and amplitude in accordance with the radial variation of the

61
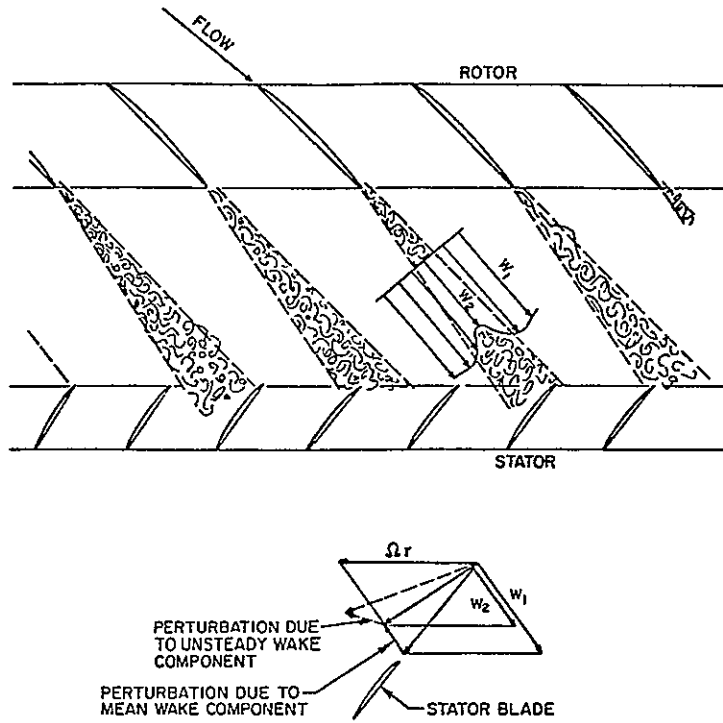
FIG. 23.   THE INTERACTION OF THE STATOR VANE ROW WITH THE MEAN
AND UNSTEADY ROTOR WAKE COMPONENTS.
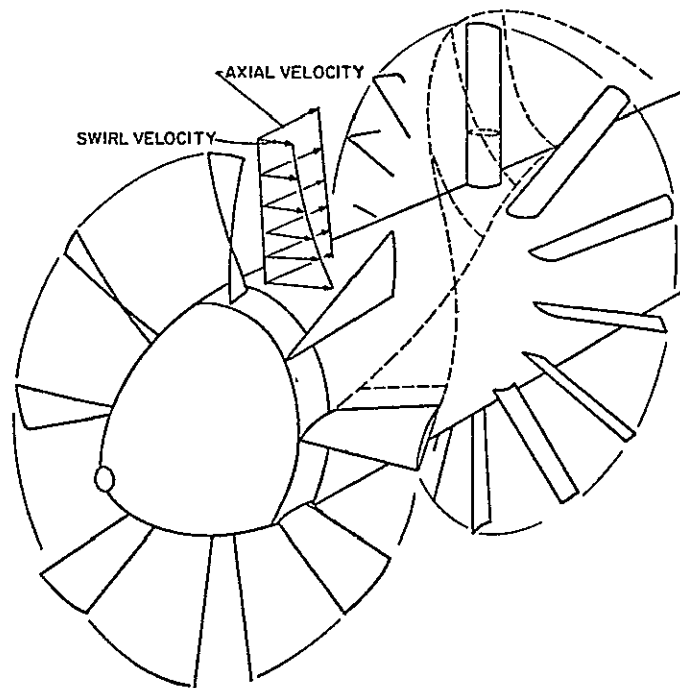


FIG. 24.   A TYPICAL ROTOR-WAKE/STATOR-VANE INTERACTION.

mean flow properties and wake strength, width, and skew. Imposed
on this traveling load distribution will be the unsteady effect
of the turbulent structure of the wake. In addition, the other
contributors to the unsteady wake component also impose fluctuating
loads on the stator vanes. The end result of all these sources of
unsteady loading of the stator vanes is to produce tonal and broad-
band noise. Only the tonal noise has been considered in the pre-
sent prediction effort.

Whether a particular source of unsteady loading produces
significant acoustic radiation depends on whether it satisfies a
trace speed criterion along the vane span. This fact has not been
generally recognized in previous fan noise analyses which usually
assume the rotor-wake/stator-vane interaction is two-dimensional
(corresponding to infinite spanwise trace speed).

The interaction of the wake with the vane produces a load
distribution which travels along the vane. Suppose the vane is
much longer than an acoustic wavelength. Following a phase front
of this load distribution, acoustic radiation can occur if the
magnitude of the load changes, the phase speed changes with time,
or if the phase speed is supersonic. These conditions are *neces-
sary* for radiation, but not *sufficient*. The interaction with
acoustic field produced by the other vanes must also be considered
before it can be established that acoustic radiation actually occurs.
Therefore, regions along the stator vane span can be expected to
be poor radiators if the phase speeds are subsonic, nearly con-
stant, and levels do not change rapidly.* Other regions may or may
not be efficient radiators depending on the behavior of the dis-
tribution of sources elsewhere on the stator. Furthermore, end
effects at the hub and tip (within approximately one half an
acoustic wavelength of the ends) make these regions potential
radiators. These considerations are justified in detail in
Chandiramani, *et al.*, (1976).

The configuration of the wakes at the QF-1B stator, and the
corresponding trace speed along the stator span, are of particular
interest because the height of a stator vane considerably exceeds
one half an acoustic wavelength. The possibility then exists
that much of the stator span may not be capable of efficient radia-
tion. At 80% speed, the blade passage frequency is approximately
2400 Hz corresponding to an acoustic wavelength of 0.47 ft. The
vane height is 1.16 ft. Therefore, $2(r_{tip}-r_{hub})/\lambda = 4.94$, which
demonstrates that the stator vane is acoustically non-compact.

---

*The rate of change of amplitude must be small compared to the
 propagation speed of the load distribution.

The configuration of the rotor wakes at the stator plane is now computed assuming the wakes are convected with the mean flow of the fan. The geometry for this calculation is illustrated in Fig. 25. Referring to Fig. 25-a, the slope of the wake in a $\theta,z$-plane at constant radius is

$$\tan\phi = \frac{1}{r}\frac{dz}{d\theta} = \frac{V_z}{V_\theta} = \frac{V_z}{\Omega r - V_{\theta f}} \tag{2}$$

where $V_z$ is the axial velocity, $V_\theta$ is the tangential velocity in rotor-fixed coordinates, $V_{\theta f}$ is the tangential velocity in stator-fixed coordinates, and $\Omega$ is the rotor shaft speed. Note that the velocity components are all functions of radius. The above expression can be solved for $\theta$ and integrated to yield the circumferential location of the wake centerline as a function of radius and downstream distance. Thus,

$$\theta = \theta_{rotor} + \int_{z_r}^{z_s} \frac{\Omega r - V_{\theta f}}{r V_z}\,dz \tag{3}$$

where the subscripts $r$ and $s$ denote the locations of the rotor trailing edge and stator leading edge, respectively.

For the QF-1B it is a good approximation to assume $\theta_r = z_r = 0$, independent of radius. In other words, the rotor blade trailing edge is very nearly on a radial line. Furthermore, the stator vanes are also very nearly radial, so that $z_s$ is also independent of radius. A table of velocity components supplied by NASA for the QF-1B showed that, to good accuracy, average values of the velocity components could be used to eliminate the dependence on z. Then, making the additional approximation that constant mass flow surfaces remain cylindrical between the rotor and stator, the previous expression simplifies to:

$$\theta = \frac{z_s}{r}\left(\frac{\Omega r - \overline{V}_{\theta f}}{\overline{V}_z}\right) \tag{4}$$

The averaged velocity components, $\overline{V}_{\theta f}$ and $\overline{V}_z$, are still dependent on radius.

64
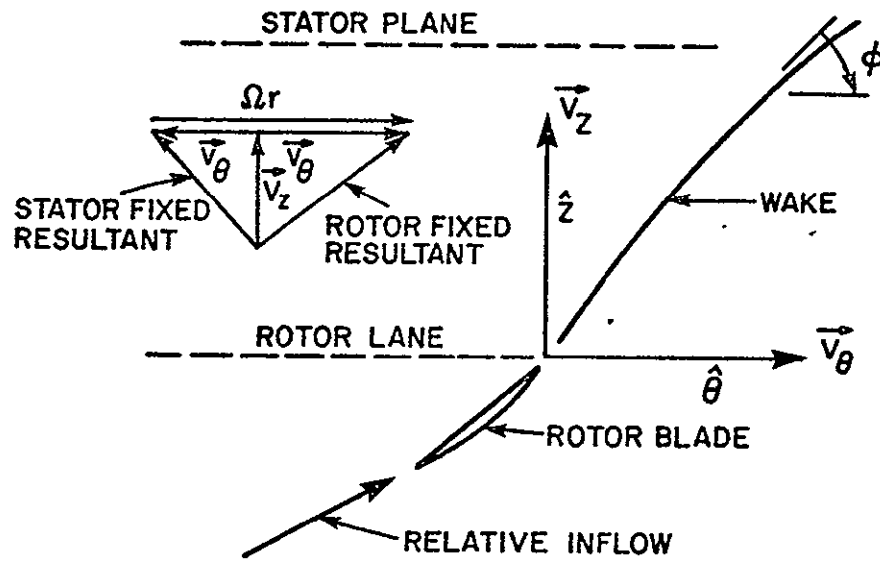
(a)   View at a Constant Radius Surface
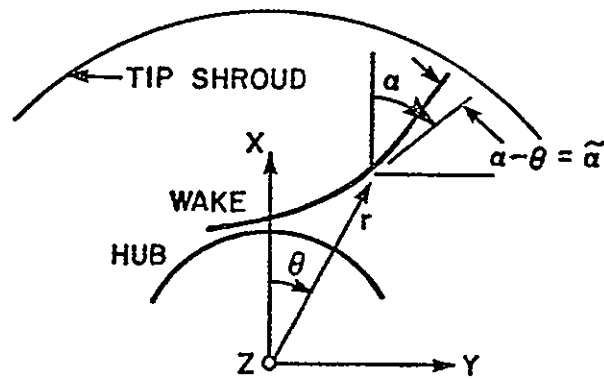


(b)   View at the Stator Inlet Plane

FIG. 25.   GEOMETRY FOR THE CALCULATION OF ROTOR WAKE
           SHAPE AND TRACE SPEED ON THE STATOR VANE

Now referring to Fig. 25-b, the slope of the wake in the x,y plane is

$$\alpha(r) = \tan^{-1}\frac{dy}{dx} \simeq \tan^{-1}\frac{\Delta(r\ \sin\theta)}{\Delta(r\ \cos\theta)} \tag{5}$$

where the incremental notation is useful when working with discrete tabulated values. The interaction angle between the wake and a radial edge is

$$\tilde{\alpha} = \alpha - \theta \tag{6}$$

The trace speed of the point of interaction along the radial edge of a stator vane is then found to be

$$V_{trace} = \frac{\Omega r}{\tan\tilde{\alpha}} \tag{7}$$

The wake configuration and the trace speed were computed using the velocity component values supplied by NASA. Figure 26 shows the wake configuration at the stator plane. Notice that a single wake simultaneously interacts with many stator vanes, in this case:

$$\left(\theta_{tip} - \theta_{hub}\right)\frac{V}{2\pi} \simeq 14\ \text{vanes} \tag{8}$$

Similarly, the number of wakes in a single vane is

$$\left(\theta_{tip} - \theta_{hub}\right)\frac{B}{2\pi} \simeq 6+\ \text{wakes} \tag{9}$$

Clearly, the interaction between the rotor wakes and stator vanes will not produce acoustic sources having a coherent constant amplitude behavior along the stator vane span.

Figure 27 shows the calculated trace speed along a stator vane. Clearly the trace speed distribution is such that the traveling load distribution induced on the vane begins to accelerate and becomes supersonic near the tip of the vane. Over the

66

ANGULAR LOCATION (DEG)
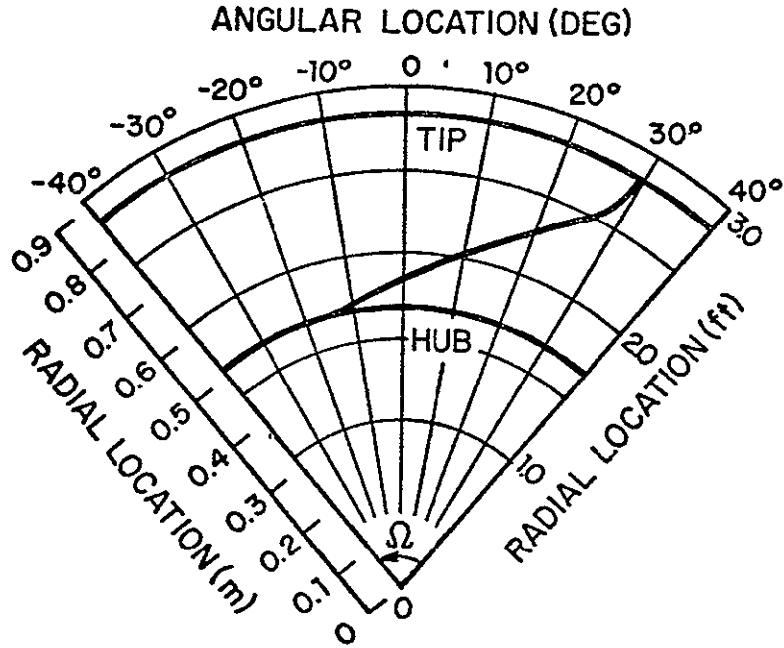


(a)   Instantaneous Wake Location at the Stator Inlet Plane
      (Rotor at 0°)

ANGULAR LOCATION (DEG)
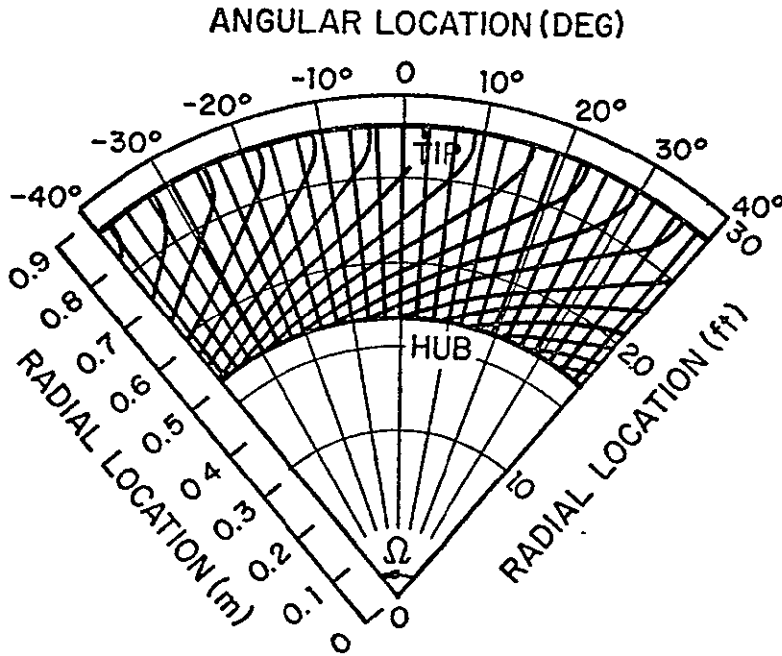


(b)   Instantaneous Location of all Wakes and Vanes at the
      Stator Inlet Plane

FIG. 26.   ILLUSTRATION OF THE WAKE SHAPE AND WAKE/VANE
           INTERACTION AT THE STATOR INLET PLANE.          67
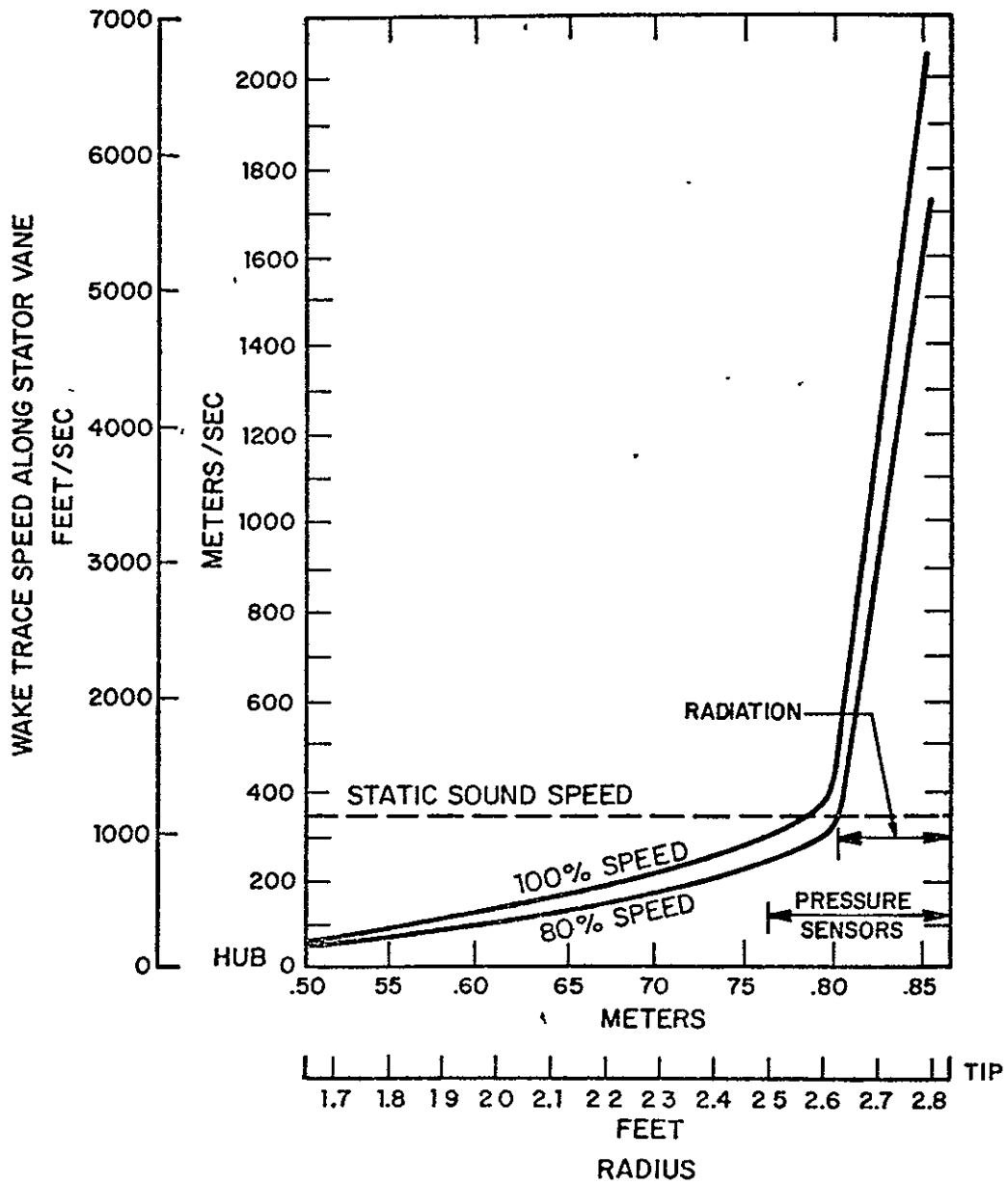
FIG. 27.  TRACE SPEED OF ROTOR WAKE ALONG A STATOR VANE
LEADING EDGE.

inner region of the vane the trace speed is subsonic and rela-
tively constant. It is assumed that the magnitude of the load
remains nearly constant over the span. This assumption is rea-
sonable because the magnitude of mean inflow velocity to the sta-
tor does not vary greatly along its span, and there is no reason
to believe that the rotor wake structure undergoes substan-
tial changes between the hub and tip. Unfortunately, no pressure
sensors were located in the middle or hub region of the vane, and
therefore, this assumption has not been experimentally verified.
Assuming that the magnitude of the load remains relatively con-
stant, it is clear from Figure 27 that the tip region of the vane
will radiate most strongly because the trace speed is supersonic
and accelerating.

The above considerations indicate that the assumption of
spanwise coherence of the acoustic sources for the stator is in-
appropriate. However, the region of significant radiation is
confined to the tip area of the stator. Due to its small size,
as indicated in Figures 26 and 27, the acoustic sources in this
tip region are essentially coherent, at least for the lowest cir-
cumferential harmonics of rotor wake structure. Thus, in the
following sections, the prediction method is exercised on the
assumption that the tip region of the vanes is the dominant noise
source and that this source behaves in a coherent, compact manner
which is consistent with the method. Because these sources
occupy only a small portion of the acoustically non-compact duct,
the predicted results for the free rotor case may be more repre-
sentative than those for a ducted rotor.

## Characterization of the Aerodynamic Response

On both the rotor and stator, pressure measurements were made
only at discrete points on the blades and vanes. The strength of
the acoustic dipole sources in the prediction method are related
to the net unsteady forces. Ideally, in order to estimate the
total forces, it is necessary to utilize information about func-
tional form of the load distribution in the spanwise and chordwise
directions. This information could come from a theoretical model
for the unsteady aerodynamic response. Many effects could be
accounted for in such a model, including spanwise and chordwise
wave number, cascade geometry, compressibility, etc. Analytical
models of the aerodynamic response which include these effects
tend to be quite complicated, and the results often cannot be
expressed in simple form.

In the present case, there is only a limited amount of reliable lift data, particularly on the rotor. Thus a refined procedure to determine the net unsteady loads is not justifiable. Furthermore, the available data shows that the reliable lift loads at different parts do not differ significantly, i.e., they tend to be within a couple of decibels. Other sources of error in the noise prediction are found to be more significant. Therefore, the unsteady load distribution has been treated as a constant value over the regions in which radiation occurs.

## Analytical Procedures

Following the approach of Heller and Widnall (1972), the method assures a point dipole model and a flat, two dimensional geometry in place of the cylindrical geometry of a ducted compressor. Some important results of the method are first reviewed. Then the procedure for estimating the noise generated by the rotor-wake/stator-vane interaction is described. Next the procedure for estimating the noise generated by the interaction between the rotor and the distorted inflow is described. This latter topic was not as extensively discussed by Heller and Widnall, hence a unified presentation of the two noise generation mechanisms is deemed worthwhile. The actual comparison between predicted and measured results is made in the next section.

*Nomenclature and Some Useful Mathematical Identities*

As in Heller and Widnall (1972), the x-direction denotes the axial or mean-flow direction in the compressor and the y-direction denotes the "straightened-out" or developed version of the circumferential direction in the compressor. Both the rotor and the stator are modelled as arrays of infinite extent in the y-direction. The respective inter-element spacings $d_r$ and $d_s$ for the rotor and stator are given by:

$$d_r = \frac{2\pi R_o}{B} \,, \tag{10}$$

$$d_s = \frac{2\pi R_o}{V} \,, \tag{11}$$

where $R_o$ is the effective radial location of the point forces acting on the rotor or stator blades, and B and V are the number of rotor blades and stator vanes, respectively.

The motion of the rotor blades and of the wakes shed by the rotor blades is represented by a uniform rectilinear motion of velocity u in the y-direction,

$$u = \Omega R_o \qquad (12)$$

where $\Omega$ is the shaft rotation speed in radians/sec. The blade passage frequency $\omega_r$, in radians/sec, is given by:

$$\omega_r = \Omega B = \frac{2\pi u}{d_r} \qquad (13)$$

The following three mathematical results are useful in deriving the necessary Fourier transforms. Throughout, unless otherwise stated, all the summations and integrals range from $-\infty$ to $+\infty$.

(1) If

$$\tilde{f}\left(k_y\right) = \frac{1}{2\pi}\int f(y)e^{-ik_y y}dy \qquad (14)$$

is the Fourier transform of $f(y)$, then $\tilde{f}\left(k_y\right)e^{-ik_y\delta}$ is the Fourier transform of $f(y-\delta)$. Similarly, if

$$\tilde{f}(\omega) = \frac{1}{2\pi}\int f(t)\, e^{i\omega t}dt \qquad (15)$$

is the Fourier transform of $f(t)$, then $\tilde{f}(\omega)\, e^{i\omega t}$ is the Fourier transform of $f(t-\tau)$.

(2)

$$\delta(ay) = \frac{1}{a}\delta(y) = \frac{1}{a}\delta(-y) \qquad (16)$$

where $\delta$ is the Dirac delta function and a is a constant. In particular,

$$\delta\left(\omega-k_y u\right) = \frac{1}{u}\delta\left(k_y - \frac{\omega}{u}\right) \qquad (17)$$

(3)

$$\sum_j e^{\pm i k_y d j} = \frac{2\pi}{d} \sum_m \delta\left(k_y - \frac{2\pi m}{d}\right) \qquad . \quad (18)$$

*Rotor-Wake/Stator-Vane Interaction*

Let $f(t)$ denote the time history of the fluctuating lift produced at each stator vane due to impingement of one rotor wake. The $\ell(t)$, the lift due to impingement of a series of equi-spaced identical wakes, is given by:

$$\ell(t) = \sum_j f\left(t - \frac{j d_r}{u}\right) \qquad (19)$$

Then $\tilde{\ell}(\omega)$, the Fourier transform of $\ell(t)$, can be expressed as:

$$\tilde{\ell}(\omega) = \frac{1}{2\pi} \int \ell(t) \, e^{i\omega t} dt, \qquad (20)$$

$$= \omega_r \, \tilde{f}(\omega) \sum_m \delta\left(\omega - m\omega_r\right) \qquad (21)$$

where $\tilde{f}(\omega)$ is the Fourier transform of $f(t)$ (see Eq. 15). Note that $\tilde{\ell}(\omega)$ gives the frequency content of the fluctuating lift as measured on a stator blade.

Similarly, the fluctuating lift $s(y,t)$ per unit length in the y direction on the stator is given by:

$$s(y,t) = \sum_\ell \sum_j f\left(t - \frac{j d_r}{u} - \frac{y}{u}\right) \delta\left(y - \ell d_s\right) \quad (22)$$

The term involving f in the above equation states that the generating mechanism of the lift field (the wakes shed by the rotor) is periodic in the y-direction with an interval $d_r$ and that it is moving in the positive y-direction with a constant velocity u. The second term involving the $\delta$ function states that the lift field is concentrated periodically at fixed point locations in

72

the y direction spaced $d_s$ apart. Consider the Fourier transform $\tilde{s}(k_y,\omega)$ of $s(y,t)$ in order to make an analogous examination of the wavenumber-frequency content of the stator lift field.

$$\tilde{s}\left(k_y,\omega\right) = \frac{1}{(2\pi)^2}\iint s(y,t)\ e^{-i(k_yy-\omega t)}\ \ dy\ dt \tag{23}$$

$$= \left\{\omega_r\ \tilde{f}(\omega)\sum_m \delta\left(\omega-m\omega_r\right)\right\}\frac{1}{d_s}\sum_n \delta\left(k_y - \frac{\omega}{u} - \frac{2\pi n}{d_s}\right) \tag{24}$$

$$= \tilde{\ell}(\omega)\ \frac{1}{d_s}\sum_n \delta\left(k_y - \frac{\omega}{u} - \frac{2\pi n}{d_s}\right) \tag{25}$$

The spectral content of $\tilde{s}(k_y,\omega)$ is sketched in Fig. 28. The circular dots in Fig. 28 lie on the straight line $\omega = k_y u$, corresponding to the term $n = 0$ in Eq. 25. These dots are separated by $\omega_r$ in frequency and by $2\pi/d_r$ in wavenumber. These dots denote essentially the wavenumber-frequency content of the rotor wake train in absence of the stator. For $u<c$, these dots lie outside the radiation region $|k_y| \leq k = \frac{\omega}{c}$, shown shaded in Fig. 28. Here c is the sound speed and k is the acoustic wavenumber magnitude.

The crosses in Fig. 28 are spaced at wavenumber separations of $2\pi/d_s$ from the circular dots and denote the presence of the stator as a scattering array. The crosses that fall in the shaded radiation region denote harmonics that can radiate to the far field, those falling outside the radiation region denote harmonics suffering "duct" cut-off.

The amplitude associated with a harmonic of Eq. 25 is $\tilde{\ell}(\omega)/d_s$. This amplitude when multiplied by $\cos\beta$ gives the drag component of the harmonic, and when multiplied by $\sin\beta$ gives the thrust component of the harmonic. Here $\beta$ is the setting angle of the stator blade at the relevant radial location. When considering the acoustic power radiated to the far field, these amplitudes must of course be replaced by squared quantities or spectral values such as:

73
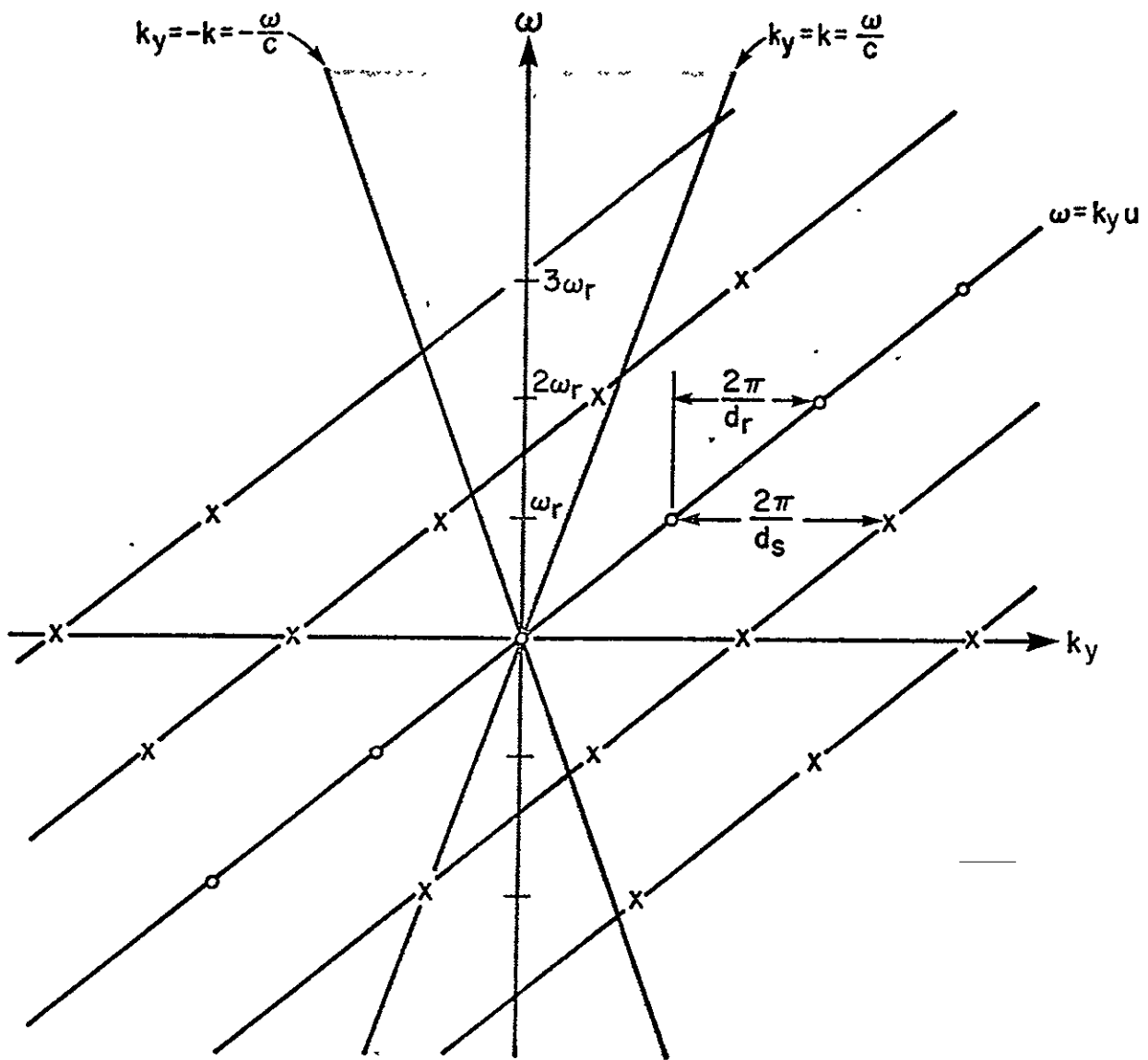
FIG. 28.   SKETCH ILLUSTRATING THE SPECTRAL CONTENT OF
$\tilde{S}(k_y,\omega)$

$$\frac{\phi_\ell(\omega) \cos^2\beta}{d_s^2} \quad \text{and} \quad \frac{\phi_\ell(\omega) \sin^2\beta}{d_s^2} \ .$$

Thus, using the results of Heller and Widnall, the frequency density $\phi_{\Pi rad}(\omega)$ of the acoustic power radiated by a harmonic (for $|k_y| < k$) is given by:

$$\phi_{\Pi rad}(\omega) = \frac{\pi R_0}{2m\rho ck} \ \frac{\phi_\ell(\omega)}{d_s^2} \left[ \frac{\left(k^2 - k_y^2\right)}{m} \sin^2\beta + k_y^2 \cos^2\beta \right], \quad (26)$$

where $\rho$ is the medium density, $\phi_\ell(\omega)$ is the frequency spectral density of the fluctuating lift at a stator blade, and $m = 2$ if the stator is located in a free-field environment, and $m = 1$ if the stator is confined in a semi-infinite duct. We note that Eq. 26 includes power radiated to both the upstream and downstream of the stator.

When more than one mode radiates to the far field at the same frequency, the far-field pressure may exhibit the influence of interference effects between the radiating modes, however, when computing the acoustic power radiated by these modes, the interference terms average out to zero. Hence, the acoustic power radiated is just the sum of the powers radiated by the individual modes.

The effective "dipole strength" or the spectrum $\phi_\ell(\omega)$ in Eq. 26 of the fluctuating lift at the stator blades is estimated from the following items of data:

(1) Frequency spectral densities $\phi_{dp}(\omega)$ of the fluctuating lift-density field (or differential-pressure field) at the stator at blade passage frequency $\omega_r$ and its harmonics.

(2) Trace speeds of rotor wakes along the stator blade spans. Only spanwise lengths $\ell_s$ where the trace speeds are supersonic are included in the calculation. These lengths $\ell_s$ invariably fall at

the tip region of the stator blade spans. Chordwise length scales $\ell_{ch}$ are taken to be the same as the stator blade chord lengths.

(3) Spanwise and chordwise coherency length scales $L_s$ and $L_{ch}$ of stator lift-density field at the blade passage frequency.

Even under the assumption that the $L_s$ and $L_{ch}$ vary inversely with frequency (a type of "similarity" hypothesis), the dimensions $\ell_s$ and $\ell_{ch}$ of the effective radiating area from a stator blade turn out to be smaller than, or comparable to, the coherency length scales $L_s$ and $L_{ch}$ for frequencies as high as $4\omega_r$. This conclusion is based on computing a length scale based on the square root of the coherence function curve shown in Fig. 21; the square root is taken in order to properly represent the behavior of the actual pressure field. Thus the effective sources at the stator tips are more or less *statistically* coherent, even though not necessarily acoustically compact.

Thus, for the frequency range of interest, $\phi_\ell(\omega)$ of Eq. 26 is given simply by:

$$\phi_\ell(\omega) = \phi_{dp}(\omega) \ (\ell_s \ell_{ch})^2 \ . \qquad (27)$$

The spectral density of the radiated power of Eq. 26 is finally converted into the spectral density $\Phi_p(\omega)$ of far-field pressure assuming isotropic spreading over a hemisphere of radius S. Thus,

$$\phi_p(\omega) = \phi_{\pi_{rad}}(\omega)\frac{\rho c}{2\pi S^2} \qquad \qquad (28)$$

*Inflow-Distortion/Rotor-Blade Interaction*

Let
$$f(t) = q(y)\big|_{y \ = \ ut} \qquad (29)$$

denote the time history of the fluctuating lift at a rotor blade due to interaction with steady inflow distortion during one full revolution. Since the flow distortion is considered steady, the pattern f(t) repeats after every time interval $\frac{2\pi}{\Omega}$, and the corresponding spatial pattern q(y) repeats after every spatial interval $2\pi R_o$. Hence the fluctuating lift $\ell(t)$ as measured at a rotor blade is given by:

76

$$\ell(t) = \sum_j f\left(t - j\frac{2\pi}{\Omega}\right) \tag{30}$$

$$= \sum_j q(ut - j2\pi R_o) \tag{31}$$

and $\tilde{\ell}(\omega)$, the Fourier transform of $\ell(t)$, is

$$\tilde{\ell}(\omega) = \frac{1}{2\pi} \int \ell(t) e^{i\omega t} dt \tag{32}$$

$$= \Omega \tilde{f}(\omega) \sum_m \delta(\omega - m\Omega) \tag{33}$$

$$= \Omega \frac{\tilde{q}}{u}(-\omega/u) \sum_m \delta(-\omega - m\Omega) \tag{34}$$

Here $\tilde{f}(\omega)$ is the (frequency) Fourier transform of $f(t)$ (see Eq. 15), and $\tilde{q}(ky)$ is the (wavenumber) Fourier transform of $q(y)$ (see Eq. 14). $\tilde{\ell}(\omega)$ gives the frequency content of the fluctuating lift as measured on a (rotating) rotor blade.

The fluctuating lift field $r(y,t)$ per unit length in the y direction *at* the rotor location (rather than moving *on* the rotating rotor) is given by:

$$r(y,t) = \sum_\ell \sum_j q(y - j2\pi R_o) \, \delta(y - \ell d_r - ut) \tag{35}$$

where the y-direction corresponds to the circumferential direction in the fan. The first term involving the q in the above equation states, as noted above, that the generating mechanism of the lift field (the steady inflow distortion) is periodic in the y-direction with an interval $2\pi R_o$ and is fixed in space. The second term involving the $\delta$ function states that the lift field is concentrated periodically at point locations in the y-direction spaced $d_r$ apart and that these point locations are moving in the y-direction with velocity u.

Consider the Fourier transform $\tilde{r}(k_y,\omega)$ of $r(y,t)$ in order to examine the wavenumber-frequency content of the rotor lift field.

$$\tilde{r}(k_y,\omega) = \frac{1}{(2\pi)^2}\iint r(y,t)e^{-i(k_y y - \omega t)}dy\ dt \qquad (36)$$

$$=\left\{\Omega\frac{1}{u}\tilde{q}\left(k_y - \frac{\omega}{u}\right)\sum_m \delta\left(k_y u - \omega - m\Omega\right)\right\}\frac{1}{d_r}\sum_n \delta\left(\frac{\omega}{u} - \frac{n\omega_r}{u}\right) \qquad (37)$$

$$= \tilde{\ell}\left(\omega - k_y u\right)\frac{1}{d_r}\sum_n \delta\left(\frac{\omega}{u} - \frac{n\omega_r}{u}\right) \qquad (38)$$

Note that in Eq. 37, as in Eq. 24, there are two infinite series of $\delta$ functions; one of these $\delta$ functions must have frequency as its argument, the other the wavenumber. The choice of the frequency argument of the $\delta$ functions in the curly brackets was fixed by the requirement of seeking connection with the measured lift spectrum $\tilde{\ell}(\omega)$ of Eq. 34. Hence the argument of the $\delta$ functions in Eq. 38 is formally the wavenumber.

The discrete frequency spectral content of $\tilde{\ell}(\omega)$ is sketched in Fig. 29, where lines A, B, C are identified. These same lines are shown by crosses in Fig. 30, where the spectral content of $\tilde{r}(k_y,\omega)$ is sketched. According to Eq. 38 these lines have a slope of $\frac{\omega}{k_y} = u$ in the $(\omega - k_y)$ plane. According to Eq. 38, also, all the rotor harmonics, whether they radiate to the far field or not, are restricted to the blade passage frequency $\omega_r$ and its harmonics. These harmonics are shown by crosses in the $\omega - k_y$ plane of Fig. 29 and are spaced at wavenumber separations of $\frac{1}{R_o}$. Only the crosses that fall in the shaded radiation region in Fig. 30, defined by $|k_y| \le k = \frac{\Omega}{c}$, correspond to rotor harmonics that radiate to the far field.

The following features of the inflow-distortion/rotor-blade interaction are novel and differ from the rotor-wake/stator-vane interaction:

(1) The amplitude for a rotor harmonic at frequency $n\omega_r$ and wavenumber $k_y$ is, according to Eq. 38, $\tilde{\ell}(n\omega_r - k_y u)/d_r$ rather than $\tilde{\ell}(n\omega_r)/d_r$.

78
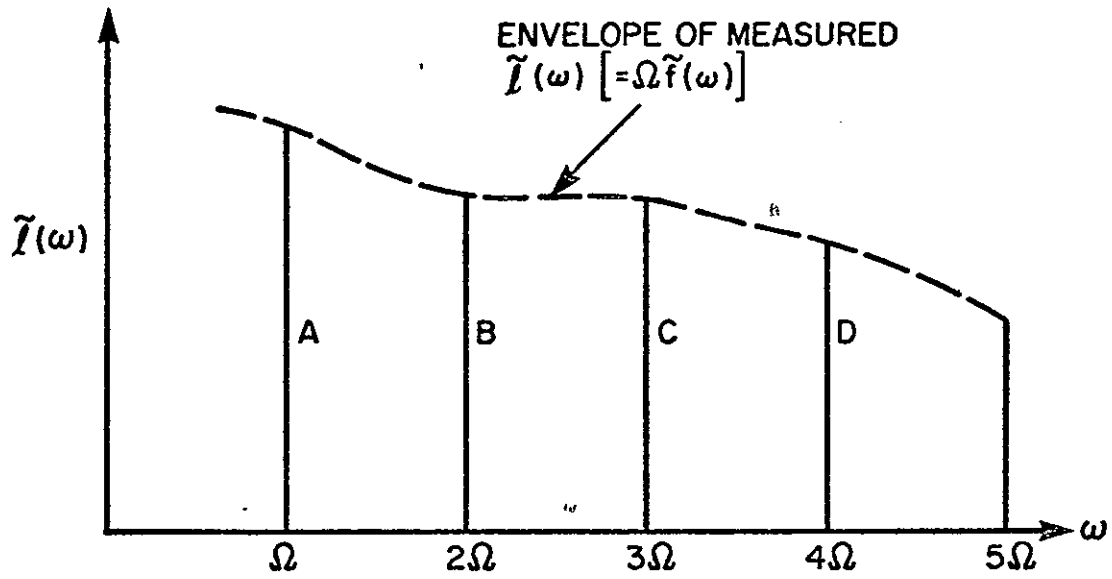
FIG. 29. TYPICAL DISCRETE FREQUENCY CONTENT $\tilde{\ell}(\omega)$ OF
FLUCTUATING LIFT ON A ROTOR BLADE.
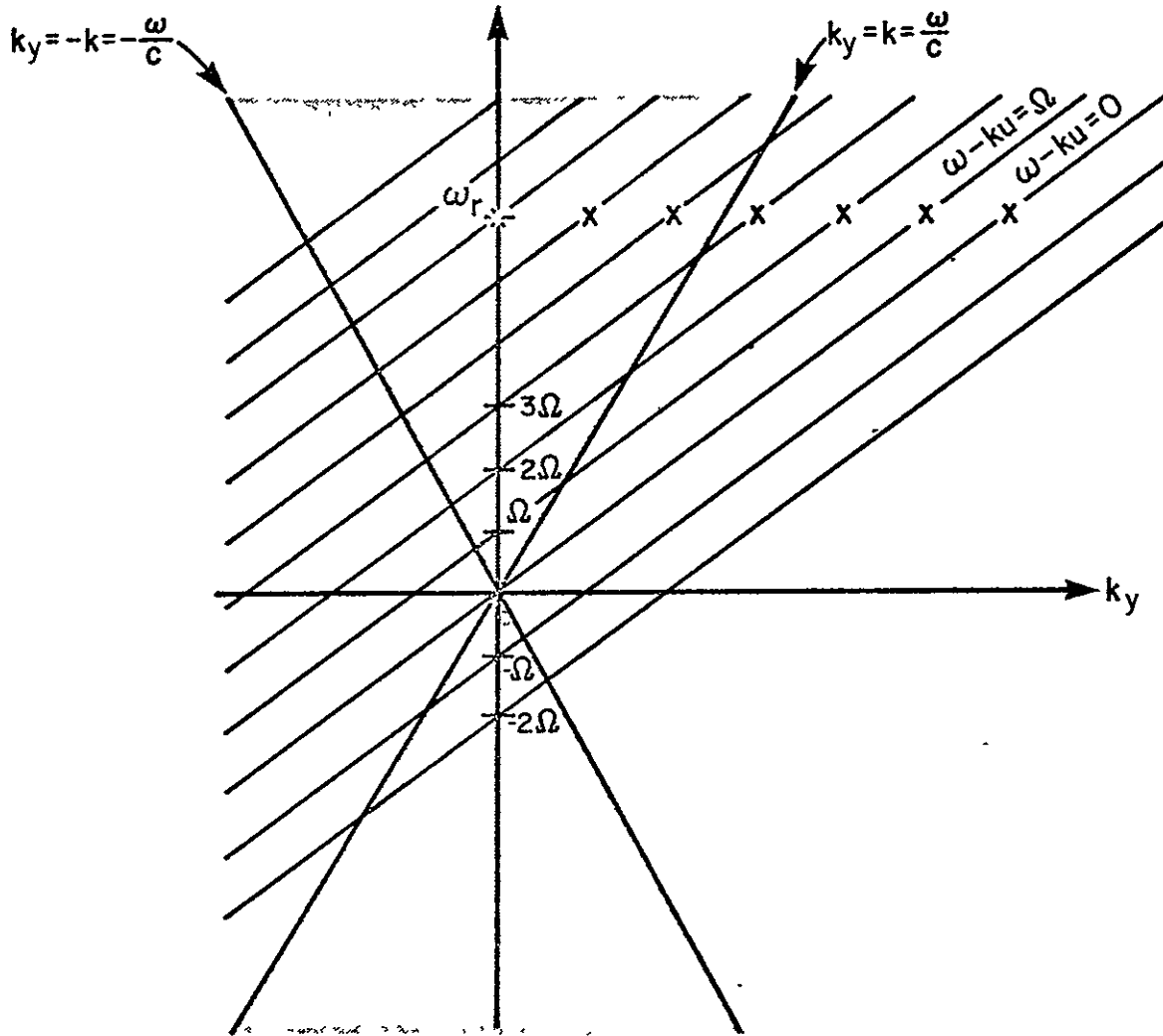
FIG. 30.   SKETCH ILLUSTRATING THE SPECTRAL CONTENT OF
$\tilde{r}(k_y, \omega)$.

(2)  The discrete frequency noise at $n\omega_r$ is caused by a multitude of rotor harmonics, with wavenumbers $k_y$ of 0, $\pm 1/R_o$, $\pm 2/R_o$ . . . ., $\pm m/R_o$, and corresponding amplitudes of $\tilde{\ell}(n\omega_r)/d_r$, $\tilde{\ell}(n\omega_r \pm \Omega)/d_r$, . . . .$\tilde{\ell}(n\omega_r \pm m\Omega)/d_r$.  The total number $(2m + 1)$ of these harmonics is given approximately by:

$$2m + 1 \simeq \frac{2n\omega_r}{c} R_o \qquad (39)$$

The contributions of all the other harmonics are cut-off.

If we replace the term $d_s^2$ in Eq. 26 by $d_r^2$, then that equation and the discussion related to it apply for the rotor harmonics as well.  As before, when more than one rotor harmonic radiates to the far field at the same frequency, the radiated acoustic power is the sum of the powers radiated by the indivi- dual harmonics.  However, in the present situation, far too many harmonics radiate.  For example, using typical values in Eq. 39, even for $n = 1$ (i.e., at the blade passage frequency), $2m + 1 \simeq 75$. Moreover, the amplitudes of the individual rotor harmonics do not vary substantially; in other words, the envelopes of the measured lift spectra (see Fig. 29) vary rather smoothly with frequency.

Hence, instead of summing over the various harmonics, an equivalent integration over wavenumber $k_y$ is performed to get the total power radiated.  The integral can be expressed as:

$$\phi_{\Pi_{rad}}(\omega) \simeq R_o \frac{\pi R_o}{2m\rho ck} \frac{<\phi_\ell(\omega)>}{d_r^2} \int_{-k}^{k} \left[ \frac{\left(k^2 - k_y^2\right)}{m} \sin^2\beta + k_y^2\cos^2\beta \right] dk_y \qquad (40)$$

where$<\phi_\ell(\omega)>$ is the "average" value of the fluctuating lift spectrum at the rotor blade, the average being performed over an appropriate frequency band around $\omega$.  The simple integration of Eq. 40 yields:

$$\phi_{\Pi_{rad}}(\omega) \simeq \frac{\pi R_o^2}{m\rho ck} \frac{<\phi_\ell(\omega)>}{d_r^2} \frac{2}{3} k^3 \left[ \frac{2}{m} \sin^2\beta + \cos^2\beta \right] \qquad (41)$$

Trivially modified versions of Eqs. 27 and 28 apply here as well, excepting that in the case of the rotor, one has to work with much scantier data for estimating the length scales $\ell_s$ and $\ell_{ch}$ of Eq. 27.

## Prediction of Sound Power Levels

Using the results of the previous section, the sound power levels for the first few harmonics of blade passage frequency can now be predicted. The levels due to rotor-wake/stator-vane interaction and due to inflow-distortion/rotor-blade interaction are predicted separately. As will be seen, the comparison with measured levels is not particularly encouraging, especially for the inflow-distortion/rotor-blade interaction. The difference between predicted and measured levels increases for the higher harmonics of blade passage frequency. A similar lack of agreement is evident in some of the results contained in the original work by Heller and Widnall (1972).

### *Rotor-Wake/Stator-Vane Interaction*

The discrete freqeuncy noise from the stator for Case 1 (80% speed) is now evaluated. The following numerical values are used in Eqs. 26, 27 and 28.

$$B = 53$$

$$V = 112$$

$$R_0 = (\text{stator tip radius}) = - \frac{\ell_s}{2}$$

$$= 2.83 - \frac{0.23}{2} = 2.715 \text{ ft}$$

$$\ell_s = 0.205 \text{ ft}$$

$$\ell_{ch} = 0.224 \text{ ft}$$

$$f_r = \frac{\omega_r}{2\pi} = 2400 \text{ Hz}$$

$$\beta \simeq 35°$$

$$S = 100 \text{ ft}$$

$$m = \begin{cases} 1 \text{ rotor confined to a semi-infinite duct} \\ 2 \text{ rotor in a free field} \end{cases}$$

Table 11 summarizes the results. Column L shows "average" values of differential pressure spectra on stator blades obtained by NASA. All numbers refer to the values of tonal peaks in the spectrum and are in units of dB re 0.0002 µbar/Hz. These levels were taken from the average decibel levels of the computed lift pressures S1/A5ℓ, S1/C1ℓ, and S1/C5ℓ, as presented in the Appendix.

Columns $P_{free}$ (for m = 2 in Eq. 26) and $P_{confined}$ (for m = 1 in Eq. 26) show the estimated far-field pressure spectra for a free stator and for a stator confined in a semi-infinite duct. Columns $P_{10-60}$ and $P_{70-160}$ show averaged decibel levels for the far-field pressure spectra, between 10°-60° and between 70°-160°, respectively, measured by NASA under relevant conditions (80% speed, radius S = 100 ft) and tabulated in the Appendix. Figure 31 illustrates the results of Table 11.

The stator is estimated not to radiate at all at the blade passage frequency $f_r$, whereas the measured far-field noise at $f_r$ is substantial. This result supports the belief that the measured far-field noise at blade passage frequency is contributed by the interaction of the steady inflow distortion with the rotor. The estimated noise at the second harmonic $2f_r$ compares reasonably well with the measured data.

However, the trend quoted above is reversed for higher harmonics. Estimated noise at $3f_r$ and $4f_r$ is seen to be higher than the measured noise, the difference becoming larger for the higher frequency. A similar trend, but of substantially larger magnitude is present also for the inflow-distortion/rotor-blade interaction.

TABLE 11.   COMPARISON OF PREDICTED AND MEASURED SOUND PRESSURE LEVELS AT THE FARFIELD MICROPHONES DUE TO ROTOR-WAKE/ STATOR-VANE INTERACTION.

| Frequency (Hz) | L | $P_{free}$ | $P_{confined}$ | $P_{10-60}$ | $P_{70-160}$ |
|---|---|---|---|---|---|
| 2400 | 154 | -- | -- | 100 | 94 |
| 4800 | 134 | 85.5 | 91.6 | 88 | 82 |
| 7200 | 130 | 89.0 | 93.4 | 78 | 75 |
| 9600 | 125 | 87.9 | 91.9 | 75 | 70 |

*Inflow-Distortion/Rotor-Blade Interaction*

The discrete frequency noise from the rotor for Case 1 - 80% speed is now evaluated, using the differential pressure spectrum RII/Al$\ell$, shown in Fig. 9c. The following numerical values were used.
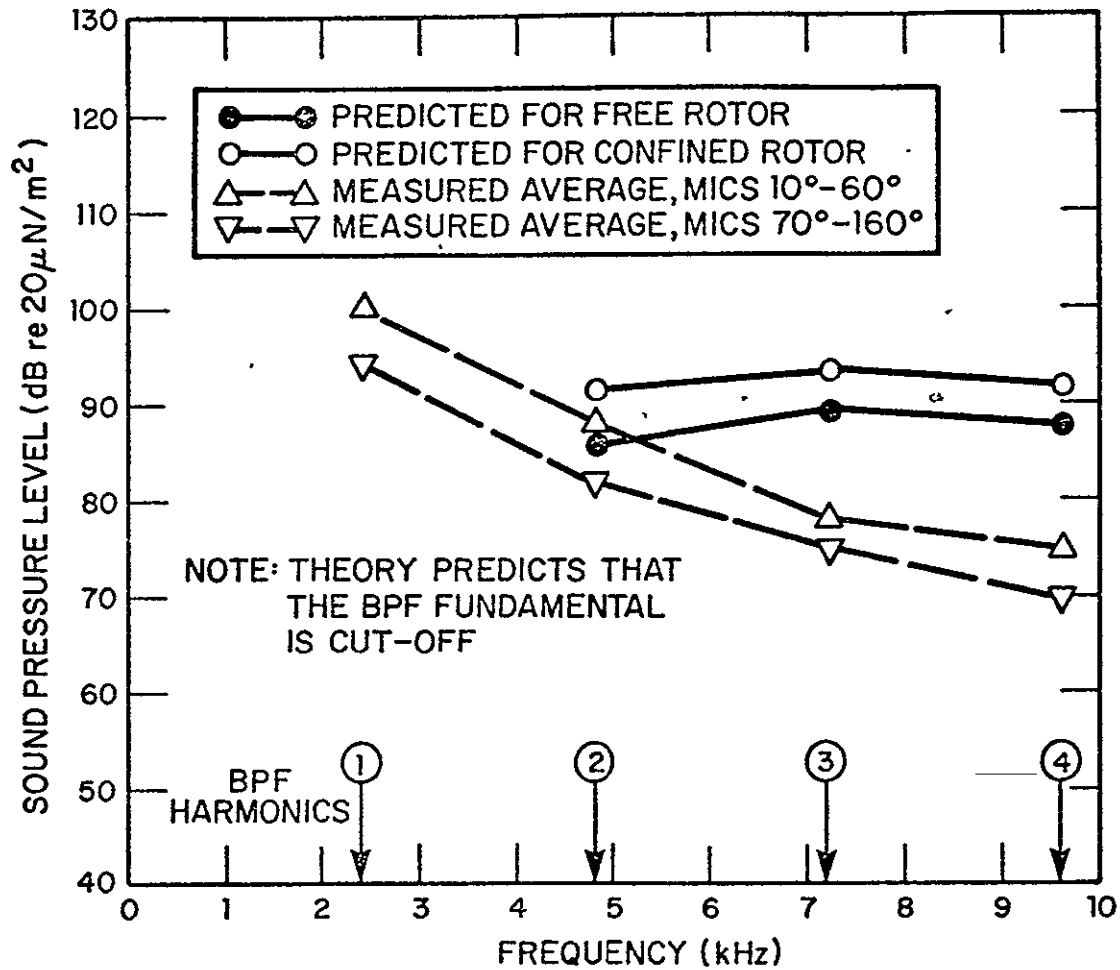
FIG. 31.  COMPARISON OF MEASURED SOUND PRESSURE LEVELS AT
THE FAR-FIELD MICROPHONES WITH PREDICTED LEVELS
DUE TO ROTOR-WAKE/STATOR-VANE INTERACTION.

84

C-2

$$B = 53$$

$$R_o = 2.81 \text{ ft}$$

$$f_r = 2400 \text{ Hz } (80\% \text{ speed})$$

$$\beta \simeq 40°$$

$$\ell_s = \ell_{ch} = 0.458 \text{ ft}$$

$$S = 100 \text{ ft}$$

Table 12 summarizes the results for the 80% speed case. Column <L> in Table 12 shows a frequency averaged value of differential pressure spectrum RII/Al$\ell$. $P_{confined}$ (for m = 1 in Eq. 41) and $P_{free}$ (for m = 2 in Eq. 41) are the estimated farfield pressure spectra under the respective assumptions concerning the rotor location. Only $P_{free}$ is shown in Table 12. $P_{confined}$ is related to $P_{free}$ by:

$$P_{confined} = P_{free} + 4.5 \text{ dB} \qquad (42)$$

Columns $P_{10-60}$ and $P_{70-160}$ in Table 12 are identical to the ones in Table 11.

TABLE 12.  COMPARISON OF PREDICTED AND MEASURED SOUND PRESSURE LEVELS AT THE FARFIELD MICROPHONES DUE TO INFLOW-DISTORTION/ ROTOR-BLADE INTERACTION AT 80% SPEED.

| Frequency (Hz) | <L> | $P_{free}$ | $P_{10-60}$ | $P_{70-160}$ |
|---|---|---|---|---|
| 2400 | 122 | 99.8 | 100 | 94 |
| 4800 | 116 | 99.8 | 88 | 82 |
| 7200 | 112 | 99.3 | 78 | 75 |
| 9600 | 110 | 99.8 | 75 | 70 |
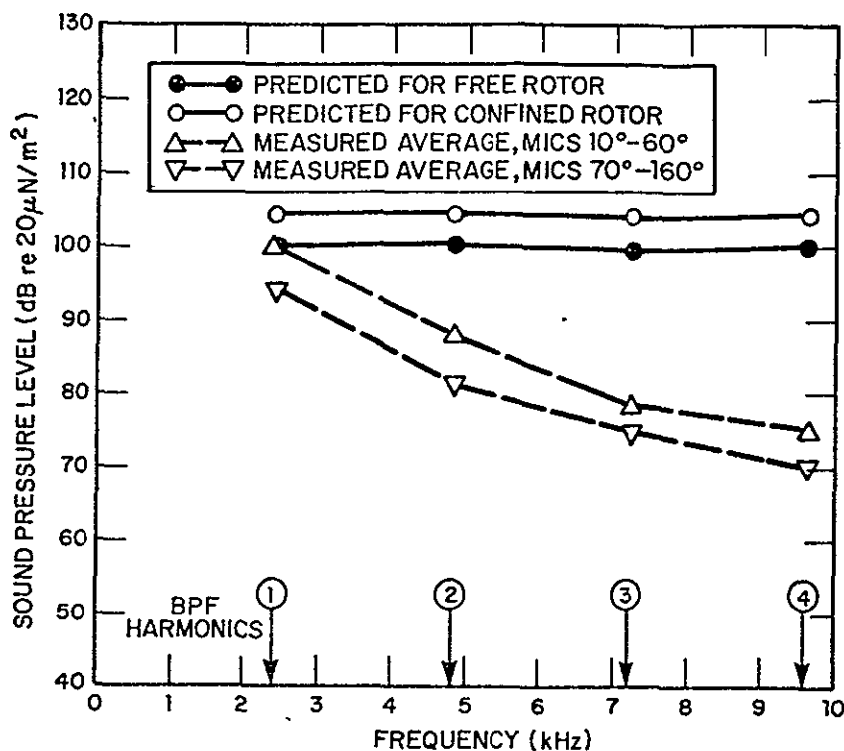
FIG. 32.    COMPARISON MEASURED SOUND PRESSURE LEVELS AT THE
FAR-FIELD MICROPHONES WITH PREDICTED LEVELS DUE TO
INFLOW-DISTORTION/ROTOR-BLADE INTERACTION
CASE 1, 80% SPEED.

As is evident from this table, the predicted results do not
agree well with the measured ones.  The disagreement is strongly
frequency dependent, thus precluding resolution on the basis of
incompatible calibrations or inappropriate choice of any frequency-
independent parameters such as $R_0$.  The extent of the disagreement
and its frequency dependence is displayed in Fig. 32.  The fre-
quency dependence of the difference between predicted and measured
levels is very strong, of the order of 30 dB per decade.

Discussion of Results

Considerable differences are evident between the predicted
results and the measured far field data.  Some differences in
level are to be expected considering the assumptions that have been
made and the uncertainties that are present.  Therefore, the
differences in the predicted and measured values for the lowest
harmonics are not viewed as being particularly serious.  However,
the significant difference in trend with increasing harmonic
number is disturbing.  The fact that the analytical model

86

overpredicts the far field levels with increasing frequency probably reflects the basic limitations of the method. This trend is much more severe for the rotor than for the stator. Some possible explanations for the discrepancy are given in this section. These can be classified as being of two types: factors affecting the accuracy of inputs to the method, and factors affecting the validity of the method itself.

*Accuracy of Inputs*

The question of the accuracy of inputs to the method centers on the values assumed for the net fluctuating forces. These values are affected by:

- the accuracy of the surface pressure measurements,

- the spanwise extent over which radiation occurs, and

- the assumed spanwise and chordwise unsteady load distribution.

Although there are clearly some discrepancies among the blade surface pressure data, it seems unlikely that this is the source of the problem. On both the rotor and stator, the data show consistent pressure signals at more than one location. Furthermore, the data seem to behave reasonably at higher harmonics.

The spanwise extent of radiation may be an important factor. On the stator, the portion of the span which is responsible for most of the radiation was chosen as being the region in which the spanwise trace speed of loads on the vane is supersonic and accelerating. Because the radiation efficiency of this region is not necessarily constant, the effective constant strength radiating area may be smaller. Furthermore, there may be force cancellation within the radiating area for higher harmonics of blade passage frequency, which are contributed by the higher circumferential harmonics of wake structure. Because the wakes are skewed, the higher circumferential harmonics lead to shorter lengths of the spanwise load distribution. When these wavelengths become shorter than the scale of the radiating region, then force cancellation will begin to occur. Indeed, this point also illustrates a basic limitation of the model, to receive more discussion later. This type of effect may be adequate, however, to explain the fact that

at higher harmonics the predicted sound power from the stator exceeds the far field power level estimated from the microphone data.

The spanwise extent of radiation for the rotor was chosen arbitrarily to be one blade chord. This dimension was chosen largely for reference purposes; there is insufficient rotor data to determine the spanwise scales of inflow disturbances. It is certain, however, that the important sources of radiation must be near the rotor tip where the relative velocity is largest due to the rotary component. The forces depend on the square of the relative velocity. The circumferential scale of inflow distortions is proportional to the inverse of the harmonic number of shaft speed. Assuming the spanwise scales are similar, the effective radiating area could be adjusted to be proportional to frequency (or even frequency squared), but even this correction is insufficient to explain the discrepancy. Note, however, that this area adjustment is not the same as accounting for force cancellation. Nor does it account for interaction of acoustic sources, which relates to the limitations of the prediction method.

Finally, the assumed spanwise and chordwise load distributions affect the accuracy of inputs. The effects of wavelength on the spanwise load distribution has already been mentioned above. The spanwise variation in magnitude has also been discussed. For the stator there is no reason to expect large spanwise variations in magnitude within the radiating region, nor are large variations indicated in the data. For the rotor, the spanwise variation in magnitude will vary as the relative velocity squared. Therefore, the magnitude decreases away from the tip region, but this variation is not particularly significant over the radiating area that has been assumed.

The lift data on the stator indicate that chordwise load variations cannot account for the overprediction of stator noise at the higher harmonics of blade passage frequency. The data show that the assumed constant chordwise load distribution will not lead to an error of more than a few decibels, even for the higher harmonics. Compare, for instance, the values of S1/A5ℓ, S1/C1ℓ, and S1/C5ℓ which are tabulated in the Appendix. Although less direct evidence is available, the same assumption can be expected to lead to errors much smaller than those required to explain the rapid increase of predicted rotor sound power level with frequency.

In summary, it is not believed that errors in the calculated inputs are responsible for the behavior of predicted sound power levels. The inputs have been calculated, however, in accordance with the assumptions of the prediction method. Namely, levels

have been obtained on the assumption that a constant, coherent, and acoustically compact unsteady load is responsible for the radiation. To the extent this is untrue, more elaborate means could be desired to correct the inputs to an equivalent unsteady load which would yield correct results when used in the prediction method. However, when this is required, it seems more reasonable and realistic to begin with a more refined prediction technique. Some limitations of the method which may explain the discrepancies in the present prediction are now discussed.

## Limitations of the Prediction Method

The question of basic limitations in the prediction method involves two related areas: the appropriateness of the blade-force/acoustic-source model; and the role of the duct acoustics. In fact, the role of these effects is such that the present method can reasonably be expected to predict levels equal to, or greater than, those actually encountered (assuming the noise sources are entirely of a dipole character).

As already mentioned, the load distribution within the radiating region of the stator span may be such that considerable cancellation of the net force occurs because the phase of the load distribution varies along the span. This effect will be especially important for higher harmonics. However, at the higher harmonics for which the radiating region can no longer be considered acoustically compact, the radiated sound power cannot be estimated by such a simple approach, particularly when the phase of the source varies along the span. Similarly, the assumption of acoustic compactness and phase coherence for sources on the rotor is questionable at the higher harmonics of blade passage frequency. Assuming the radial scale of disturbances entering the rotor is similar to the circumferential scale, then this condition can definitely occur on the rotor for higher harmonics. For the QF-1B, this basic limitation of the method may be more important for the rotor than for the stator, since the spanwise region of stator radiation is quite small. In any event, because the method assumes the sources are compact and coherent, the radiation efficiency of these sources will be overestimated. The overestimation will be most serious at higher harmonics. The difference between predicted and measured levels is consistent with this expectation.

Now consider the problem from the standpoint of duct acoustics. The propagation of acoustic modes in cylindrical and annular ducts has been discussed in detail by Tyler and Sofrin (1960). Spinning disturbance patterns are found to radiate when a certain

critical spinning mode (measured at the tip radius) is exceeded.
The modes can be described in terms of characteristic functions
which depend on the number of circumferential lobes, the hub/tip
ratio, and the radial order (number of radial nodes) of the
disturbance pattern. For a fixed lobe number and hub/tip ratio,
any radiating disturbance pattern can be described by a summation
of the characteristic functions over all radial orders. The
critical spinning speed at which radiation occurs for a disturbance
described by a given characteristic function depends on the lobe
number, the hub/tip ratio, and the radial order. This speed is
always supersonic. The speed required for radiation increases as
the radial order increases. Thus, even though a disturbance is
spinning at a given supersonic speed (measured at the tip radius),
it will not radiate if it corresponds exactly to a characteristic
function of a sufficiently high radial order.

In contrast, the prediction method ignores the effect of
radial order as the criterion for acoustic radiation. The under-
lying assumptions of the method make the condition for radiation
simply that the tip speed of a spinning disturbance becomes super-
sonic. The previous discussions have shown, however, that the
radial order of disturbances on both the rotor and stator is quite
high. For instance, six wake phase fronts were calculated to
intersect a given stator vane. Similarly for the rotor, assuming
the radial and circumferential disturbance length scales are
similar, the radial order can be estimated by:

$$\frac{r_{tip} - r_{hub}}{2\pi r_{tip}/q}$$

where q is the harmonic number of rotor shaft speed. Since radia-
tion occurs for harmonics centered around $q = nB$, the average
radial order for the nth harmonic of blade passage frequency is:

$$\frac{nB}{2\pi}\left(1 - \frac{r_{hub}}{r_{tip}}\right) \approx 4n$$

The above suggests that much of the acoustic excitation on
the QF-1B corresponds to duct modes of high radial order. Since
many of these duct modes will be cut-off, this effect may help
explain the discrepancy between the predicted and measured loads,
particularly the very large differences that occur for the rotor

90

levels at higher harmonics. In summary, on a fan such as the QF-1B, neglecting the effect of radial structure in the excitation of duct modes can potentially lead to serious errors. To verify that this effect is responsible for the difference in trend between predicted and measured results would require very detailed information about the rotor surface pressures and a very sophisticated analysis procedure.

# SUMMARY OF RESULTS

Because the text divides naturally into two parts, data analysis and noise prediction, many of the important results have been reviewed and summarized at the appropriate point in the test. However, the most important results obtained in these two areas are summarized below.

## Data Analysis

The spectra from the far field microphone data were reasonably typical of a fan stage operating at subsonic tip speed. Tones at the harmonics of blade passage frequency rise above a broadband distribution. Both the tonal and broadband levels decreased with increasing frequency, with the tones also becoming less prominant relative to the broadband. Tones at the harmonics of rotor shaft speed were also present but they had much lower levels and were often difficult to distinguish from the broadband distribution.

Unsteady surface pressures were measured on the rotor blades and stator vanes using flush-mounted sensors. Pressure spectra measured on the stator vane were qualitatively similar to the far field noise spectra except for the presence of numerous spurious peaks associated with vane vibration modes. The stator spectrum is produced primarily by the aerodynamic interaction of the vanes with rotor wake. The highest tone levels occurred again at blade passage frequency.

On the other hand, spectra measured by sensors on the moving rotor showed only the peaks at the harmonics of rotor shaft speed rising about a broadband distribution. This behavior occurs because the rotating sensor effectively surveys the (circumferential) harmonic structures of inflow distributions to the rotor. Since the pressures measured are predominantly aerodynamic rather than acoustic, the tone at blade passage frequency has no special distinction.

A number of analysis methods were tried to study the nature of tones in the spectra. The analysis showed that random turbulent processes play a very important role in the generation of fan noise tones. The most successful approach involved the use of probability density analysis which allows the determination of the relative contributions of periodic and random contributions to the tone levels. Time history studies of the blade passage frequency tones on the stator were also performed. The waveform was displayed after passing the signal through a narrowband filter centered on blade passage frequency.

92

The probability density analysis of isolated blade passage frequency tones on the stator indicated surprisingly little sinusoidal character. However, the time history studies showed that the waveform exhibits a systematic zero crossing behavior as compared to narrowband noise. The random character of the blade passage tones in the stator data indicates that the wakes striking the stator blades, although systematic in time, have a strongly stochastic amplitude character.

The rotor data tones at the harmonics of shaft rotation speed have probability characteristics which depend on harmonic number. A strong sinusoidal character was evident for the fundamental. The second harmonic was less sinusoidal than the fundamental, while the third harmonic was only slightly sinusoidal. The higher harmonics appeared as Gaussian noise, in spite of the fact that they stand out strongly in the spectral data.

The probability density analysis of blade passage tones in the far field microphone data showed these tones to be almost entirely Gaussian in character. Because the stator is cut off at the fundamental of blade passage frequency, this far field tone is due to the rotor alone. This fact helps to explain why the far field blade passage tone displays a greater degree of randomness than the corresponding stator surface pressure signals.

Coherence and time delay studies were made to learn more about the rotor-wake/stator-vane interaction. Spurious phase delays in the data prevented the use of the time delay information. However, useful coherence data was obtained showing that the spectral coherence of the blade passage tone falls off gradually to about 0.3 between the stator leading and trailing edge. In sufficient data was available to definitely confirm a similar trend in the spanwise direction.

Prediction Method

Unsteady pressure levels on the blades and vanes were used in a fan noise prediction method and the results were compared with the measured far field noise levels. The prediction method, developed by Heller and Widnall (1972), assumes that acoustic dipoles produced by the net unsteady forces on the blades and vanes are responsible for fan noise. Since the prediction method assumes spanwise coherent and acoustically compact sources, certain modifications were required to apply the method to the QF-1B fan configuration.

93

The rotor-wake/stator-vane interaction geometry was determined assuming that the wakes are convected with the mean flow. The swirl velocity component skews the rotor wake so that the hub region leads the top region. As a result, the interaction between the wakes and vanes is completely three-dimensional. For the QF-1B, it was found that six or more wakes simultaneously interact with a single vane. Using the interaction geometry, the trace speed of the wake phase fronts along the vane span was computed. Only the regions of the span for which the trace speed is supersonic or accelerating can be efficient radiators. The region near the vane tips was found to be the only region which meets this criterion. These radiating regions were therefore considered to be the only important radiating areas in the pre-determined stator noise radiation.

The interaction of the rotor blades with inflow distortions was treated in more detail in the original work by Heller and Widnall (1972). The present work shows that the only rotor sensor shaft speed harmonics which contribute to the harmonic of blade passage frequency is in a band centered around the harmonic at blade passage frequency. All the other harmonics are cut off.

The comparison of predicted and measured levels shows a general agreement for the lower harmonics. However, the predicted levels significantly exceed the measured levels at the higher harmonics. The sources of disagreement are believed to be related to the differences between the assumptions underlying the prediction method and the physical behavior of the actual fan configuration. The potential sources of disagreement were discussed in detail. It is believed that the inability of the prediction method to fully account for the lack of spanwise coherence as it effects the propagation of acoustic modes is an important contributor to the difference between predicted and measured values.

# REFERENCES

Bendat, J.S. and Piersol, A.G., *Random Data: Analysis and Measurement Procedures*, Wiley-Interscience, New York, 1971.

Chandiramani, K.L. and Smullin, J.I., "Design Techniques for Suppressing Discrete Frequency Noise from High Speed Compressors," to be published, 1976.

Hanson, D.B., "Spectrum of Rotor Noise Caused by Atmospheric Turbulence," *JASA*, 56, 1, pp 110-126, 1974.

Heller, H.H. and Widnall, S.E., "The Role of Fluctuating Forces in the Generation of Compressor Noise," NASA CR-2012, 1972.

Goldstein, A.W., Lucas, J.G. and Balombin, J.R., "Acoustic and Aerodynamic Performance of a 6-foot-diameter Fan for Turbofan Engines. II-Performance of QF-1 Fan in Nacelle Without Acoustic Suppression, NASA TN D-6080, 1970.

Leonard, B.R., Schmiedlin, R.F., Stakolich, E.G., and Neumann, H.E., "Acoustic and Aerodynamic Performance of a 6-foot-diameter Fan for Turbofan Engines. I-Design of Facility and QF-1 Fan," NASA TN-5877, 1970.

Povinelli, F.P., Dittmar, J.H. and Woodward, R.P., "Effects of Installation Caused Flow Distortion on Noise from a Fan Designed for Turbofan Engines," NASA TN D-7076, 1972.

Rice, S.E., "Mathematical Analysis of Random Data," *Selected Papers on Noise and Stochastic Processes*, edited by N. Wax, Dover Publications, New York, 1954.

Tyler, J.M. and Sofrin, T.G., "Axial Flow Compressor Noise Studies," Trans. *SAE*, Vol. 70, pp. 309-332, 1962.

APPENDIX

SUMMARY OF BLADE PASSAGE TONE LEVELS
ON THE STATOR BLADES AND IN THE FAR FIELD

TABLE A-1. SUMMARY OF BLADE PASSAGE TONE LEVELS IN STATOR BLADE
PRESSURE AND FAR FIELD NOISE DATA.

| Location | Pressure, Suction, Lift or Noise | Case No. | rpm (%) | Pressure Level in dB Vs. Frequency of Tone | | | |
|---|---|---|---|---|---|---|---|
| | | | | 1st tone | 2nd tone | 3rd tone | 4th tone |
| S1/A1 | suction | 2 | 60 | 140.7 | 122.1 | 130.3 | 121.9 |
| | | 2 | 70 | 130.1 | – | – | 125.6 |
| | | 2 | 80 | 136.3 | 126.0 | 127.1 | – |
| | | 1 | 80 | 140.0 | 127.0 | 122.8 | – |
| | | 2 | 90 | 146.7 | 139.2 | – | – |
| SI1/A1 | suction | 2 | 60 | 129.1 | 121.4 | – | – |
| | | 2 | 70 | 131.3 | 124.0 | – | – |
| | | 2 | 80 | 141.3 | – | – | – |
| | | 1 | 80 | 143.1 | 132.5 | – | – |
| | | 2 | 90 | 148.0 | 139.2 | – | – |
| SIII/A1 | suction | 2 | 60 | 138.4 | 128.4 | 127.1 | – |
| | | 2 | 70 | 137.7 | 128.4 | – | – |
| | | 2 | 80 | 144.2 | 136.5 | – | – |
| | | 1 | 80 | 148.8 | 134.9 | 130.0 | – |
| | | 2 | 90 | – | – | – | – |
| SI/A2 | pressure | 2 | 60 | 147.5 | 136.0 | 138.8 | 126.1 |
| | | 2 | 70 | 148.9 | 135.8 | 134.6 | 129.0 |
| | | 2 | 80 | 148.9 | 138.2 | 135.1 | 129.0 |
| | | 1 | 80 | 153.0 | 135.6 | 136.1 | 133.5 |
| | | 2 | 90 | 148.7 | 148.2 | 136.0 | – |
| | suction | 2 | 60 | 156.4 | 144.5 | 142.3 | – |
| | | 2 | 70 | 146.4 | 142.2 | 130.1 | 128.1 |
| | | 2 | 80 | 145.6 | 137.3 | – | – |
| | | 1 | 80 | – | – | – | – |
| | | 2 | 90 | 141.3 | – | – | – |
| | lift | 2 | 60 | 153.6 | 137.0 | 133.2 | 127.3 |
| | | 2 | 70 | 148.9 | 133.4 | 132.3 | 127.7 |
| | | 2 | 80 | 148.9 | 136.1 | 135.7 | 130.0 |
| | | 1 | 80 | – | – | – | – |
| | | 2 | 90 | 142.1 | 142.7 | 130.6 | – |

TABLE A-1. (*Continued*).

| Location | Pressure, Suction, Lift or Noise | Case No. | rpm (%) | Pressure Level in dB Vs. Frequency of Tone | | | |
|---|---|---|---|---|---|---|---|
| | | | | 1st tone | 2nd tone | 3rd tone | 4th tone |
| SI/A3 | pressure | 2 | 60 | 148.4 | 120.6 | 124.2 | – |
| | | 2 | 70 | 151.6 | 132.1 | 126.0 | 121.5 |
| | | 2 | 80 | 151.1 | 138.9 | 128.6 | 127.1 |
| | | 1 | 80 | 153.8 | 133.6 | 128.5 | 124.0 |
| | | 2 | 90 | 143.9 | 138.1 | 131.5 | – |
| SI/A4 | suction | 2 | 60 | 146.5 | 126.2 | 127.9 | 129.0 |
| | | 2 | 70 | 148.1 | 133.4 | 127.8 | 128.5 |
| | | 2 | 80 | 151.0 | 131.9 | 134.7 | 128.1 |
| | | 1 | 80 | 152.1 | 134.1 | 130.8 | – |
| | | 2 | 90 | 149.3 | 138.0 | 134.0 | – |
| SI/A5 | pressure | 2 | 60 | 127.3 | – | 114.4 | – |
| | | 2 | 70 | 129.9 | 117.8 | 111.8 | 111.2 |
| | | 2 | 80 | 134.1 | 118.0 | 114.3 | 107.4 |
| | | 1 | 80 | 150.5 | 132.6 | 132.0 | 122.2 |
| | | 2 | 90 | 135.3 | 125.7 | 113.5 | – |
| | section | 2 | 60 | 143.0 | 127.9 | 131.3 | 128.6 |
| | | 2 | 70 | 147.2 | 132.2 | – | 124.9 |
| | | 2 | 80 | 149.6 | 132.4 | 134.0 | 128.1 |
| | | 1 | 80 | 148.0 | 130.6 | 124.5 | 122.5 |
| | | 2 | 90 | 146.9 | 142.2 | 130.7 | – |
| | lift | 2 | 60 | 141.1 | 121.2 | 126.3 | 122.2 |
| | | 2 | 70 | 142.2 | 128.8 | – | 117.7 |
| | | 2 | 80 | 146.3 | 130.0 | 131.7 | 126.9 |
| | | 1 | 80 | 153.5 | 132.0 | 130.3 | 126.0 |
| | | 2 | 90 | 143.1 | 139.8 | 127.9 | – |
| SI/B1 | pressure* | 2 | 60 | 80.5 | – | 78.4 | – |
| | | 2 | 70 | 79.1 | 73.3 | – | – |
| | | 1 | 80 | 156.0 | 135.0 | 130.8 | 125.0 |
| | | 2 | 90 | 96.9 | 83.7 | – | – |

*Data between Case 1 and Case 2 are inconsistent.

TABLE A-1. (*Continued*).

| Location | Pressure, Suction, Lift or Noise | Case No. | rpm (%) | Pressure Level in dB Vs. Frequency of Tone | | | |
|---|---|---|---|---|---|---|---|
| | | | | 1st tone | 2nd tone | 3rd tone | 4th tone |
| SI/B1 | suction | 2 | 60 | 153.5 | – | 143.8 | 142.7 |
| | | 2 | 70 | 151.1 | 141.1 | – | 150.3 |
| | | 2 | 80 | 160.3 | 143.2 | 150.6 | – |
| | | 1 | 80 | 147.2 | 126.2 | – | – |
| | | 2 | 90 | 164.4 | 153.8 | 139.1 | – |
| | lift | 2 | 60 | 149.0 | – | 138.1 | 137.9 |
| | | 2 | 70 | – | – | – | – |
| | | 2 | 80 | – | – | – | – |
| | | 1 | 80 | 163.3 | 139.1 | – | – |
| | | 2 | 90 | – | – | – | – |
| SI/C1 | pressure | 2 | 60 | 138.3 | 126.3 | 128.9 | 117.1 |
| | | 2 | 70 | 144.3 | 130.9 | 123.4 | 122.5 |
| | | 2 | 80 | 151.4 | 134.0 | 129.3 | 124.0 |
| | | 1 | 80 | 153.2 | 134.2 | 130.3 | 125.0 |
| | | 2 | 90 | 144.9 | 140.1 | 131.1 | – |
| | suction | 2 | 60 | 144.0 | 127.1 | 123.1 | – |
| | | 2 | 70 | 143.8 | 135.0 | – | – |
| | | 2 | 80 | 157.8 | 139.2 | 129.7 | – |
| | | 1 | 80 | 155.7 | 136.0 | – | – |
| | | 2 | 90 | 150.1 | 144.2 | 133.2 | – |
| | lift | 2 | 60 | 140.5 | 125.4 | 129.3 | 117.9 |
| | | 2 | 70 | 144.2 | 131.0 | 123.1 | – |
| | | 2 | 80 | – | – | – | – |
| | | 1 | 80 | 153.7 | 135.8 | 129.9 | 125.7 |
| | | 2 | 90 | 147.3 | 140.4 | 134.2 | – |

TABLE A-1.  (*Continued*).

| Location | Pressure, Suction, Lift or Noise | Case No. | rpm (%) | Pressure Level in dB Vs. Frequency of Tone | | | |
|---|---|---|---|---|---|---|---|
| | | | | 1st tone | 2nd tone | 3rd tone | 4th tone |
| SI/C2 | pressure | 2 | 60 | 142.0 | 124.8 | 121.3 | 121.1 |
| | | 2 | 70 | 143.1 | 132.9 | 124.1 | 124.5 |
| | | 2 | 80 | 146.5 | 133.4 | 129.1 | 122.8 |
| | | 1 | 80 | 150.3 | 134.0 | 129.8 | 123.5 |
| | | 2 | 90 | 145.1 | 136.6 | 133.5 | – |
| | suction | 2 | 60 | 141.8 | 119.2 | 118.8 | 108.5 |
| | | 2 | 70 | 141.8 | 126.1 | 118.1 | 111.2 |
| | | 2 | 80 | 136.6 | 127.1 | 121.7 | – |
| | | 1 | 80 | – | – | – | – |
| | | 2 | 90 | 153.5 | 142.8 | – | – |
| | lift | 2 | 60 | 140.0 | 118.6 | 116.6 | 112.0 |
| | | 2 | 70 | 137.0 | 124.1 | 116.0 | 114.9 |
| | | 2 | 80 | 146.0 | 134.9 | 129.9 | 123.7 |
| | | 1 | 80 | – | – | – | – |
| | | 2 | 90 | 151.0 | 144.3 | 135.3 | – |
| SI/C5 | pressure | 2 | 60 | 142.0 | 122.3 | 128.0 | 122.7 |
| | | 2 | 70 | 138.0 | 128.3 | 124.2 | 125.0 |
| | | 2 | 80 | 142.0 | 131.1 | 131.2 | 119.1 |
| | | 1 | 80 | 148.2 | 132.9 | 129.2 | 119.0 |
| | | 2 | 90 | 146.1 | 139.0 | 127.6 | – |
| | suction | 2 | 60 | 141.9 | – | 132.3 | 122.4 |
| | | 2 | 70 | 139.0 | 131.1 | – | 130.7 |
| | | 2 | 80 | 145.0 | 131.1 | 131.0 | – |
| | | 1 | 80 | 149.0 | 131.8 | 124.8 | 123.8 |
| | | 2 | 90 | 150.1 | 143.1 | 131.0 | – |
| | lift | 2 | 60 | 138.7 | 119.9 | 116.6 | 111.7 |
| | | 2 | 70 | 138.2 | 129.1 | – | 128.8 |
| | | 2 | 80 | 154.1 | 142.2 | 142.1 | – |
| | | 1 | 80 | 154.0 | 134.8 | 128.8 | – |
| | | 2 | 90 | 151.2 | 143.9 | 129.7 | – |

TABLE A-1.  (*Continued*).

| Location | Pressure Suction, Lift or Noise | Case No. | rpm (%) | Pressure Level in dB Vs. Frequency of Tone | | | |
|---|---|---|---|---|---|---|---|
| | | | | 1st tone | 2nd tone | 3rd tone | 4th tone |
| SI/Dl | suction* | 2 | 60 | 104.0 | – | 105.5 | 96.0 |
| | | 2 | 70 | 106.1 | 102.1 | – | 106.0 |
| | | 2 | 80 | 118.2 | 111.0 | 112.0 | 107.9 |
| | | 1 | 80 | 151.6 | 135.5 | – | 124.5 |
| | | 2 | 90 | 126.1 | 126.0 | 114.0 | – |
| FF 0° | noise | 2 | 60 | 93.1 | 86.2 | 80.3 | – |
| | | 2 | 70 | 96.3 | 87.7 | 79.9 | – |
| | | 2 | 80 | 102.1 | 92.0 | 83.9 | 78.1 |
| | | 1 | 80 | – | – | – | – |
| | | 2 | 90 | 103.0 | 92.0 | 82.9 | – |
| | | | 90 (repeat) | 102.7 | 91.1 | 82.0 | – |
| FF 10° | noise | 2 | 60 | 94.8 | 86.5 | 79.9 | 76.1 |
| | | 2 | 70 | 96.0 | 88.9 | 83.5 | – |
| | | 2 | 80 | 101.8 | 91.2 | 84.3 | 76.2 |
| | | 1 | 80 | 95.0 | 84.0 | 76.3 | – |
| | | 2 | 90 | 102.8 | 91.7 | 82.3 | – |
| FF 20° | noise | 2 | 60 | 94.9 | 87.1 | 80.6 | 74.5 |
| | | 2 | 70 | 96.0 | 89.1 | 81.0 | 75.4 |
| | | 2 | 80 | 98.0 | 90.9 | 81.1 | 75.0 |
| | | 1 | 80 | 93.5 | 78.9 | 68.4 | – |
| | | 2 | 90 | 102.9 | 93.0 | 81.7 | – |
| FF 30° | noise | 2 | 60 | 93.1 | 87.2 | 79.1 | 76.1 |
| | | 2 | 70 | 96.2 | 89.1 | 83.1 | 76.0 |
| | | 2 | 80 | 102.5 | 93.0 | 85.9 | 77.0 |
| | | 1 | 80 | 100.5 | 90.5 | 80.5 | 75.2 |
| | | 2 | 90 | 104.0 | 91.1 | 82.2 | – |

*Data between Case 1 and Case 2 are inconsistent.

TABLE A-1. (*Continued*).

| Location | Pressure, Suction, Lift or Noise | Case No. | rpm (%) | Pressure Level in dB Vs. Frequency of Tone | | | |
|---|---|---|---|---|---|---|---|
| | | | | 1st tone | 2nd tone | 3rd tone | 4th tone |
| FF 40° | noise | 2 | 60 | 94.6 | 88.1 | 82.4 | 76.9 |
| | | 2 | 70 | 100.1 | 91.1 | 85.0 | 79.5 |
| | | 2 | 80 | 105.1 | 94.0 | 86.2 | 79.4 |
| | | 1 | 80 | 102.8 | 90.4 | 80.8 | 75.2 |
| | | 2 | 90 | 106.2 | 95.0 | 86.8 | – |
| FF 50° | noise | 2 | 60 | 95.7 | 88.1 | 82.9 | 76.3 |
| | | 2 | 70 | 98.7 | 91.1 | 84.3 | 79.2 |
| | | 2 | 80 | 104.1 | 93.0 | 85.5 | 78.5 |
| | | 1 | 80 | 102.3 | 91.8 | 81.2 | 74.5 |
| | | 2 | 90 | 105.9 | 94.0 | 84.0 | – |
| FF 60° | noise | 2 | 60 | 91.2 | 86.7 | 81.1 | 76.0 |
| | | 2 | 70 | 99.0 | 90.0 | 83.6 | 78.1 |
| | | 2 | 80 | 105.0 | 95.1 | 87.1 | 78.6 |
| | | 1 | 80 | 103.5 | 89.6 | 80.6 | 76.1 |
| | | 2 | 90 | 104.8 | 93.6 | 83.1 | – |
| FF 70° | noise | 2 | 60 | 90.2 | 85.9 | 80.3 | 72.0 |
| | | 2 | 70 | 99.0 | 92.1 | 85.2 | 78.3 |
| | | 2 | 80 | 102.2 | 93.7 | 83.8 | 78.1 |
| | | 1 | 80 | 98.0 | 85.0 | 76.4 | 70.8 |
| | | 2 | 90 | 104.1 | 95.1 | 83.9 | – |
| | | | 90 (repeat) | 104.6 | 93.3 | 83.0 | – |
| FF 80° | noise | 2 | 60 | 88.7 | 80.8 | 75.5 | 69.4 |
| | | 2 | 70 | 94.6 | 85.2 | 79.8 | 73.5 |
| | | 2 | 80 | 100.1 | 89.0 | 82.1 | 75.0 |
| | | 1 | 80 | 97.0 | 84.1 | 75.0 | 69.5 |
| | | 2 | 90 | 102.2 | 90.6 | 81.7 | – |

TABLE A-1. (*Continued*).

| Location | Pressure, Suction, Lift or Noise | Case No | rpm (%) | Pressure Level in dB Vs. Frequency of Tone | | | |
|----------|----------------------------------|---------|---------|-----------|-----------|-----------|-----------|
| | | | | 1st tone | 2nd tone | 3rd tone | 4th tone |
| FF 90° | noise | 2 | 60 | 89.1 | 81.1 | 75.0 | 70.2 |
| | | 2 | 70 | 93.9 | 83.2 | 77.1 | 72.0 |
| | | 2 | 80 | 99.4 | 87.2 | 79.4 | – |
| | | 1 | 80 | 93.5 | 83.1 | 77.1 | 71.0 |
| | | 2 | 90 | 100.6 | 87.8 | 79.5 | – |
| FF 100° | noise | 2 | 60 | 91.3 | 82.2 | 76.2 | 73.0 |
| | | 2 | 70 | 95.3 | 83.9 | 78.6 | 73.3 |
| | | 2 | 80 | 100.0 | 89.1 | 83.5 | 78.4 |
| | | 1 | 80 | 97.0 | 86.4 | 80.8 | 75.0 |
| | | 2 | 90 | 103.0 | 90.6 | 83.0 | – |
| FF 110° | noise | 2 | 60 | 93.6 | 84.6 | 77.5 | – |
| | | 2 | 70 | 95.0 | 85.2 | 81.1 | 76.6 |
| | | 2 | 80 | 99.3 | 89.1 | 84.1 | 78.2 |
| | | 1 | 80 | 95.2 | 84.0 | 79.6 | 72.2 |
| | | 2 | 90 | 102.1 | 90.1 | 85.0 | – |
| FF 120° | noise | 2 | 60 | 95.0 | 84.2 | 81.1 | – |
| | | 2 | 70 | 95.3 | 87.4 | 82.4 | 78.0 |
| | | 2 | 80 | 99.7 | 91.3 | 86.8 | – |
| | | 1 | 80 | 98.1 | 86.5 | 83.8 | – |
| | | 2 | 90 | 101.7 | 93.5 | 87.2 | – |
| FF 130° | noise | 2 | 60 | 93.1 | 84.7 | 81.4 | – |
| | | 2 | 70 | 95.3 | 88.0 | 83.8 | – |
| | | 2 | 80 | 100.9 | 94.0 | 88.0 | 80.1 |
| | | 1 | 80 | 96.7 | 85.2 | 81.0 | – |
| | | 2 | 90 | 101.2 | 94.0 | 86.3 | – |

TABLE A-1. (*Continued*).

| Location | Pressure, Suction, Lift or Noise | Case No. | rpm (%) | Pressure Level in dB Vs. Frequency of Tone | | | |
|----------|-----------------------------------|----------|---------|-----------|-----------|-----------|-----------|
| | | | | 1st tone | 2nd tone | 3rd tone | 4th tone |
| FF 140° | noise | 2 | 60 | 93.5 | 88.7 | 82.8 | 77.8 |
| | | 2 | 70 | 97.1 | 87.7 | 82.0 | – |
| | | 2 | 80 | 98.1 | 89.1 | 83.2 | 78.2 |
| | | 1 | 80 | 94.0 | 82.3 | 75.4 | – |
| | | 2 | 90 | 98.8 | 90.4 | 84.3 | – |
| FF 150° | noise | 2 | 60 | 91.8 | 85.2 | – | – |
| | | 2 | 70 | 91.6 | 86.1 | 78.9 | – |
| | | 2 | 80 | 93.7 | 85.5 | – | – |
| | | 1 | 80 | 88.2 | 75.8 | 72.0 | – |
| | | 2 | 90 | 95.1 | 83.0 | – | – |